PB 264 304

REPORT NO. FRA/ORD-76-295.I

AERODYNAMIC FORCES ON FREIGHT TRAINS
Volume I - Wind Tunnel Tests of Containers and Trailers on Flatcars

Andrew G. Hammitt

Andrew G. Hammitt Assoc.
30813 Marne Drive
Rancho Palos Verdes CA 90274

DECEMBER 1976

FINAL REPORT

Prepared for

U.S. DEPARTMENT OF TRANSPORTATION
FEDERAL RAILROAD ADMINISTRATION
Office of Research and Development
Washington DC 20590

NOTICE

This document is disseminated under the sponsorship of the Department of Transportation in the interest of information exchange. The United States Government assumes no liability for its contents or use thereof.

NOTICE

The United States Government does not endorse products or manufacturers. Trade or manufacturers' names appear herein solely because they are considered essential to the object of this report.

Technical Report Documentation Page

1. Report No.	2. Government Accession No.	3. Recipient's Catalog No.
FRA/ORD-76/295.I		

4. Title and Subtitle	5. Report Date
AERODYNAMIC FORCES ON FREIGHT TRAINS Volume I--Wind Tunnel Tests of Containers and Trailers on Flatcars	December 1976
	6. Performing Organization Code
7. Author(s)	8. Performing Organization Report No.
Andrew G. Hammitt	DOT-TSC-FRA-76-30,I
9. Performing Organization Name and Address	10. Work Unit No. (TRAIS)
Andrew G. Hammitt Assoc.* 30813 Marne Drive Rancho Palos Verdes CA 90274	RR616/R7309
	11. Contract or Grant No.
	DOT-TSC-1002-1
	13. Type of Report and Period Covered
12. Sponsoring Agency Name and Address	Final Report March 1975-June 1976
U.S. Department of Transportation Federal Railroad Administration Office of Research and Development Washington DC 20590	14. Sponsoring Agency Code

15. Supplementary Notes

*Under contract to: U.S. Department of Transportation
Transportation Systems Center
Kendall Square
Cambridge MA 02142

16. Abstract

The aerodynamic forces on trailers and containers on flatcars have been measured in wind tunnel tests. The forces were measured on the central car of a five-car train consisting of a locomotive, three flatcars with various loadings and a boxcar. Tests were made over a range of yaw angles and with different loadings. Standard trailers, containers and flatcars were tested as well as a variety of modifications designed to improve the aerodynamic performance. In addition to the railroad-car tests, a series of blocks simulating containers and trailer bodies were tested to determine the effect of gap spacing, corner radius, and surface roughness. The flatcars loaded with containers were found to have about forty percent less drag than when loaded with trailers. Various modifications that reduced the frontal area of the trailers or filled in the empty space between the trailer body and the car were all found to be effective in reducing the drag. Gap spacing size had little effect until it became of the order of the body width, and then the drag increased with increased spacing. Side and lift forces are chiefly caused by yaw angle and side area. The forces act near the centroid of the side area, but when the gap spacing becomes large they move farther forward. The research reported is intended to increase the knowledge base in understanding the aerodynamic drag component of trail resistance.

17. Key Words	18. Distribution Statement
Freight Car Aerodynamics TOFC and COFC Aerodynamics Train Resistance	DOCUMENT IS AVAILABLE TO THE U.S. PUBLIC THROUGH THE NATIONAL TECHNICAL INFORMATION SERVICE, SPRINGFIELD, VIRGINIA 22161

19. Security Classif. (of this report)	20. Security Classif. (of this page)	21.
UNCLASSIFIED	UNCLASSIFIED	ce

Form DOT F 1700.7 (8-72) Reproduction of completed page authorized

PREFACE

The research reported in this document was sponsored by the Office of Research and Development of the Federal Railroad Administration under its Improved Rail Freight Service Program. It represents one part of an effort to obtain greater fuel economy in the movement of freight by rail vehicles. This report is the first in a series on the aerodynamic drag of freight trains. A second volume giving the results of full scale measurements of aerodynamic forces of containers and trailers on flatcars is anticipated, and a third volume shall provide wind tunnel data on other types of freight car.

METRIC CONVERSION FACTORS

Approximate Conversions to Metric Measures

Symbol	When You Know	Multiply by	To Find	Symbol
		LENGTH		
in	inches	2.5	centimeters	cm
ft	feet	30	centimeters	cm
yd	yards	0.9	meters	m
mi	miles	1.6	kilometers	km
		AREA		
in^2	square inches	6.5	square centimeters	cm^2
ft^2	square feet	0.09	square meters	m^2
yd^2	square yards	0.8	square meters	m^2
mi^2	square miles	2.6	square kilometers	km^2
	acres	0.4	hectares	ha
		MASS (weight)		
oz	ounces	28	grams	g
lb	pounds	0.45	kilograms	kg
	short tons (2000 lb)	0.9	tonnes	t
		VOLUME		
tsp	teaspoons	5	milliliters	ml
Tbsp	tablespoons	15	milliliters	ml
fl oz	fluid ounces	30	milliliters	ml
c	cups	0.24	liters	l
pt	pints	0.47	liters	l
qt	quarts	0.95	liters	l
gal	gallons	3.8	liters	l
ft^3	cubic feet	0.03	cubic meters	m^3
yd^3	cubic yards	0.76	cubic meters	m^3
		TEMPERATURE (exact)		
°F	Fahrenheit temperature	5/9 (after subtracting 32)	Celsius temperature	°C

Approximate Conversions from Metric Measures

Symbol	When You Know	Multiply by	To Find	Symbol
		LENGTH		
mm	millimeters	0.04	inches	in
cm	centimeters	0.4	inches	in
m	meters	3.3	feet	ft
m	meters	1.1	yards	yd
km	kilometers	0.6	miles	mi
		AREA		
cm^2	square centimeters	0.16	square inches	in^2
m^2	square meters	1.2	square yards	yd^2
km^2	square kilometers	0.4	square miles	mi^2
ha	hectares (10,000 m^2)	2.5	acres	
		MASS (weight)		
g	grams	0.035	ounces	oz
kg	kilograms	2.2	pounds	lb
t	tonnes (1000 kg)	1.1	short tons	
		VOLUME		
ml	milliliters	0.03	fluid ounces	fl oz
l	liters	2.1	pints	pt
l	liters	1.06	quarts	qt
l	liters	0.26	gallons	gal
m^3	cubic meters	35	cubic feet	ft^3
m^3	cubic meters	1.3	cubic yards	yd^3
		TEMPERATURE (exact)		
°C	Celsius temperature	9/5 (then add 32)	Fahrenheit temperature	°F

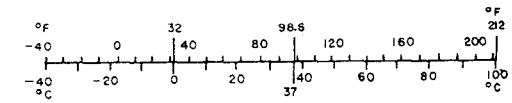

CONTENTS

ILLUSTRATIONS

ILLUSTRATIONS (Continued)

ILLUSTRATIONS (Continued)

ILLUSTRATIONS (Continued)

ILLUSTRATIONS (Continued)

TABLES

NOMENCLATURE

a	constant term in formula, Figures 2 and 43
A	frontal area
b	linear term in formula, Figures 2 and 43
c	square term in formula, Figure 43
C	coefficient
C_D	drag coefficient based on frontal area
C_{DC}	cross flow drag coefficient based on side area
C_L	lift coefficient based on frontal area
C_Y	side force coefficient based on frontal area
C_{Yc}	side force coefficient due to second order term based on frontal area
E	energy
g	factor in side force relation
h	height
k	roughness height
K	aerodynamic resistance coefficient, Figure 2 and "modified Davis Formula"
n	number of axles
R	resistance force
V	velocity
W	weight car per axle in tons
λ	body length over height
ρ	density of air
ϕ	angle of yaw

Flat Cars	
TTX	Standard without bridge plate
TTXR	Standard with bridge plate
TTXA	TTX aero fairing
TWC	Trailer well car
CWC	Container well car
CWCA	CWC with aero fairing

Containers	
CS	Smooth container with sharp edge
CSA	Smooth container with front edge rounded to r = .1 (width)

Location On Railroad Car	
F	Front
R	Rear

NOMENCLATURE (Continued)

Coupling Distance

Normal	60"
Close Coupled 1	30"
Close Coupled 2	15"

Other

E	Empty
W	Wheel trucks removed
Rr	Rearward facing

Trailers

TS	AMT* refrigerator van
Tr	AMT* exterior post van
TM	TS modified to moving van
TSA	TS with full aero fairing
TH	TS with height increase to 14 ft.

*Plastic model kit manufactured by AMT, Troy, Michigan.

EXECUTIVE SUMMARY

The aerodynamic resistance of railroad trains is a subject which has been considered for many years. Some of the first measurements seem to have been made by Gross (Reference 7) in 1898 and included the introduction of the wind tunnel as an engineering tool. Notable later works were the measurements made on the test car Louisiana by the Electric Railroad Commission in 1906 (Reference 3) and the 1926 paper by Davis (Reference 2). With the introduction of piggyback freight, it was observed that the aerodynamic resistance of such trains was higher than for other types. Changes to the Davis formula for resistance were suggested giving increased aerodynamic resistance (Reference 14). In the present study the aerodynamic resistance of trailers and containers on flat cars was measured for a variety of configurations using models tested in a wind tunnel.

The importance of aerodynamic drag on the total resistance of a train has been considered as well as the effect on operating costs. For high speed runs and high railroad car utilization, the fuel and locomotive operational cost required to overcome the aerodynamic drag can be large, about $4,000 per year for 100,000 miles per year at 60 mph service for the trailer on flat car configuration. However, the practical conditions of railroad operation make it unreasonable to consider extensive streamlining that would interfere with cargo handling operations. The use of containers instead of trailers is one change which is known to give lower aerodynamic resistance. Various other configurations such as well cars have also been considered in this series of tests.

The wind tunnel as a means of aerodynamic testing has been well established for airplane development but has not yet been completely accepted for railcar testing. It is a convenient way of measuring aerodynamic forces that separates the aerodynamic from the rolling resistance and allows data to be obtained relatively cheaply and expeditiously. However, the inexact simulation of the ground plane causes some questions as well as the use of reduced scale models. The past use of the wind tunnel in railroad and automotive testing has established that the measurements are reasonably reliable, especially for comparisons between different configurations. A subsequent part of this program is the verification of the wind tunnel tests by measurement of the aerodynamic forces on trailers mounted on flat cars.

These tests are expected to be run at the Transportation Test Center at Pueblo, Colorado.

The initial wind tunnel tests were on a series of five blocks simulating containers or trailer bodies. Aerodynamic forces were measured on the third or middle block. Tests were run at a variety of yaw angles using different nose radii and different spacings between the blocks. A series of pictures were also taken using tufts to provide flow visualization. These pictures show that the flow between the blocks is less than might be expected even for large gap spacings at large angles of yaw. The drag increases as the gap spacing increases but there is little effect until the gap is somewhere between a half to one block width long. For smaller gaps, the sharp cornered blocks give less drag than those with larger corner radii and the opposite is true for larger gaps. The drag is independent of yaw angle for small gap spacing but does increase considerably at larger gap spacings for the smaller block nose radii. The side forces and rolling moments depend on the yaw angle. Their magnitude increases with increased gap size.

The railroad car tests confirm the reduced aerodynamic drag of containers over trailers on flat cars which had been determined by full scale observations. The tests also show a major increase in drag caused by crosswinds that is larger than that caused by the same strength headwind. Empty spaces along the train caused by unloaded flat cars or cars with only one trailer increase the drag. While the drag of an empty car is less than a loaded car, the increase in drag on the following loaded car almost equals the decrease. If loaded and empty cars are in the same train, a considerable decrease in aerodynamic drag can be obtained by grouping the empty and loaded cars together.

Several modified flat car and trailer designs were tested including well cars. Streamlining the body of the TTX car was tried with little resulting improvement. A well car in which the trailer wheels were submerged in a well between the rail trucks was tested and showed considerable drag reduction as might be expected. Any modification reducing the open space between the trailer body and the car decreases the drag. A shortened container well car in which two containers are carred stacked on top of each other proved to have very low aerodynamic drag when end fairings were added.

Side forces and rolling moments depend on yaw angle and side area as expected. The force is roughly at the midpoint of the side area. The lift forces also vary in roughly the same way as the side forces. Lift forces are small at zero yaw angle. The lift force also depends on the side area rather than the planform area as might have been expected.

1. BACKGROUND

The measurement of the tractive resistance of railroad trains has been a subject of interest for more than 100 years. Notwithstanding this long history, engineering data is not yet available for making accurate predictions of such resistance. The rolling resistance is hard to measure and the parameters which affect it are hard to control. The wind tunnel is a good way of measuring aerodynamic forces but has not yet become a thoroughly reliable and trusted means of measuring aerodynamic forces for railroad trains operating on the ground. The principal reasons for this are the lack of proper ground plane simulation and the old classic problem of Reynolds number extrapolation. In full scale tests of total resistance, it is difficult to separate aerodynamic from rolling resistance.

One of the early full scale measurements of freight train resistance was done by Professor Schmidt at the University of Illinois in 1910 (Reference 1). Many of these early results have been compiled by Davis (Reference 2) in his 1926 paper. This is a classic paper that treats all forms of railroad resistance and can still be considered one of the authorities in this field. While much of the early work consisted of overall resistance measurements, the work of the Electric Railway Commission (Reference 3) is noted as an early and careful attempt to measure aerodynamic resistance alone. A street car was suspended by means of a balance on a railway flatcar and the aerodynamic resistance of the street car measured as the flatcar was moved at different speeds.

A surge of interest in the aerodynamic resistance of railway trains occurred during the 1930's particularly with respect to high speed streamlined passenger trains. At this time, several investigators used wind tunnels as means of determining the aerodynamic effects. The work of Tietjens and Ripley at Westinghouse (Reference 4), Klemin at New York University (Reference 5), and Johansen at London Midland and Scottish Railway (Reference 6) are all examples of the application of wind tunnel aerodynamic testing to determine and improve the aerodynamic resistance of passenger trains.

These were not the first use of the wind tunnel to test the aerodynamic resistance of trains. Even before the wind tunnel had been developed for testing of airplanes, W. F. M. Goss had built a wind tunnel at Purdue in 1896 and performed tests on railway trains (Reference 7).

Following World War II the interest in the aerodynamic resistance of trains was somewhat reduced particularly in the United States. There have been a few wind tunnel tests of special train configurations such as that of Lesher at the University of Michigan (Reference 8) and that of Burlage at Case Institute (Reference 9). Since the 1960's, interest in Europe and Japan has increased. The Japanese have done considerable work particularly aimed at the development of their high speed Tokaido line (Reference 10) and the French have built a special wind tunnel at Saint Cyr L'Ecole for the testing of railway trains (Reference 11). The test section of the usual wind tunnel is too short relative to its diameter to be used efficiently for railroad train testing. The French tunnel is designed to overcome this difficulty by providing a long test section and a boundary layer control system to make this long test section effective.

In recent years the interest in the aerodynamic resistance of freight trains has increased in the United States. One reason for this has been the introduction of new car designs which have a higher aerodynamic resistance. Rack cars and piggyback cars are examples. Practical experience on the railroads has shown that the power required to pull a train of rack or piggyback cars is higher than for the standard cars. Wind tunnel tests were made by Matthews and Barnett (Reference 12) in 1968 on automobile rack car configurations. These tests did demonstrate the high aerodynamic resistance of rack cars and showed ways in which it could be reduced. Luebke (Reference 13) compared the wind tunnel results with full scale test data and was able to show a reasonable agreement between the two. Other full scale tests of piggyback configurations have demonstrated the large drag of such arrangements. Such tests as those run by the Eric Lackawanna (Reference 14) and the Santa Fe (Reference 15), as well as several tests reported by Luebke (Reference 13) run on the New York Central and Chesapeake and Ohio show increased drag.

Compilations of existing data appear in several books and reports. The American Railway Engineering Association handbook (Reference 16) has a chapter which discusses rolling resistance and aerodynamic resistance. The aerodynamic drag of railway vehicles is also covered by Hoerner (Reference 17) and Hammitt (Reference 18). Both of these references are more oriented to passenger than freight type of service.

2. TRAIN RESISTANCE — INTRODUCTION

The work of Davis (Reference 2) in 1926 is classic in the field and is the principle reference even today. The situation is complicated by the introduction of a different relation, referred to as the "modified Davis Formula" by the AREA (Reference 16), which seems to have been originated by the Canadian National Railroad. The two formula as applied to conventional freight cars are as follows:

$$\frac{R}{Wn} = 1.3 + \frac{29}{W} + .045\ V + .0005\ A\ \frac{V^2}{Wn} \qquad \text{Davis}$$

$$\frac{R}{Wn} = 0.6 + \frac{20}{W} + 0.01\ V + .07\ \frac{V^2}{Wn} \qquad \text{"modified Davis"}$$

where R is resistance in pounds, W is weight per axle in tons, n is number of axles and V is velocity in miles per hour.

The aerodynamic terms listed are for conventional freight cars. Davis (Reference 2) gives the frontal area of a freight car as 85 to 90 sq. ft. so the coefficients of the velocity squared term differ by about 35 percent. The coefficients of the other terms are even more different. The basic assumption in both these formulas seems to be that there is a term which is independent of velocity, which breaks up into one part which depends on weight and one which depends on the number of axles, a term which is linear with velocity and depends on weight, and a term which is independent of weight and depends on velocity squared. This last term is usually considered to be the aerodynamic resistance which is a reasonable assumption. It is hard to give substantial reasons for limiting the rolling resistance effects to the constant and linear term but it seems to be generally accepted. Davis quotes authority for his selection of the parameters, but the considerable difference between his values and the so called "modified formula" is disturbing. Figure 1 shows the total resistance of a 75 ton freight car, the weight of a loaded TTX car, calculated by both of these methods and the contributions made by the different terms.

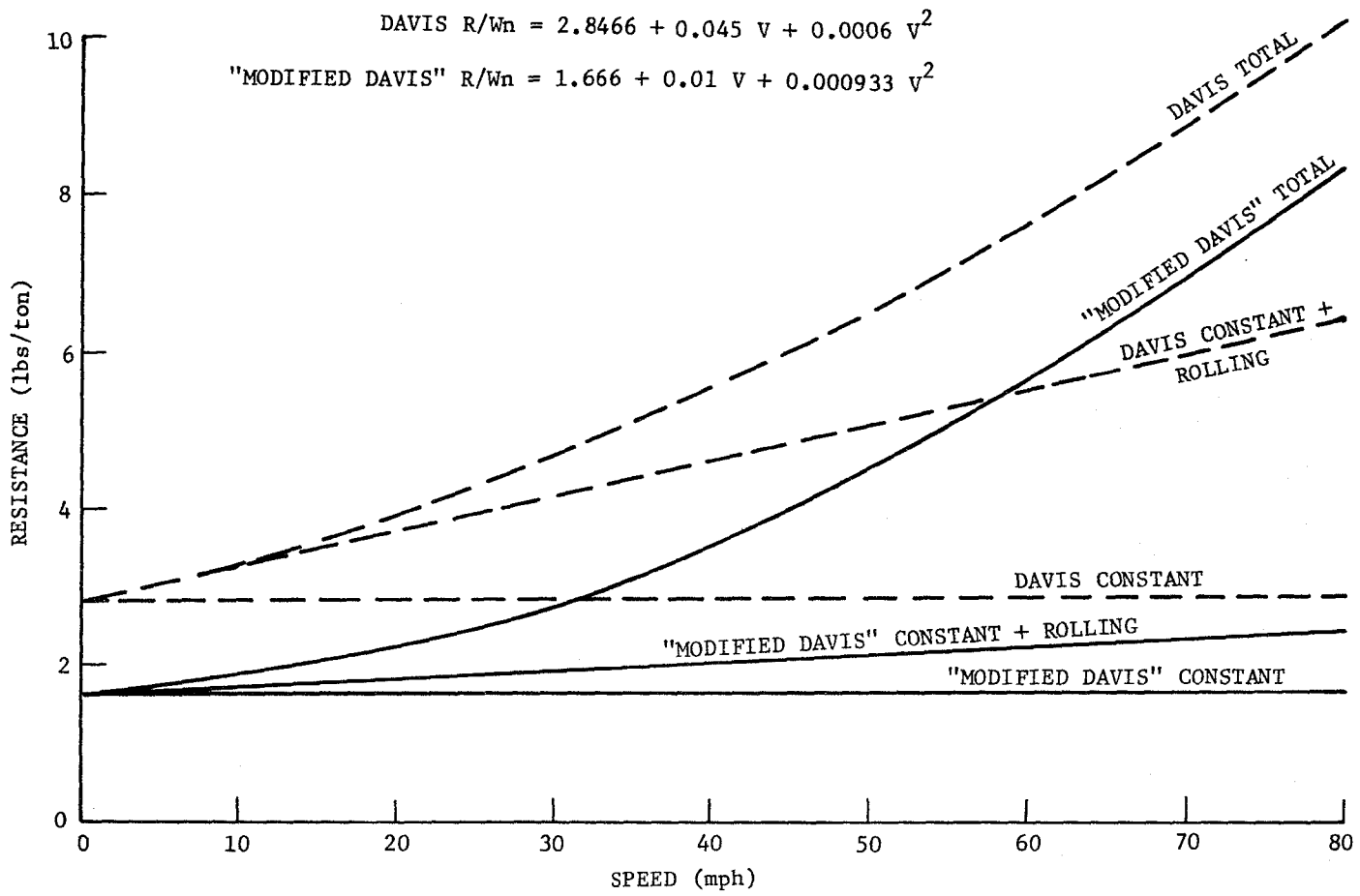

Figure 1. Resistance of 75 ton 4 axle freight cars from Davis and "Modified Davis" formula as a function of speed. Curves show the effect of different terms in formulas.

Another source of resistance information is the work of Tuthill (Reference 19). This work is a follow up of the earlier work of Schmidt (Reference 1) which was also done at the University of Illinois. Tuthill does not attempt to separate the various physical effects. However, he does provide empirical curve fits to his data in the form of coefficients to a constant, first, and second order velocity term. These fits are made for cars of different weights. The coefficients so determined are shown in Figure 2 compared with those from the Davis and "modified Davis" formulas. The coefficients from the various sources seem to bear little relation to each other. The dependence of the Tuthill square term, aerodynamic coefficient, on weight does not seem logical. The scatter in the Tuthill coefficients seems to illustrate the difficulty of determining a set of several coefficients from a series of test data which is itself subject to random scatter. Tuthill's results for resistance are compared with those calculated by the Davis and "modified Davis" formulas in Figure 3. While there is considerable discrepancy, the differences are not as large as the difference in the coefficients.

There are some recent results particularly applicable to the TOFC and COFC operations. The work of Luebke (Reference 13) and that done by the Erie Lackawanna (Reference 14) are in this class. In both of these instances total resistance has been determined and then the aerodynamic part calculated by subtracting out the rolling resistance using the "modified Davis" formula. Luebke gives the following results for the aerodynamic coefficient K, the coefficient of the V^2 term in the "modified Davis" formula. The relation between K and C_dA will be discussed later.

	K	C_dA (ft^2)	C_dA (m^2)
TOFC (C&O tests)	0.16	63	5.85
COFC (NYC tests)	0.0935	37	3.44
TOFC (EL tests)	0.20	78	7.24

Luebke justifies the difference between the Erie Lackawanna results and the Chesapeake and Ohio results by the fact that Erie Lackawanna only used data from runs at about 50 mph and he shows that the Chesapeake and

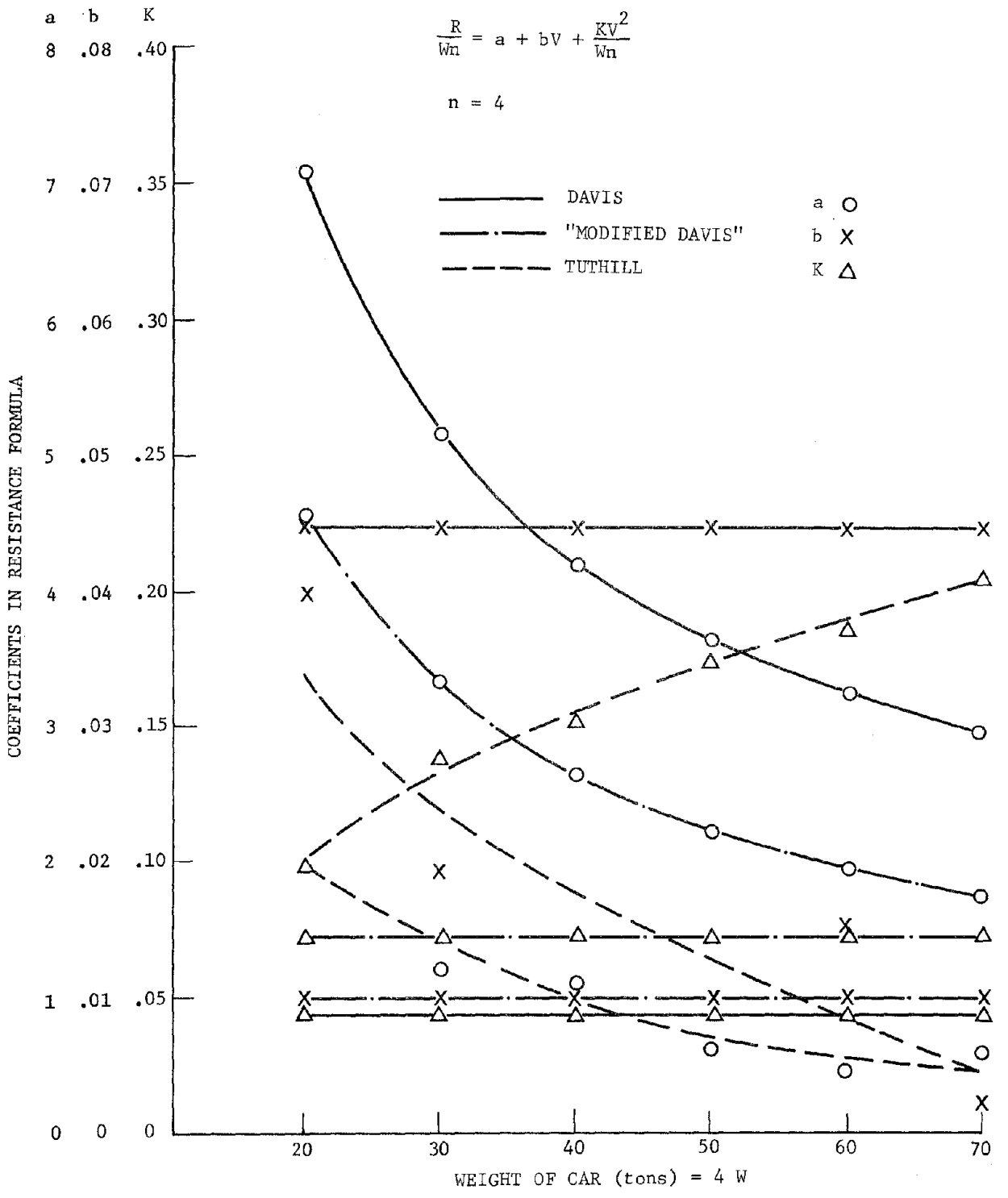

Figure 2. Comparison of coefficients in the Davis and "Modified Davis" resistance formulas and those determined by Tuthill (Ref. 19) as a function of car weight.

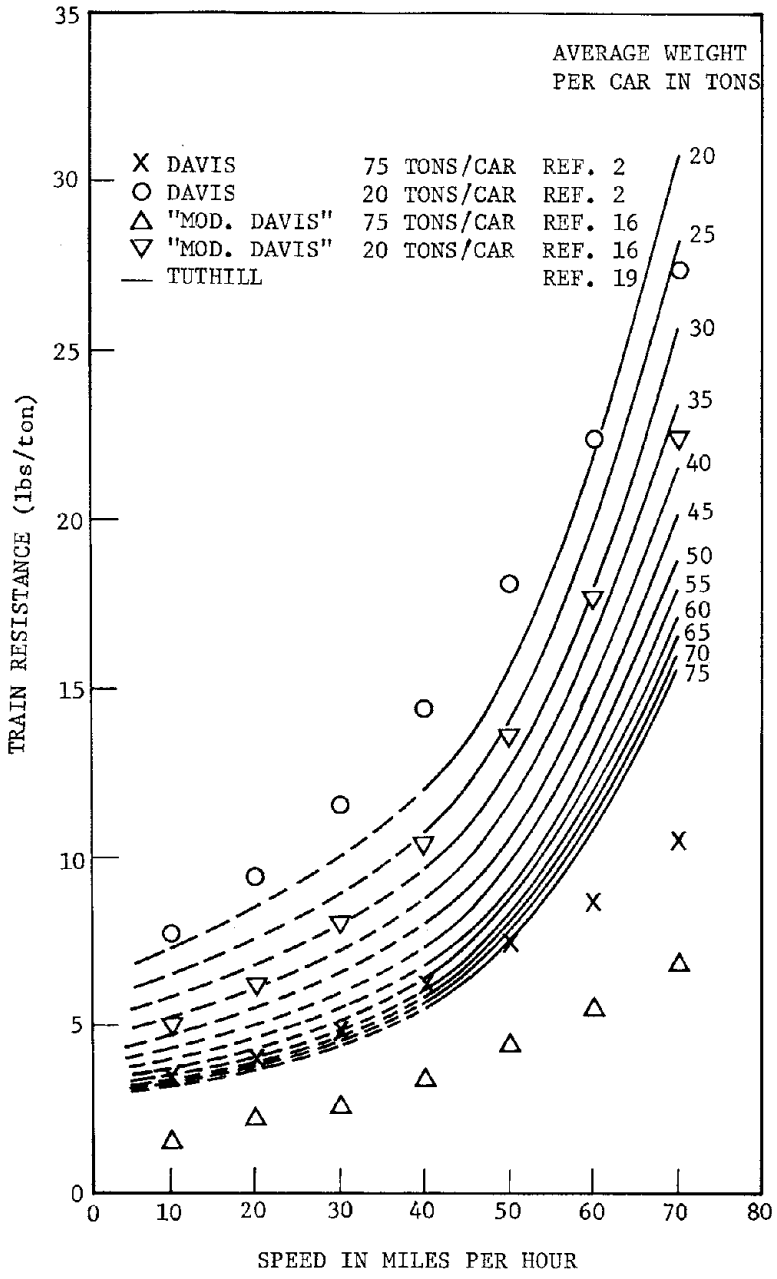

Figure 3. Relation of resistance to speed for various weights per car calculated by various methods.

Ohio results give about the same coefficient when only the data from runs at this speed are considered. While this may explain the difference between the two results, it is disturbing in that it suggests that, with data reduced in this way, the aerodynamic coefficient depends upon the speed at which the tests are run.

At this point it is probably worth taking a moment to discuss the form of expression used in these formulas. The aerodynamic basic relation for resistance is:

$$R = \frac{1}{2} \rho V^2 \, C_d A$$

C_d is dimensionless and the other quantities may be in any consistent units. To reduce this to the form of the Davis formulas, a particular value of the density of the air must be assumed. If the air density is taken as .002377 slugs/ft^3 the relation becomes:

$$R = .002556 \, V^2 \, C_d A$$

in which R is in pounds, V is in mph, and $C_d A$ is in ft^2. $C_d A$ is called the drag area and is a convenient quantity in which to work, especially for shapes for which a basic characteristic area is not well defined. The relation between $C_d A$ and K, the resistance coefficient of the "modified Davis" formula, is

$$C_d A \ (ft^2) = 391.1 \ K \quad \text{or} \quad C_d A \ (m^2) = 36.33 \ K$$

The drag area, and other force areas, are the quantities that will primarily be used to specify the resistance and other forces or railroad cars in this report.

Tests have also been run by the Santa Fe Railroad on both TOFC and COFC (Reference 15). The Santa Fe made no attempt to determine separate aerodynamic and rolling resistance coefficients from this data. Figures 4 and 5 show calculations of the aerodyanmic coefficients using the assumption that the air was still, Figure 4, and the winds as reported in the tests, Figure 5. This has been done using the Davis and "modified Davis" formulas for rolling resistance. If the wind is neglected, the use of the Davis formula gives relatively constant

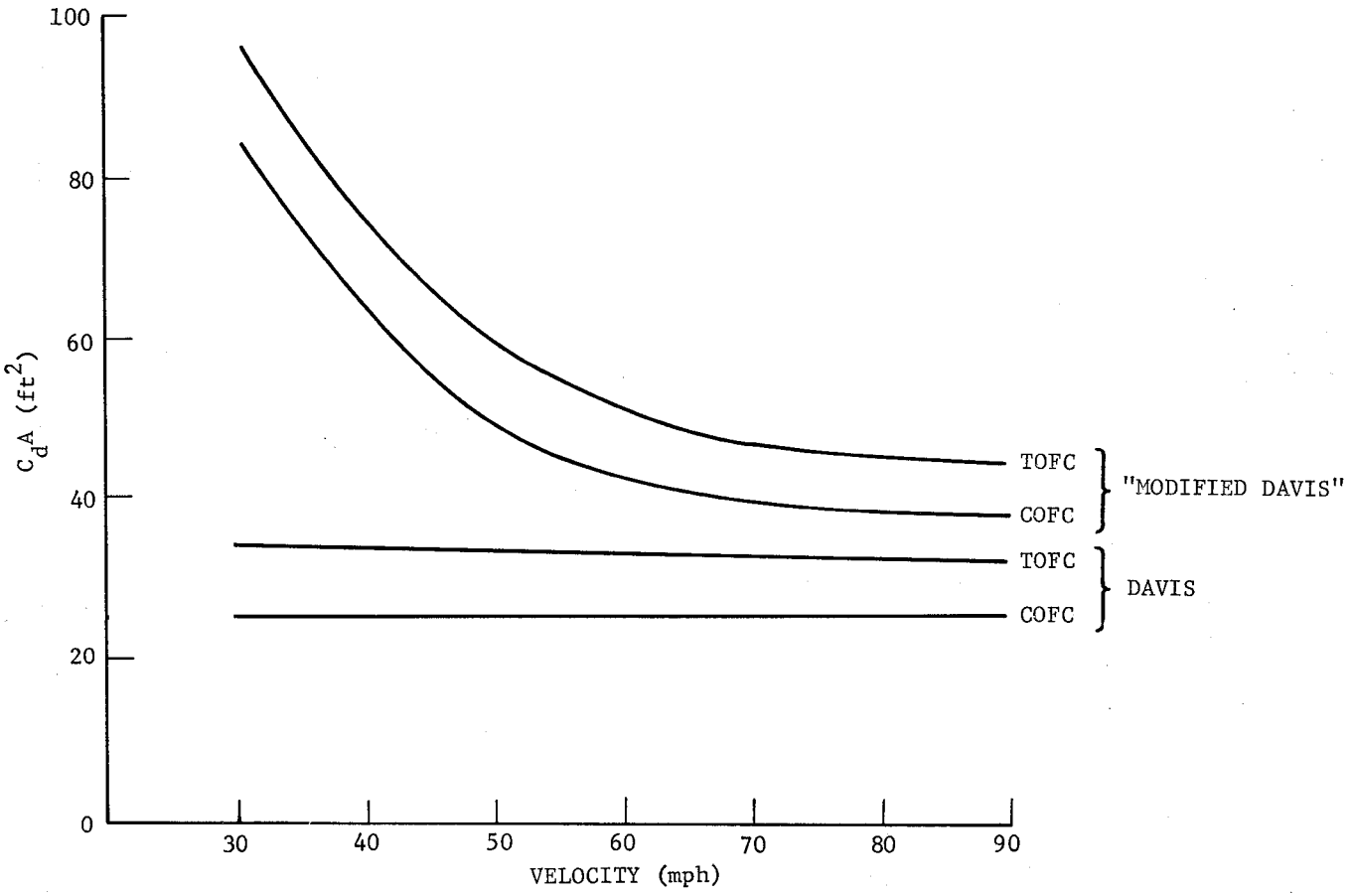

Figure 4. Aerodynamic drag for TOFC and COFC calculated from full scale test data using Davis and "Modified Davis" formulas for rolling resistance, assuming still air conditions. Data from Santa Fe (Ref. 15)

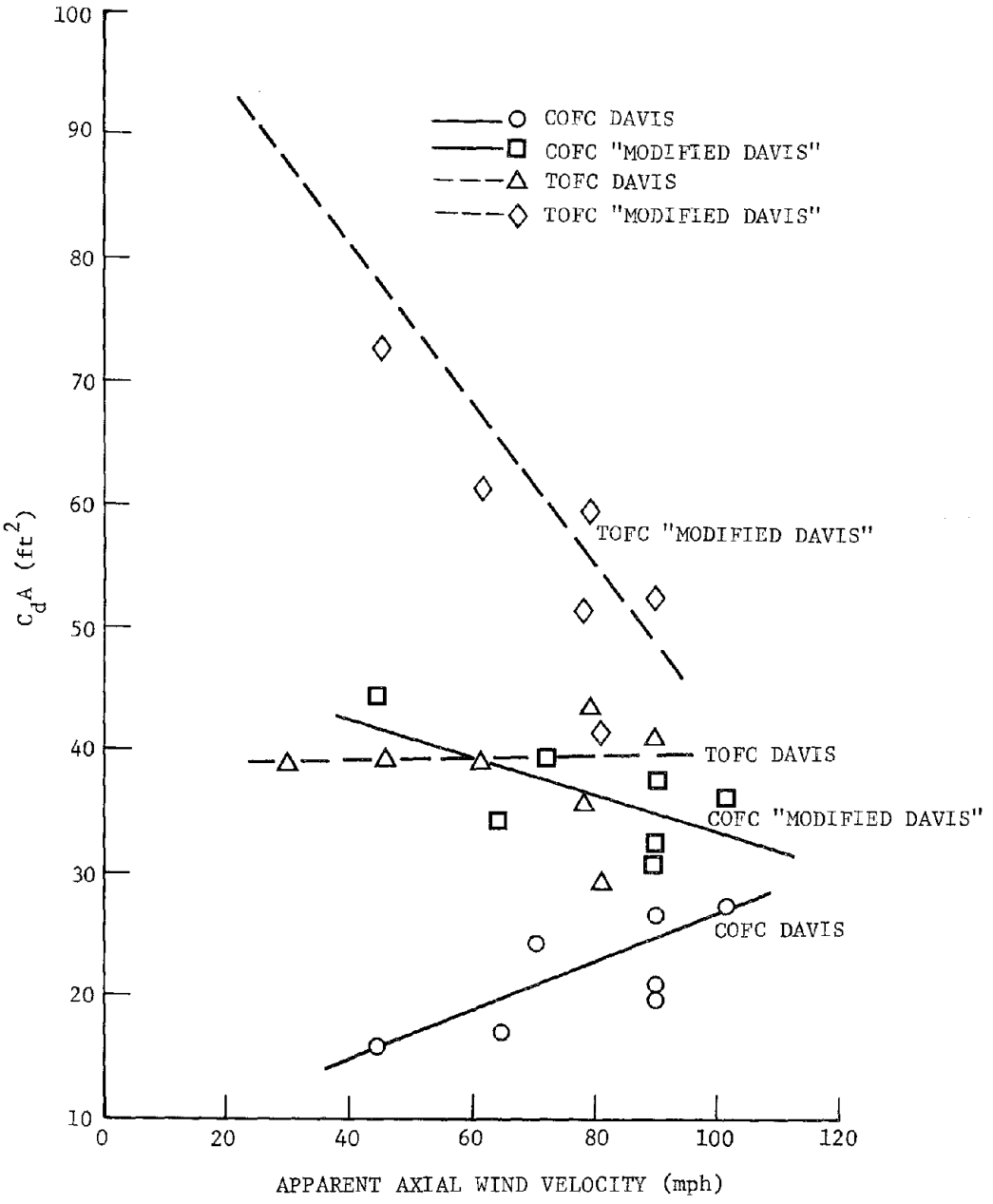

Figure 5. Aerodynamic drag for TOFC and COFC calculated from full scale test data using Davis and "Modified Davis" formulas for rolling resistance, using winds reported in the tests. Data from Santa Fe (Ref. 15)

aerodynamic resistance coefficients over the entire speed range while use of the "modified Davis" formula does not. However, the difference in drag between TOFC and COFC is not large. If the measured wind is included, the results shown in Figure 5 are obtained. A drag area independent of speed is obtained only for the TOFC configurations using the Davis formula. One would expect the drag area to increase with yaw angle. There appears to be no correlation of this type. Both ways of reducing the data show a decrease of drag area with speed when the "modified Davis" formula is used. This result seems to be consistent with the reason Luebke gave for the discrepancy between the Chesapeake and Ohio and Erie Lackawanna aerodynamic coefficients and makes one feel that the "modified Davis" formula may not be an improvement. The inclusion of the winds in the reduction of the data increases the differences between the TOFC and COFC aerodynamic coefficients. This is because the winds were ahead of the train during the COFC tests and behind the train during the TOFC tests. The difference is roughly consistent with the difference between the two configurations suggested by Luebke.

One must conclude that the available full scale tests are not adequate to define the aerodynamic drag of railroad freight cars. The most obvious reason for this is the difficulty of determining what part of the total drag is caused by aerodynamics. One solution would be to obtain better ways of predicting the rolling resistance; however, this may be simply a way of shifting the responsibility away from the aerodynamicist.

3. ECONOMIC EFFECT OF A CHANGE IN RESISTANCE

The air resistance of a high speed freight train is a major contributer to the overall resistance of the train, Figure 1. A reduction in the aerodynamic resistance would result in a direct saving in the power expended in pulling the train. Since the aerodynamic drag increases as the square of the speed, while other resistances rise less rapidly, aerodynamics is of increasing importance as the speed increases.

A reduction in required power reduces the cost of railway operation in two different ways. It reduces the fuel expended and it reduces the maintenance and operating costs of locomotives. The fuel costs are almost directly related to the change in power. The capital and maintenance costs depend more on the number of power units used on a particular train than on the actual power used. It is reasonable to assume that the number of power units will be reduced as the power required is reduced but, since locomotives only come in integral units, small reductions in required power may not allow a reduction in power units. If the power unit is sized by the requirement to climb a governing grade at low speed (where aerodynamic resistance is unimportant) then reduced aerodynamic resistance will not allow a reduction in power units. The problem here is the efficiency of power unit utilization. Nevertheless, for present purposes, it is only reasonable to assume that the utilization, on the average, would be the same for trains of different aerodynamic resistances.

The energy saved by a specified change in aerodynamic resistance can be expressed by the relation

$$\Delta E = .002868\ \rho\ V^2\ \Delta C_d A$$

where ΔE is in hp hrs per mile, ρ in slugs per ft^3, V in mph and $\Delta C_d A$ (the change in drag area) in ft^2. If sea level air density is used, the relation becomes

$$\Delta E = 6.817(10^{-6})\ V^2\ \Delta C_d A$$

In order to determine the cost of the additional energy it is necessary to know the cost of the fuel and the maintenance and capital costs of the locomotives. The fuel consumption of a railroad locomotive is on the order of .056 gallons of fuel per hp hr. This number is consistent with the basic information on diesel engines and with the information obtained from References 20 and 21. Reference 20 used .0606 and Reference 21 gives .056. The cost of the fuel has changed considerably during the past few years and it is difficult to fix a lasting value. Reference 20, written in 1969, used $.10 per gallon and Reference 21 gives $.269 per gallon as a current price in May 1975. Using the current figures from Reference 21, the fuel cost is $.015 per hp hr. Maintenance and capital cost are given in Reference 20 as $.0034 per hp hr and in Reference 21 as $.006 per hp hr. Using the later and more current figure, the total cost of both fuel and equipment is $.021 per hp hr. It is interesting to note that the proportion of the total cost attributable to fuel has not changed appreciably since 1969, that fuel costs are now 71 percent of the total and were 64 percent in 1969.

Since firm data is not yet available on the aerodynamic drag of piggyback freight, it seems best to evaluate the economic savings as a function of the appropriate parameters and then to indicate the value of these parameters based on the available data. Figure 6 shows the energy in hp hr per car mile as a function of speed and C_dA. Figure 7 shows the cost per car mile caused by aerodynamic drag as a function of these same parameters, and Figure 8 the cost per year based on the average national car usage of 100,000 miles per year.

Based on the available data on the aerodynamic resistance of TOFC and COFC operations, reasonable values of C_dA are 70 ft^2 (6.50 m^2) for TOFC and 37 ft^2 (3.43 m^2) for COFC. As an example, it can be determined from Figure 8 that the use of containers instead of trailers in 60 mph service would result in an annual savings per car of $1,700. From Figure 9, the savings that would be accomplished by this same change in C_dA as a function of speed and miles per year can be determined. These figures can be used to determine the economic advantages caused by the aerodynamic drag of the different configurations considered in this report.

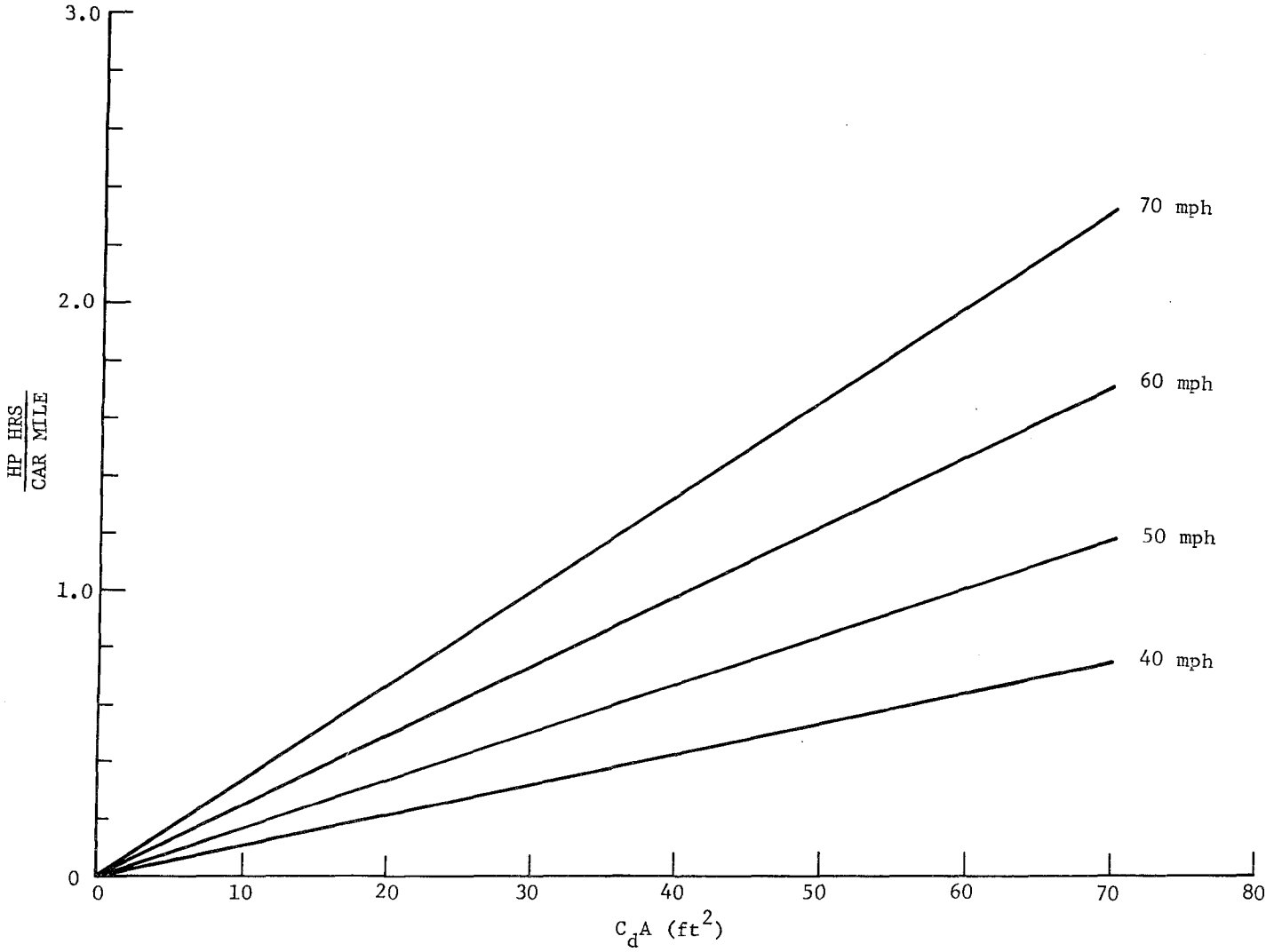

Figure 6. Energy required per car mile to overcome aerodynamic resistance at different speeds as a function of drag area.

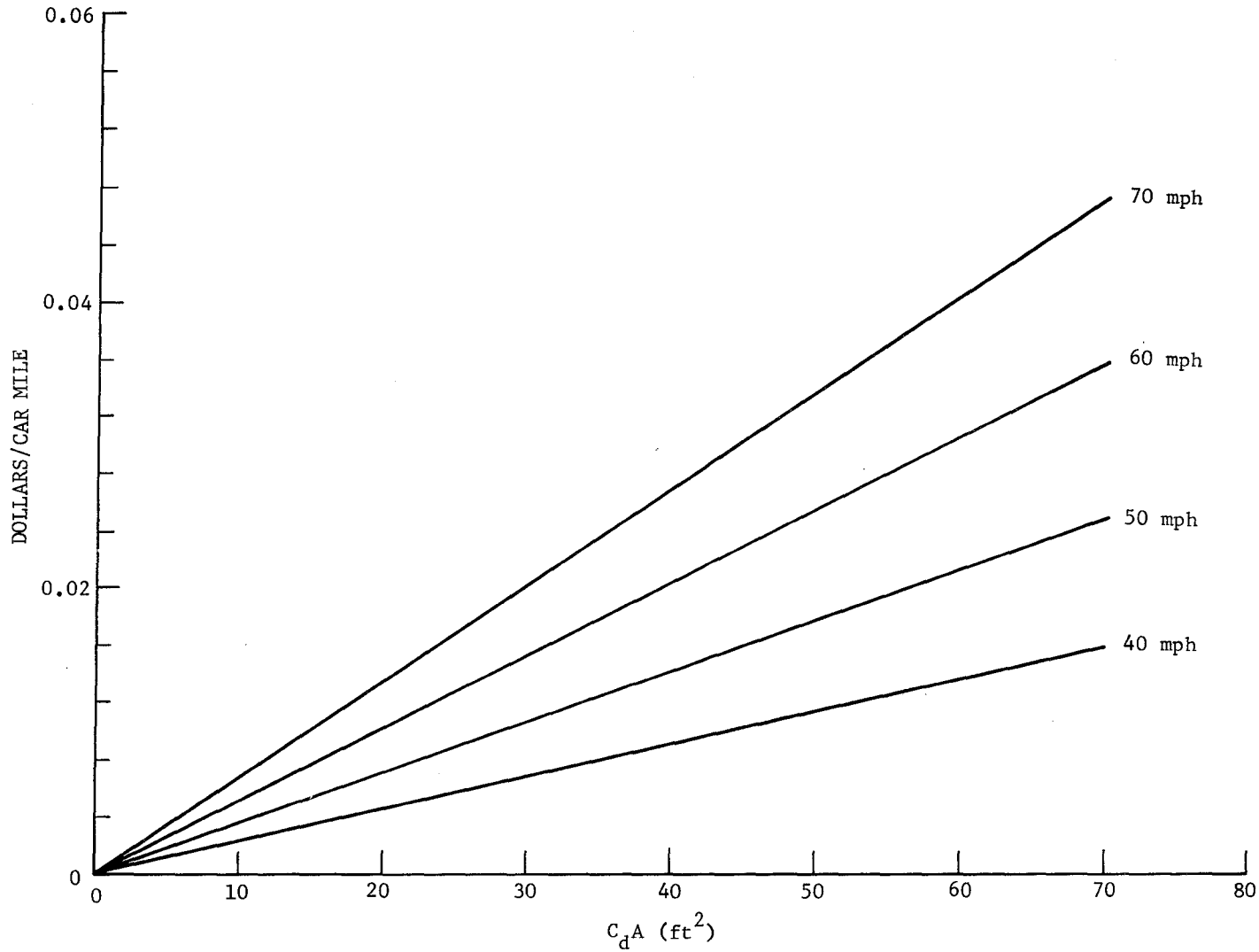

Figure 7. Cost per car mile required to overcome aerodynamic resistance as a function of drag area.

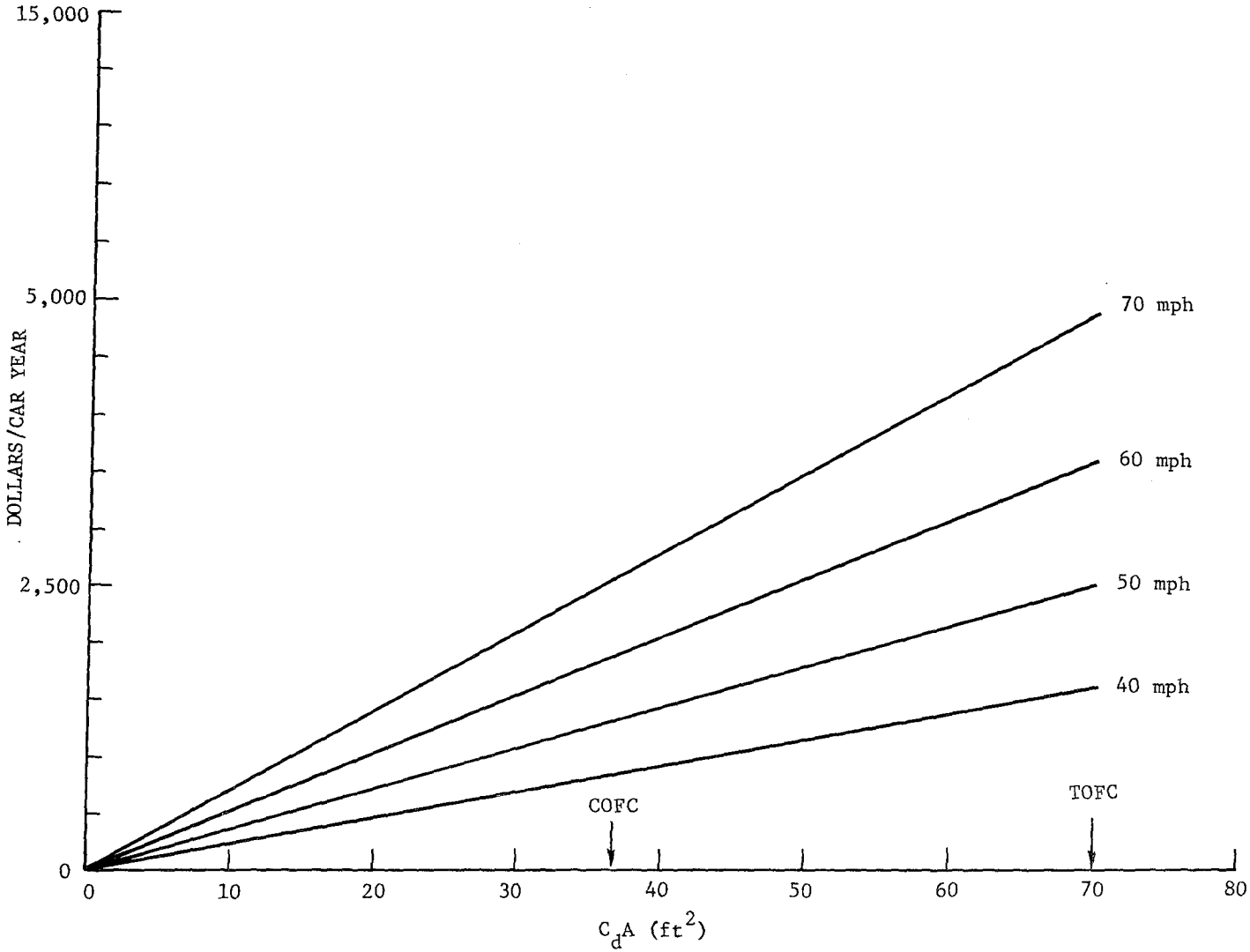

Figure 8. Cost per car year, based on use of 100,000 miles per year, of overcoming aerodynamic resistance for different speeds as a function of drag area. Typical values of drag area for TOFC and COFC are shown.

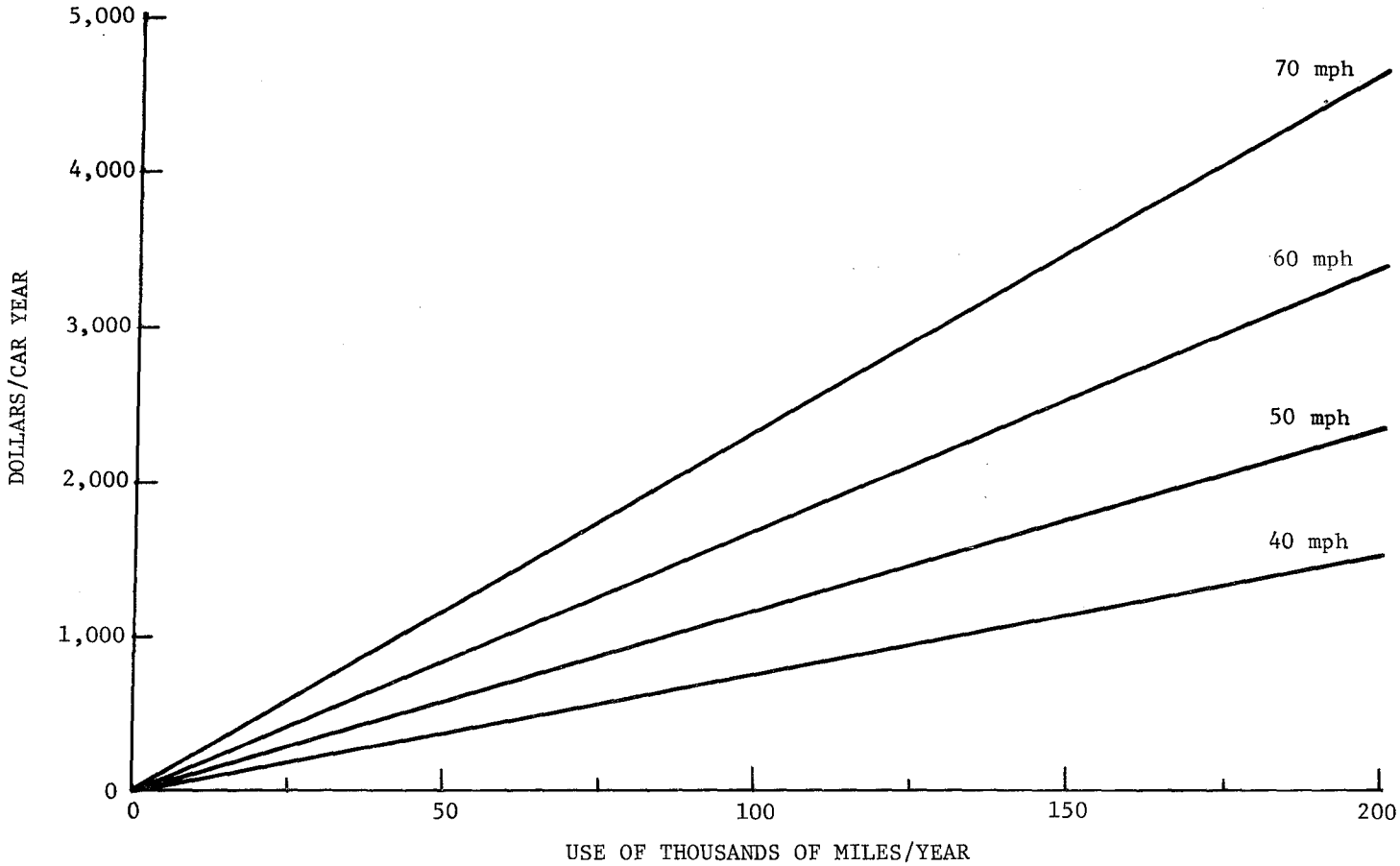

Figure 9. Difference in cost per car year as a function of use for overcoming aerodynamic resistance between TOFC and COFC based on drag area of 70 and 37 square feet, respectively.

4. RESTRICTIONS IMPOSED BY OPERATING PRACTICE

A survey of railway operating practice was conducted in order to determine the conditions under which railroad piggyback operations were conducted. A short exposure to railway loading yard practice soon convinces one that the equipment must be rugged and designed for rapid handling. Any changes that would increase the difficulty of handling the equipment in the loading and unloading process is not likely to be economically viable.

The relative merits of container and trailers is an example. Containers seem to have all of the advantages from the point of view of line hauling. They are lighter in weight, give a lower center of gravity, and have considerably less aerodynamic resistance. Their disadvantages are that they require a trailer bed on which to be loaded that must be stored and available when the container is to be unloaded. They also are not suitable for circus style (drive on) loading and unloading but require relatively expensive side or overhead loading equipment. At present their use seems to be pretty much restricted to maritime cargoes, for which trailers are unsuitable, and the land connections for these cargoes.

Containers overcome many of the line haul disadvantages of trailers. Their main disadvantages over the standard box car is the reduced loading per unit length caused by the reduced height and width, and the aerodynamic losses caused by the increased gaps between the containers on successive cars. The Southern Pacific has suggested a container well car design in which two containers are stacked on top of each other in a well between the wheels of the car. This design increases the weight per unit length of the train.

The great advantage of trailers is that they can be circus loaded when side loading equipment is not available and that a side loader can set them directly on the ground without waiting for a trailer bed to be brought. Circus loading is particularly important in small freight terminals where side loading equipment is not available. The importance of circus loading seems to be decreasing as piggyback traffic increases

and more yards obtain side loading equipment. If it is satisfactory to design equipment not suitable for circus loading, then better solutions for trailers become obvious. A well car in which the wheels are located in wells between the trucks is one solution. Such an arrangement requires the trailers to be loaded facing in opposite directions and the wheels submerged in a well. These conditions pretty well require side loading. It also lowers the center of gravity and decreases the frontal area of the loaded car. Other streamlining suggestions would be fairing pieces to go under and/or between trailers. It seems necessary to add such fairing pieces after trailers have been loaded and the cost of this additional loading operation is likely to prove prohibitive. Changes may restrict the flexibility of a car so that it is only suitable for trailers or containers. This restriction complicates the railway operation, but must be evaluated in individual situations.

5. WIND TUNNEL TESTS

An effective way of investigating the aerodynamic drag of piggyback configurations is by means of wind tunnel tests. Wind tunnel tests have been made on automobile rack cars which are somewhat similar to the piggyback freight configuration and do show high aerodynamic drag (Reference 12), but no TOFC and COFC configurations have previously been tested in wind tunnels. The wind tunnel testing provides a means of testing many configurations at minimum expense. However, data from wind tunnel tests must be scaled to full size and the results suffer from a questionable simulation of the ground plane.

The purpose of the present investigation was to obtain basic information applicable to railroad train aerodynamics and particularly TOFC and COFC configurations. The aerodynamic resistance of the standard configurations and of modified configurations designed to decrease the air resistance was determined.

5.1 GROUND PLANE SIMULATION

A basic difficulty in wind tunnel testing of ground vehicles is simulating the ground plane. The problem is in modeling the motion between the vehicle and the ground plane that exists in the prototype. The four techniques that have been used and were considered are:

1. Moving belt ground plane
2. Image method
3. Ground board
4. Tunnel floor.

The moving belt method is the only one that simulates the motion between the vehicle and the ground and, therefore, appears to be the correct method. There are, however, practical difficulties associated with its use that make results obtained by this method no more reliable than by the other simpler methods. These difficulties are the control of the vertical position of the belt and the inability to support the model from the tunnel floor. Results obtained by this method do not appear to be critically different from those by other methods.

The image method is based on the conclusion from steady inviscid flow theory that the ground plane and the plane of symmetry between a model and its image will both be streamlines. This technique avoids the boundary layer which will exist on any stationary ground plane but does not properly simulate the viscous effects on the real ground plane. Even though the plane of symmetry must be a streamline in steady flow, it may not be so in the unsteady flow between and behind the models which may exist with this test configuration. It also requires twice as many models.

The use of a ground plane or the tunnel wall are very similar techniques. Installing a ground plane which has a leading edge only a short distance ahead of the model provides a thinner boundary layer at the model than would be the case if the test were run using the tunnel wall as the ground plane. Both of these methods are relatively simple.

Studies made comparing the results from the different test methods do not show substantial differences (References 22 and 23). The ground plane method was selected for the present program.

If the ground plane method is used, it is relatively simple to model the roadbed and track. However, it is not clear that this is really an advantage. Most wind tunnel tests of railroad vehicles have not modeled the track. One case in which this was done is in the tests by Lesher (Reference 8). The problem is that the roadbed and track provide added friction over that of a smooth surface. Since the viscous force on the roadbed is in the opposite direction in the wind tunnel and prototype cases, it is a questionable advantage. For these reasons a smooth track was used for locating the non-metric cars.

5.2 MODELS

The selection of the model scale was a compromise between several different considerations. The availability of models was one important criterion in the selection of the scale to be used. Scale model railroad equipment is available in 1/93 scale (HO gauge), 1/48 scale (O gauge) and some in 1/25 scale. Semitrailers are also available in 1/48, 1/43, and

1/25 scale. Unfortunately, the 40 foot trailers are not available in the 1/48 scale and the TTX flatcar is also not available. Containers do not appear to be available as models but they are the simplest to build.

Aerodynamic scaling laws are well understood. Much experience has been gained with wind tunnel testing and the way in which such data can be extrapolated to full scale. As long as the velocities are low enough so that the air is not compressed (velocities well below the speed of sound) then all pressures are proportional to the dynamic pressure ($1/2\ \rho V^2$). If all forces and moments are divided by the dynamic pressure and appropriate areas and lengths, the dimensionless aerodynamic coefficients are obtained. These coefficients are independent of velocity and scale but do depend upon the Reynolds number, $\rho V\ L/\mu$. In a wind tunnel test, it would be desirable to simulate the Reynolds number of the prototype as accurately as possible. Since the model is of reduced linear scale, some compensation can be obtained by increasing the velocity and density of the flow. Some wind tunnels have been built to operate at higher than atmospheric pressure to achieve higher density. Testing in such facilities is considerably more expensive than in unpressurized tunnels and is not warranted in the present program. If the velocity obtained in the wind tunnel is increased over that of the prototype, the Reynolds number simulation can also be improved. The increase in velocity somewhat compensates for the decrease in scale. This approach was used in the present tests. Most of the tests were run at a velocity of 153 mph (246 Km/hr) giving a dynamic pressure of 60 pounds per ft^2 (292 kg/m^2). Some runs were made at lower velocities and dynamic pressures to see if there was any pronounced variation of the aerodynamic coefficients with dynamic pressure.

Considerable experience has been developed with Reynolds number extrapolation methods but such methods are never perfect. Drag on a TOFC and COFC car is principally caused by separation and only secondarily by skin friction. Drag of blunt bodies becomes quite independent of skin friction once the Reynolds number is greater than the critical value which causes the boundary layer to become turbulent before the separation point. Table 1 shows the Reynolds numbers of full size trains and models based on a number of characteristic dimensions. The critical Reynolds

TABLE 1. CHARACTERISTICS OF WIND TUNNEL MODELS

REYNOLDS NUMBER

(Based on velocity of 75 mph (121 Km/hr) for prototype and 150 mph (241 Km/hr) for model and vehicle dimensions indicated.)

Scale	Trailer Width	Car Length	Trailer Length
Prototype	$60.00(10^5)$	$66.00(10^6)$	$30.00(10^6)$
$\frac{1}{43}$	$2.79(10^5)$	$3.09(10^6)$	$1.39(10^6)$

ROUGHNESS

Roughness height for no Re effect on skin friction ($Re_k = 10^2$)
$k \approx 10^{-3}$ in. = .0025 cm

number for a sphere is about $5(10^5)$. It is reasonable to compare the Reynolds number of the sphere with that based on length for the railroad cars or trailers. If this is done, it is seen that the Reynolds number based on length for each of the two model scales is considerably greater than the critical value.

The skin friction along a smooth surface decreases as the Reynolds number increases. On this basis it might be expected that the skin friction on the prototype will be less than on the model. However, if the surface is rough, then the skin friction coefficient becomes independent of Reynolds number. The surface roughness required to cause the skin friction to become independent of Reynolds number is also shown in Table 1. The surface roughness of the prototype would be expected to be greater than this critical roughness and, therefore, it would seem desirable to have the surface roughness of the model also greater than this value. Actually, the surface roughnesses of the models are probably not important since the large scale roughnesses caused by protuberances and gaps between vehicles are responsible for most of the drag and should ensure Reynolds number independence. Based on these considerations, there seemed no need for using models larger than the 1/43 scale.

Since tests were done on a fixed ground plane, the thickness of the boundary layer compared with the height of the model is important. The thickness of the boundary layer as a function of the distance from the leading edge of the ground plane is shown in Figure 10.

The 10 foot diameter GALCIT wind tunnel at California Institute of Technology was selected for these tests. This tunnel is equipped with a 12 foot ground plane. The 1/43 scale was selected as the best compromise. This allowed plastic model kits to be used for the trailers of which many were required. The railroad cars had to be built specially. A drawing of the model train located on the 12 foot ground board is shown in Figure 11. Because of the small frontal area of the model, the extensions of the ground plane beyond the ends of the train were found to be adequate. Wind tunnel blockage ratio was also not a problem with the small models used in this experiment. Even at a 30° yaw angle, the blockage ratio was only 0.06. The aerodynamic coefficients

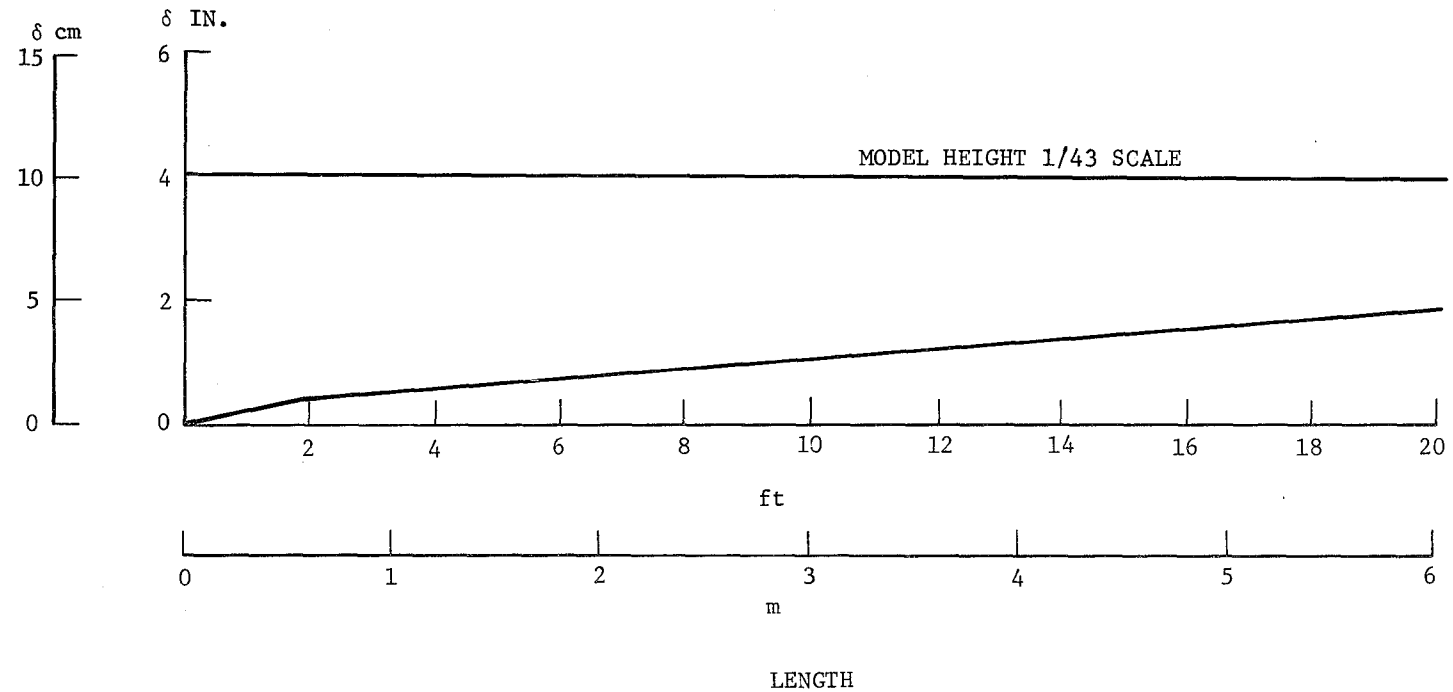

Figure 10. Boundary layer on ground board compared with train height

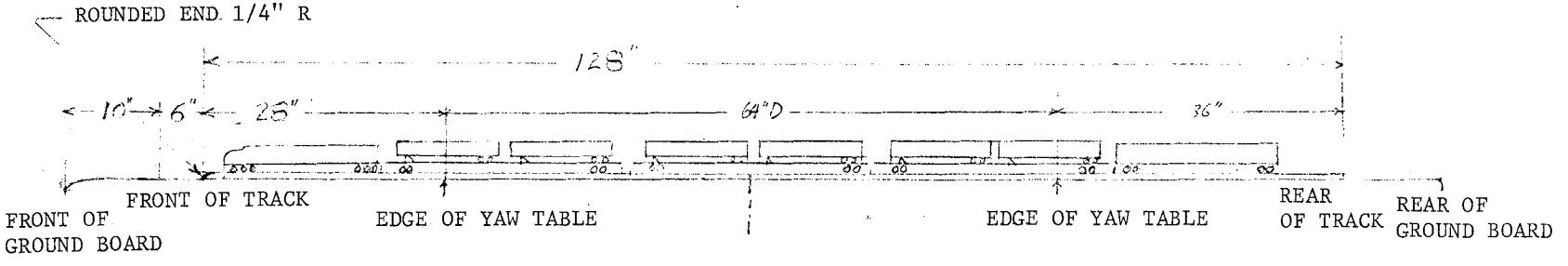

Figure 11a. Model train located in wind tunnel on ground plane.

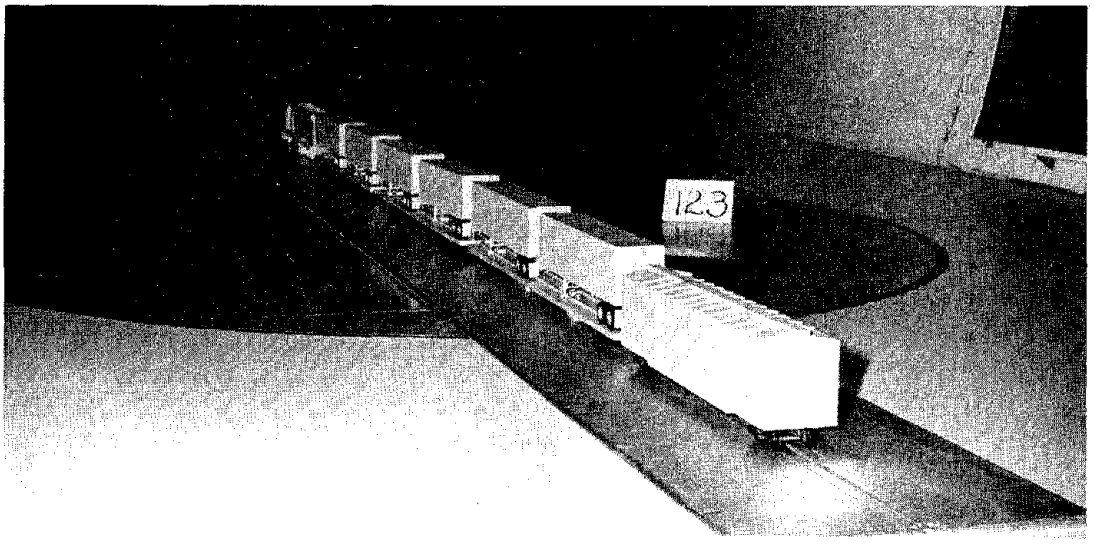

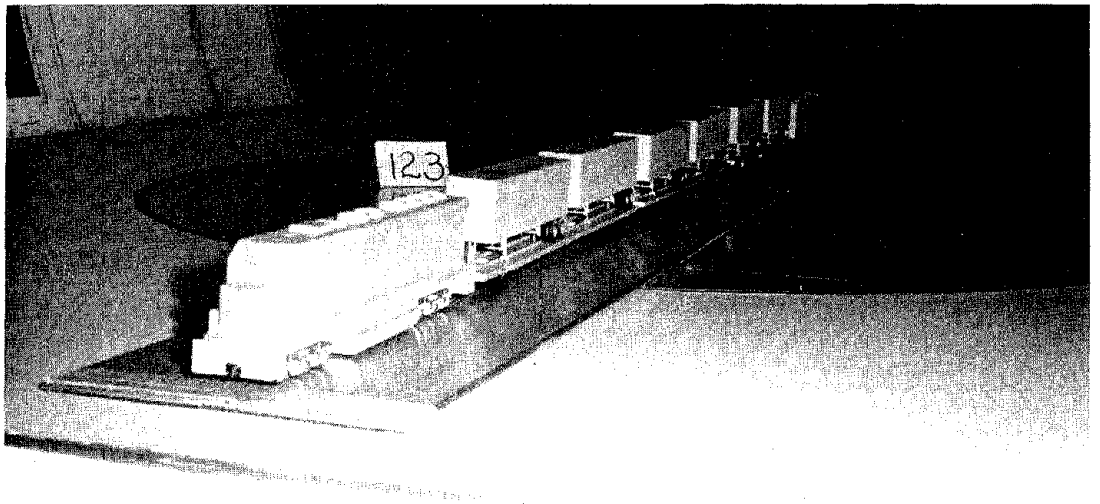

Figure 11b. Model train mounted in wind tunnel

found by this study should be directly applicable to full scale situations at all velocities.

5.3 WIND TUNNEL TEST CONFIGURATIONS

Both basic shape block models and models of railroad car configurations were tested. Only limited information is available on the forces on a series of basic shape blocks lined up behind each other. The object of these tests was to determine the effect of spacing and corner radius on a line of such blocks. Tests were also made of actual models of railroad equipment. These consisted of TTX cars with different loadings of trailers and containers. Modified railroad car, trailer, and container models were also tested in order to assess the effects of various modifications.

The basic block tests used a series of five blocks on which the force on the central block only was measured. The different configurations are listed in Table 2 and are shown in Figures 12 and 13. All of the blocks were the same size, and are 1/43 scale models of 40 foot containers. Blocks of different nose radius, rear radius, and surface roughnesses were provided. A list of the different configurations tested is shown in Table 3.

For the railroad model tests, a train consisting of five cars was used: a locomotive, three flat cars, and a box car. Measurements were made on only the middle flat car. The locomotive and the box car are used as initial and closing cars. The loadings on the three flat cars were varied in order to simulate different conditions. While the conditions to which a car is exposed vary along the length of the train, the restrictions of the size of the wind tunnel prevented the use of a longer train. By locating the metric car between two other similar cars a typical position of a car in a long train was simulated as well as possible. A determination of how conditions would vary along the length of a long train was beyond the capabilities of the present program and wind tunnel tests in general.

The railroad cars, and trailers, used in the tests are shown in Figures 14 through 23 and are listed in Tables 4 and 5. The trailers were

found by this study should be directly applicable to full scale situations at all velocities.

5.3 WIND TUNNEL TEST CONFIGURATIONS

Both basic shape block models and models of railroad car configurations were tested. Only limited information is available on the forces on a series of basic shape blocks lined up behind each other. The object of these tests was to determine the effect of spacing and corner radius on a line of such blocks. Tests were also made of actual models of railroad equipment. These consisted of TTX cars with different loadings of trailers and containers. Modified railroad car, trailer, and container models were also tested in order to assess the effects of various modifications.

The basic block tests used a series of five blocks on which the force on the central block only was measured. The different configurations are listed in Table 2 and are shown in Figures 12 and 13. All of the blocks were the same size, and are 1/43 scale models of 40 foot containers. Blocks of different nose radius, rear radius, and surface roughnesses were provided. A list of the different configurations tested is shown in Table 3.

For the railroad model tests, a train consisting of five cars was used: a locomotive, three flat cars, and a box car. Measurements were made on only the middle flat car. The locomotive and the box car are used as initial and closing cars. The loadings on the three flat cars were varied in order to simulate different conditions. While the conditions to which a car is exposed vary along the length of the train, the restrictions of the size of the wind tunnel prevented the use of a longer train. By locating the metric car between two other similar cars a typical position of a car in a long train was simulated as well as possible. A determination of how conditions would vary along the length of a long train was beyond the capabilities of the present program and wind tunnel tests in general.

The railroad cars, and trailers, used in the tests are shown in Figures 14 through 23 and are listed in Tables 4 and 5. The trailers were

1/43 models of 40 foot highway trailers made from plastic model kits*. Models were made of the TTX flatcar. Three other flatcars were designed and constructed as shown. The streamlined TTX car is very similar to the actual TTX car except that the underbody has been streamlined by covering over all the protruding framework. The trailer well car was designed to provide a lowered space between the trucks for locating the trailer wheels. Such a car reduces the overall height of the trailer and blocks much of the open space underneath the trailer. The container well car was suggested by the Southern Pacific. A well is provided between the trucks and two containers are stacked on top of each other resulting in a total height a little higher than a normal trailer on a flatcar. Streamlined end blocks were also provided for this car to fill the space over the trucks and tests were performed both with and without these blocks. A variety of trailer configurations were also provided. The plastic model kits were available for two configurations, a smooth sided trailer with small corregations running horizontally along the sides and a trailer with side reinforcings consisting of vertical posts. The smooth sided trailer was considered to be the standard configuration but some tests were made using the vertical post trailer. The smooth sided trailer was also modified in several different ways. It was modified to the typical furniture van configuration by dropping the floor level down to the centers of the wheels except for the forward part of the trailer where it connects to the tractor. Another modification was to provide a full skirt extending completely down to the deck of the car covering the hitch mechanism of the TTX car as well as the wheels and underbody of the trailer. A higher trailer was also made by raising the top of the standard trailer by the full scale equivalent of a foot.

The container models were those used in the basic block test series. Only the sharp cornered container models and a modified container model with a nose radius equal to a 1.6 foot full scale radius were used.

*The plastic model kits used were the Fruehauf Reefer (with refrigeration unit removed) and Fruehauf Exterior Post Van made by AMT.

TABLE 2. BASIC BLOCK MODELS

These blocks also used as containers on railroad cars

Corner Shape	Surface
Sharp	Smooth
R = .05 one end top and both sides Sharp one end top and both sides	Smooth
R = .1 one end top and both sides Sharp one end top and both sides	Smooth
R = .2 one end top and both sides Sharp one end top and both sides	Smooth
Sharp	Vertical posts
R = .2 one end top and both sides Sharp one end top and both sides	Vertical posts
R = .2 one end, both sides only Sharp one end, both sides only	Smooth
R = .2 both ends, top and both sides	Smooth

Blocks are 1/43 scale models of 40 ft (12.2 m) long by 8 ft (2.44 m) wide by 8.5 ft (2.6 m) high containers.

Radius (R) expressed in units of block widths.

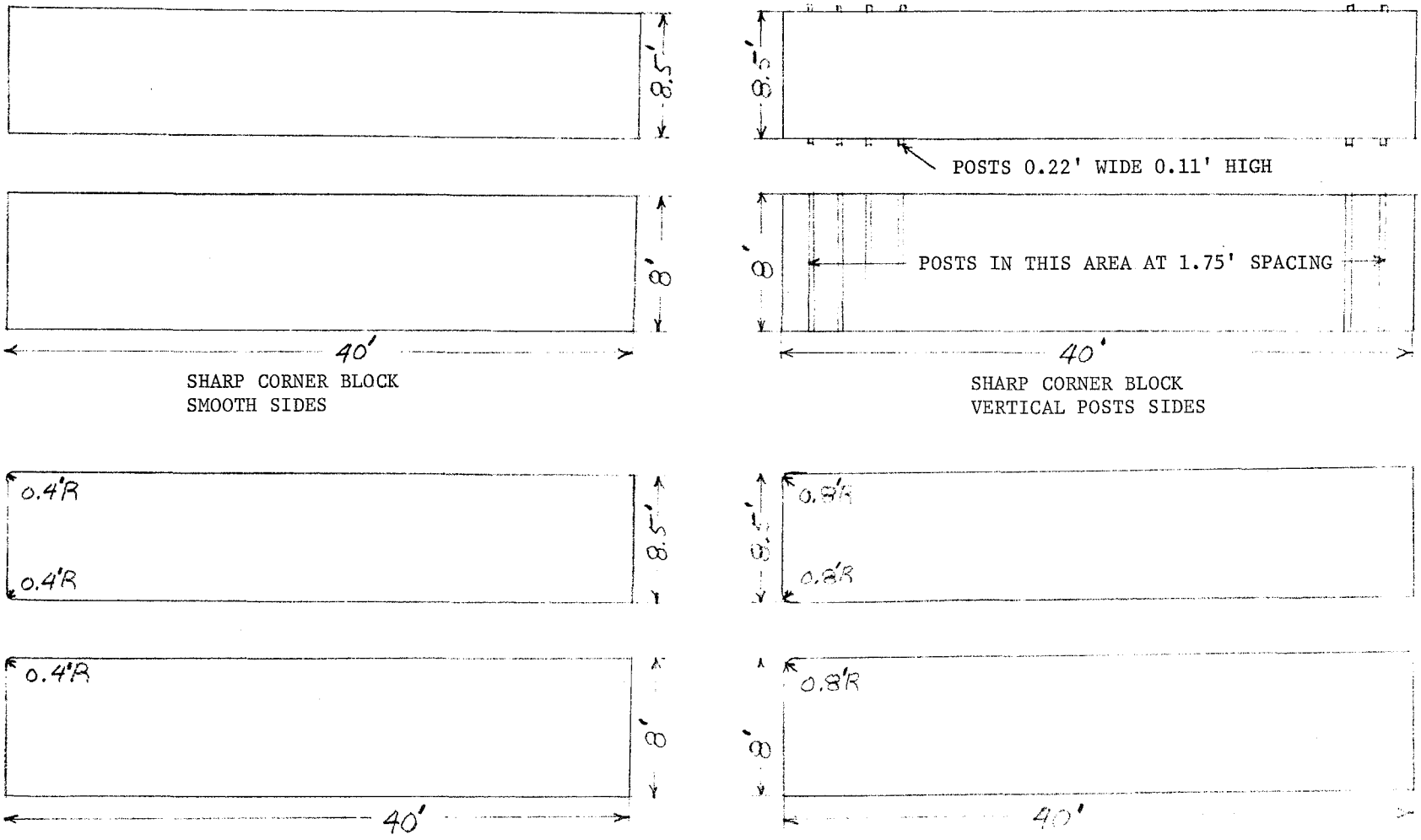

Figure 12. Basic block models - 4 configurations

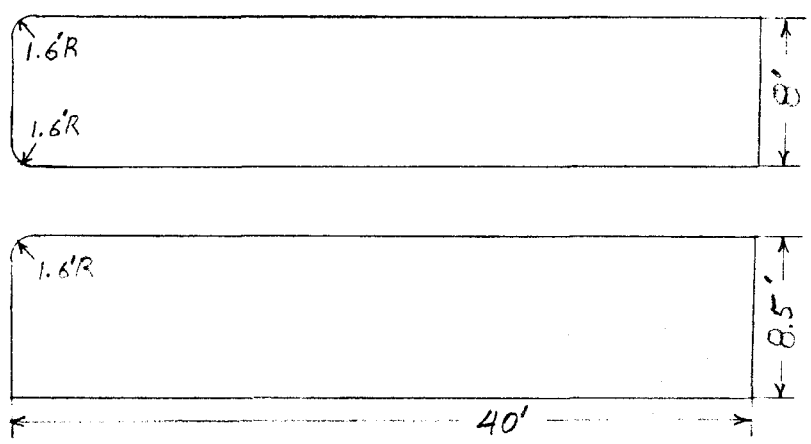

R = 0.2 W FRONT TOP AND SIDES
SMOOTH SIDES

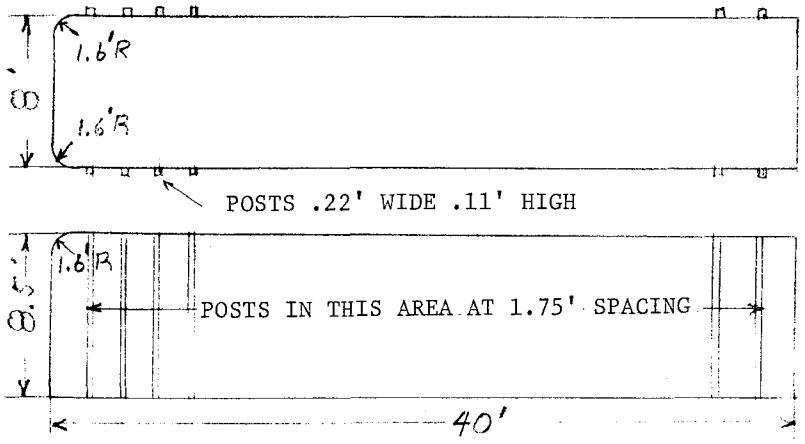

R = 0.2 FRONT TOP AND SIDES
VERTICAL POST SIDES

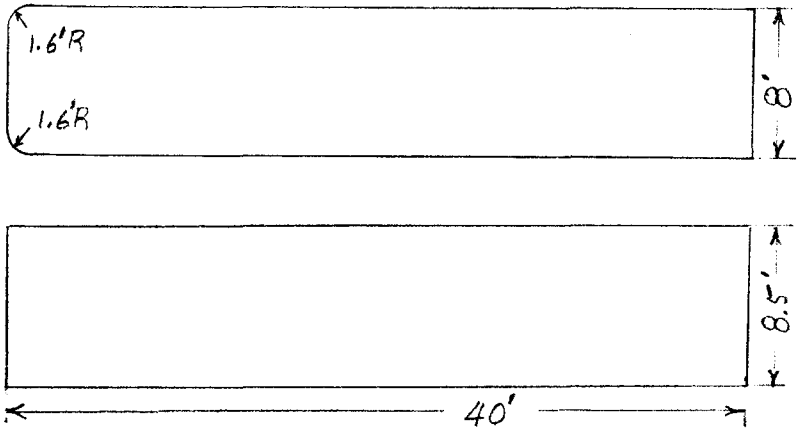

R = 0.2 W FRONT SIDES ONLY
SMOOTH SIDES

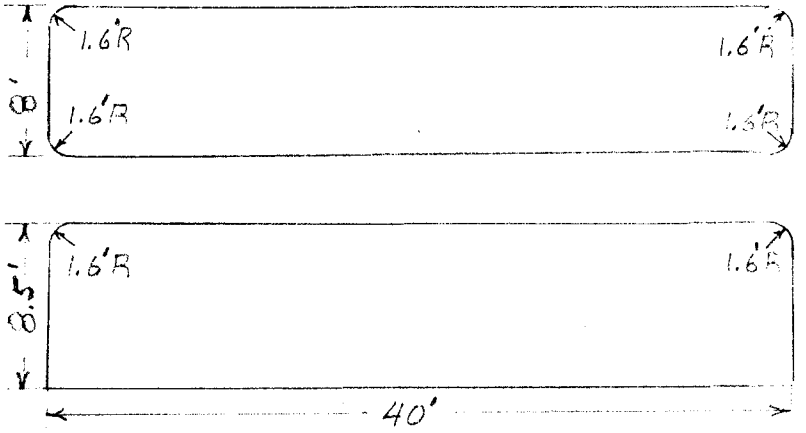

R = 0.2 W BOTH ENDS TOP AND SIDES
SMOOTH SIDES

Figure 13. Basic block models - 4 additional configurations

TRAILER TRAIN

Flush decked flatcar equipped with dual hitches. Rated capacity is 150,000 lbs. All basic dimensional data is shown on general arrangement diagram below. Built by Bethlemem Steel Company.

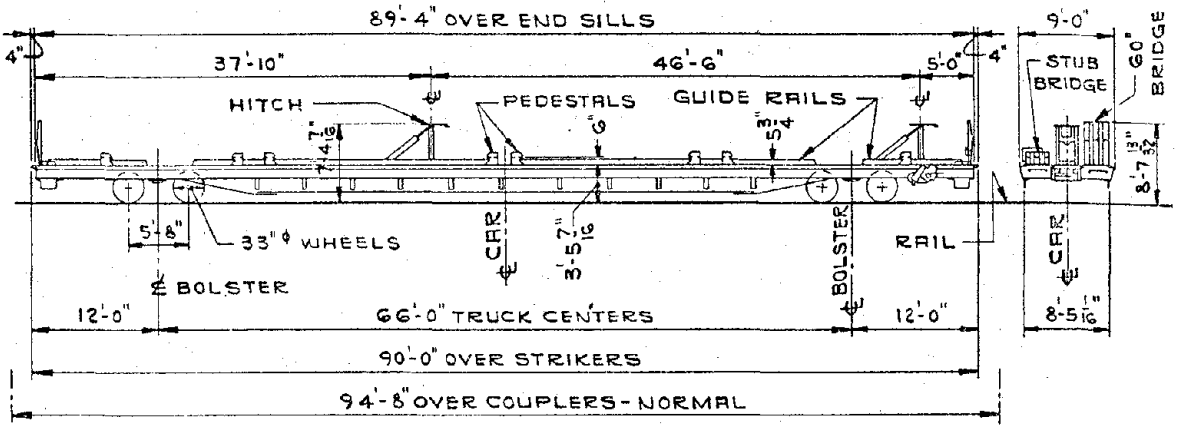

Figure 14a. TTX Car

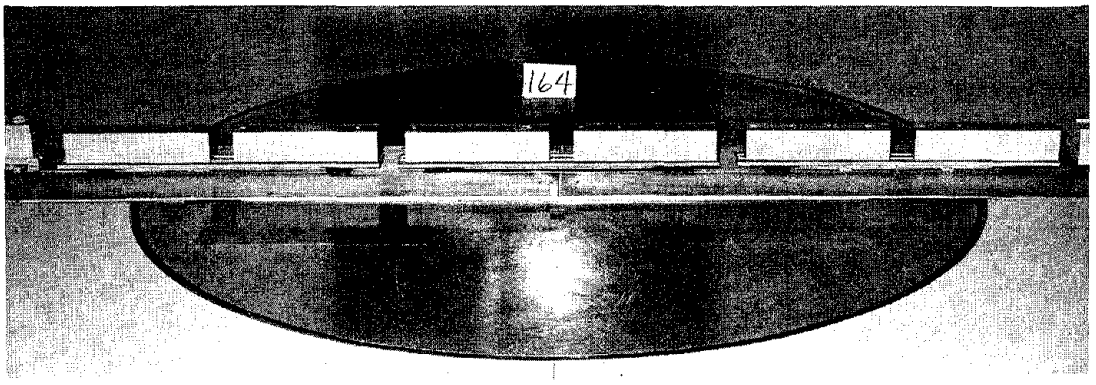

Figure 14b. TTX car with containers in wind tunnel.

TABLE 3. BASIC BLOCK TEST

Tests run over a range of yaw angles between 0 and 30° and gap spacings.

Block Shape Corner Radius	Block Surface	Gaps Between Blocks†
Sharp R = 0	Smooth	.05, .1, .2, .4, 1, 2, 4, 6, ∞
Round front* R = .05	Smooth	0.1, 0.4, 2, 4
Round front R = .1	Smooth	0.1, 0.4, 2, 4
Round front R = .2	Smooth	0.1, 0.4, 2, 4, 6, ∞
Sharp	Vertical posts	0.1, 0.4, 2, 4
Round front R = .2	Vertical posts	0.1, 0.4, 2, 4
Round sides** R = .2	Smooth	0.1, 0.4, 2, 4
Round front R = .2	Smooth	0.1, 0.4, 2, 4
Round rear R = .2	Smooth	0.1, 0.4, 2, 4

*Side and top edge rounded, corner radius (R) expressed in units of block width.

**Side edge rounded but not top.

†Gaps expressed in units of block widths.

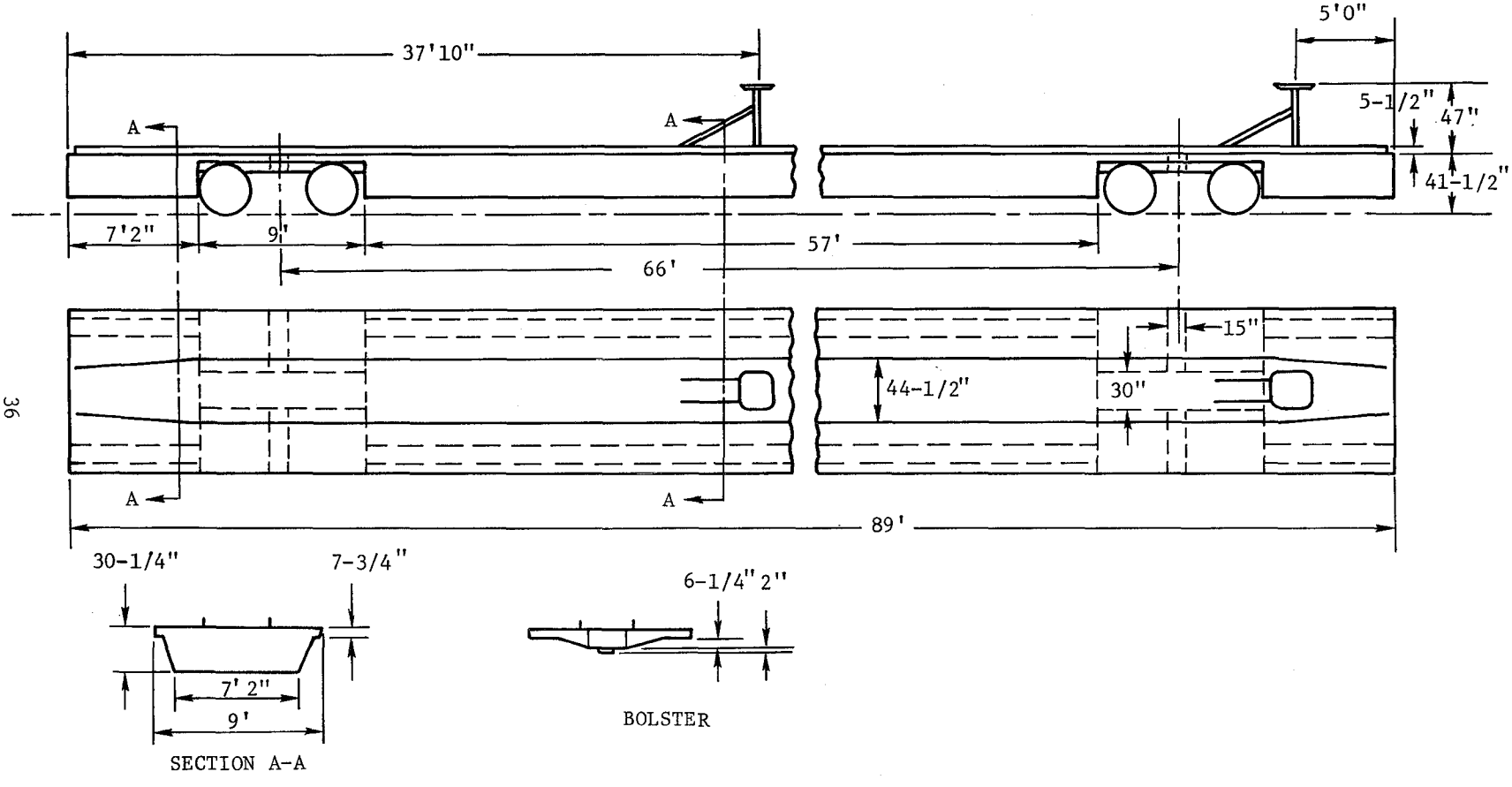

Figure 15a. Aerodynamically streamlined TTX car - TTXA

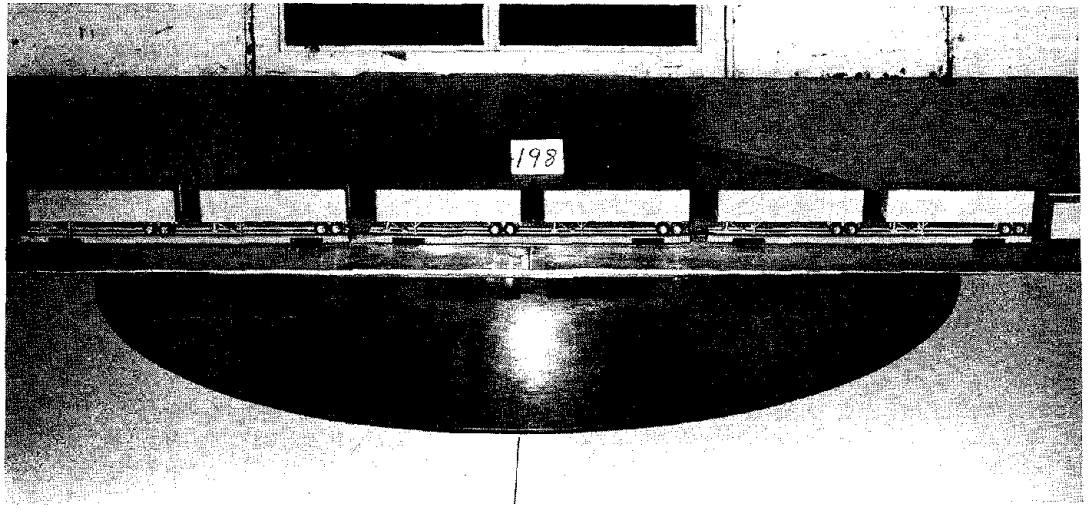

Figure 15b. TTXA car with trailers in wind tunnel

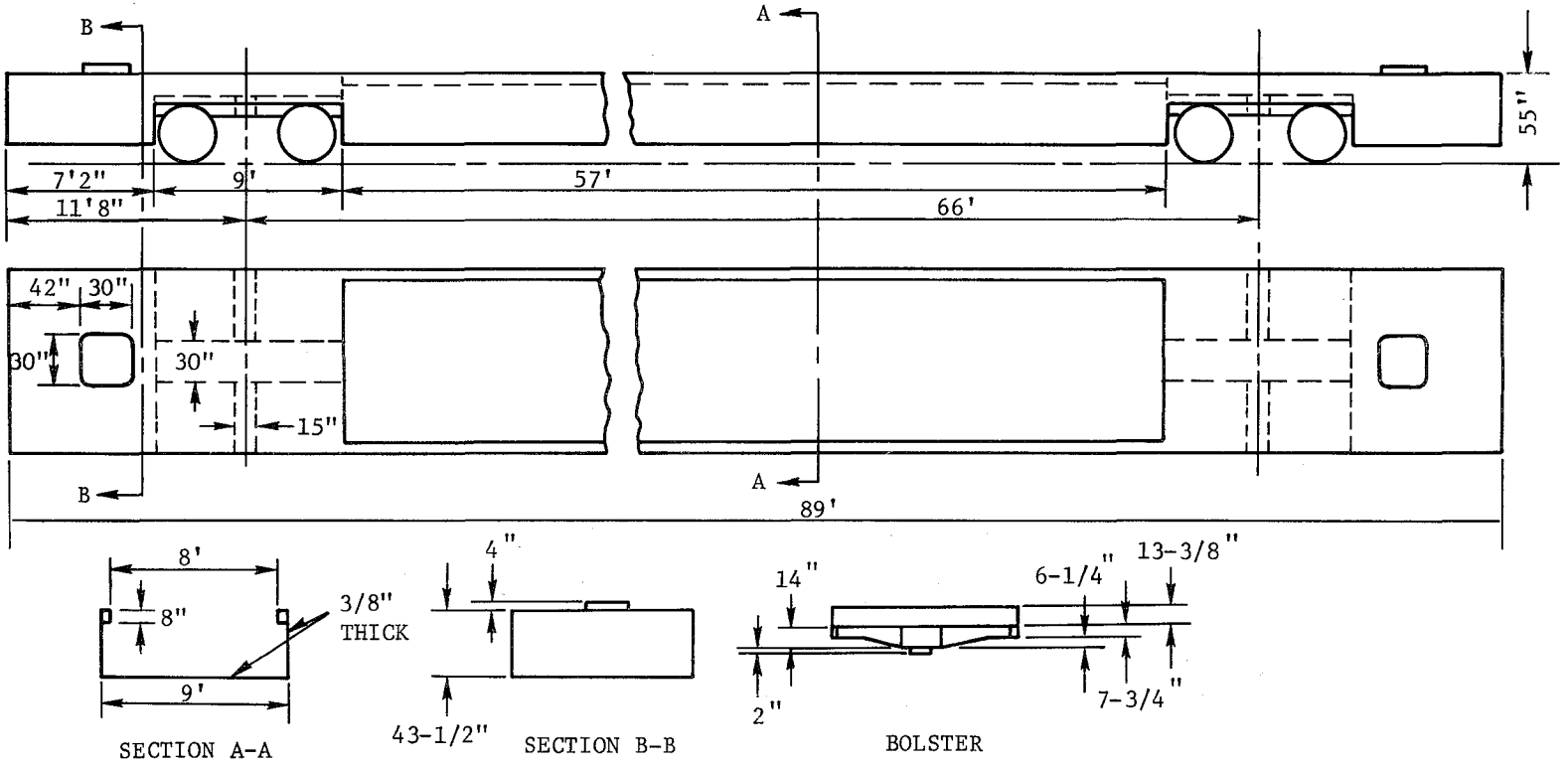

Figure 16a. Trailer well car - TWC

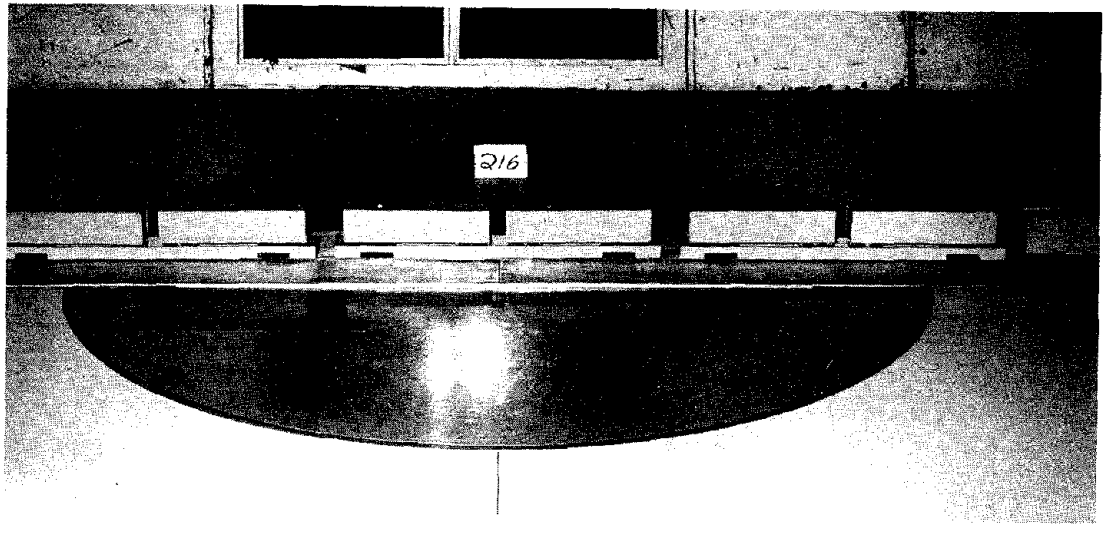

Figure 16b. TWC car with trailers in wind tunnel

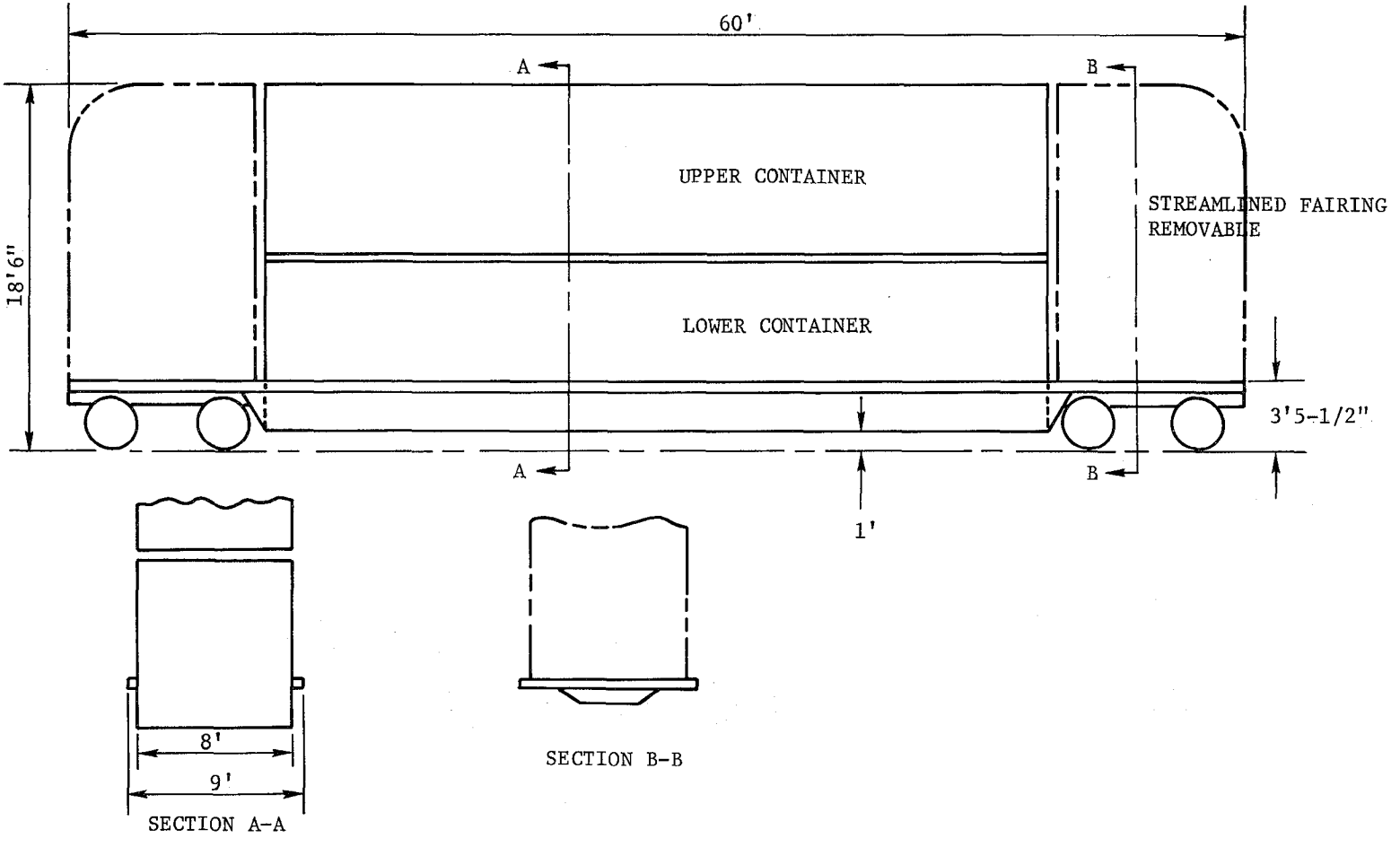

Figure 17a. Container well car - CWC

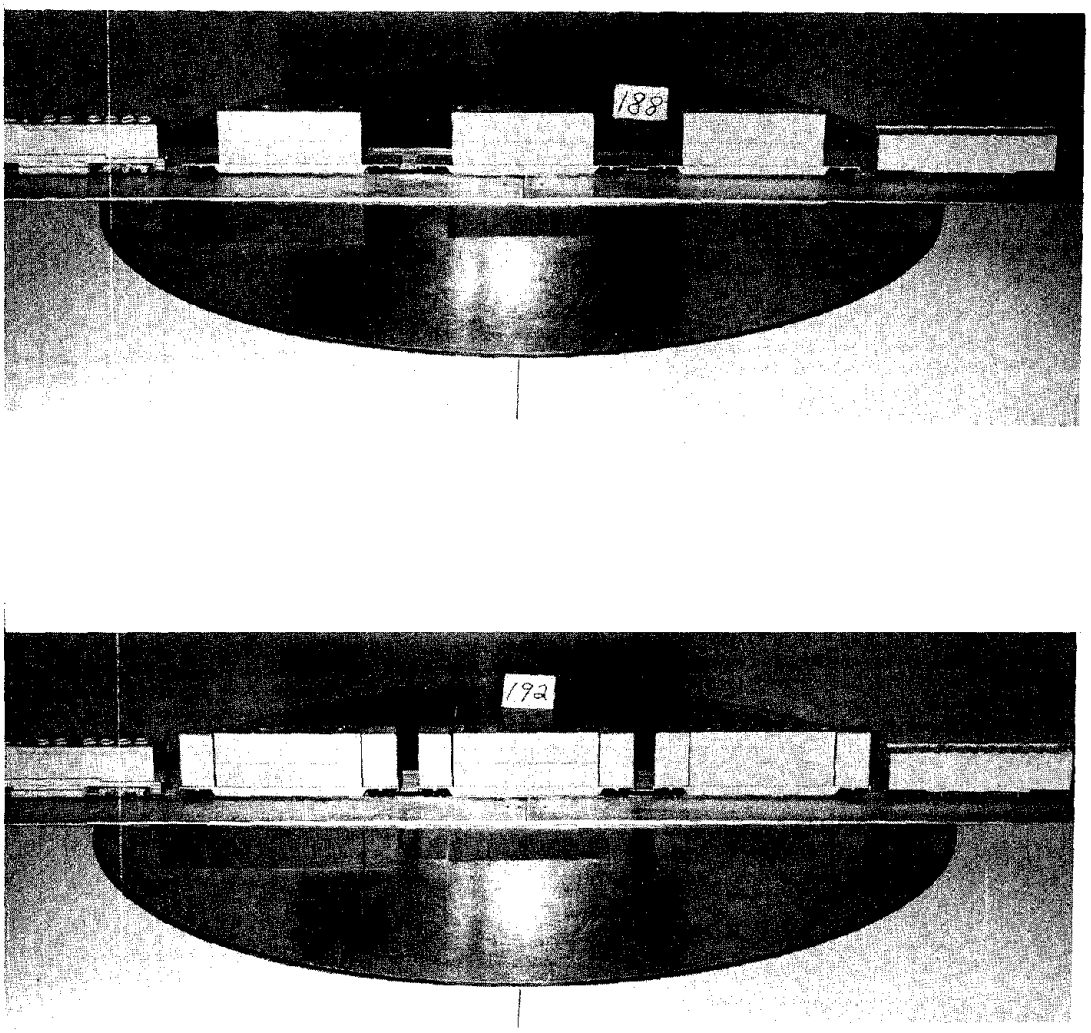

Figure 17b. CWC car with containers in wind tunnel both with and without aerodynamic fairings.

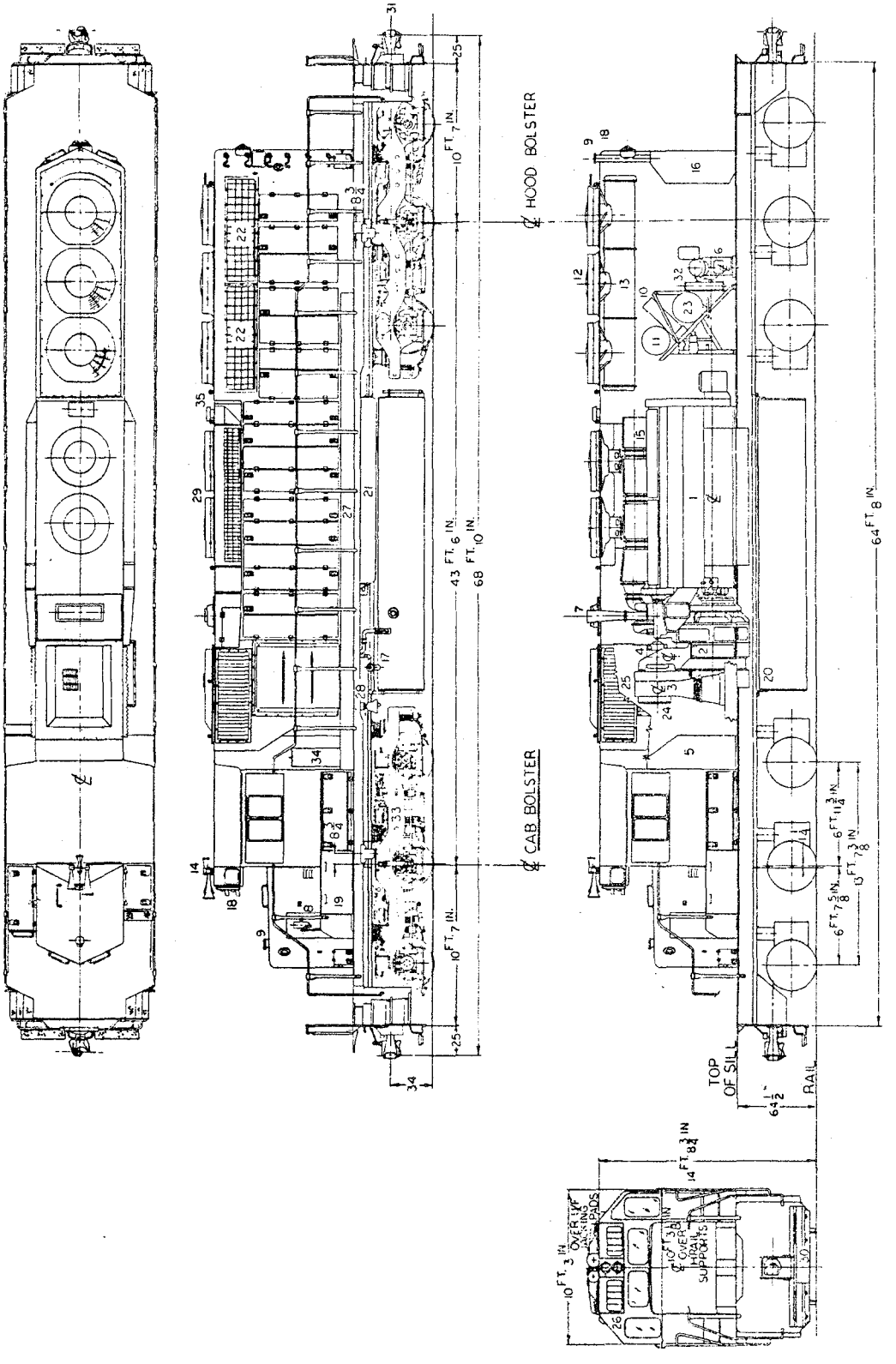

Figure 18. Diesel Electric Locomotives: General Motors SD 45-2.

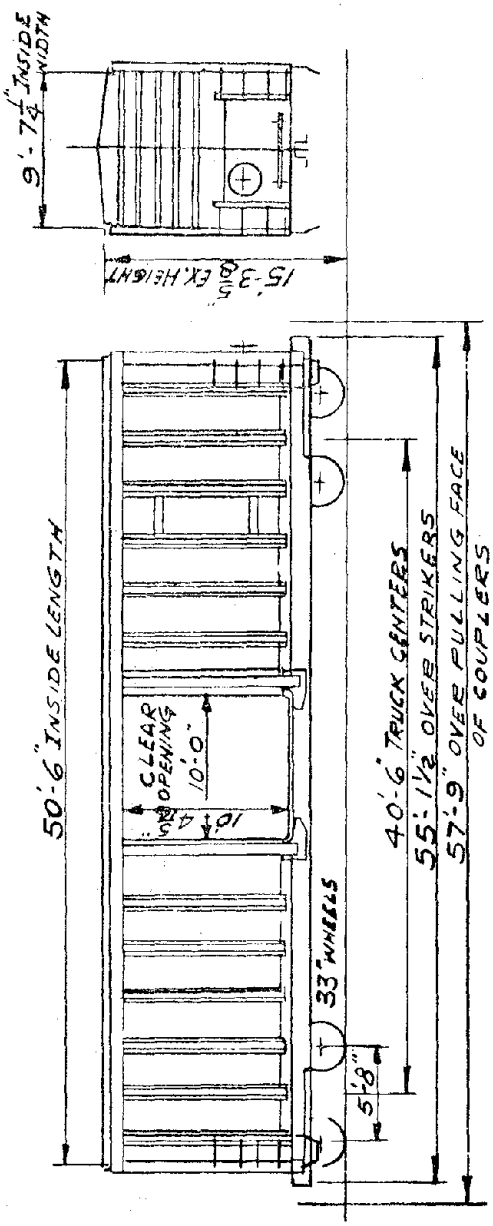

Figure 19. Union Pacific Box car, Class BF 70-10

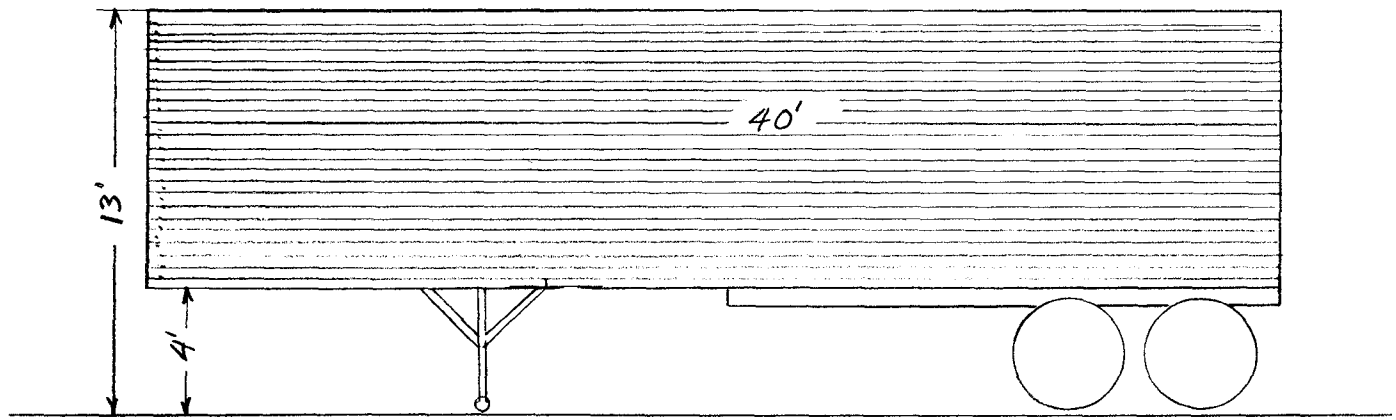

Figure 20a. Smooth sided van - small horizontal corrugations

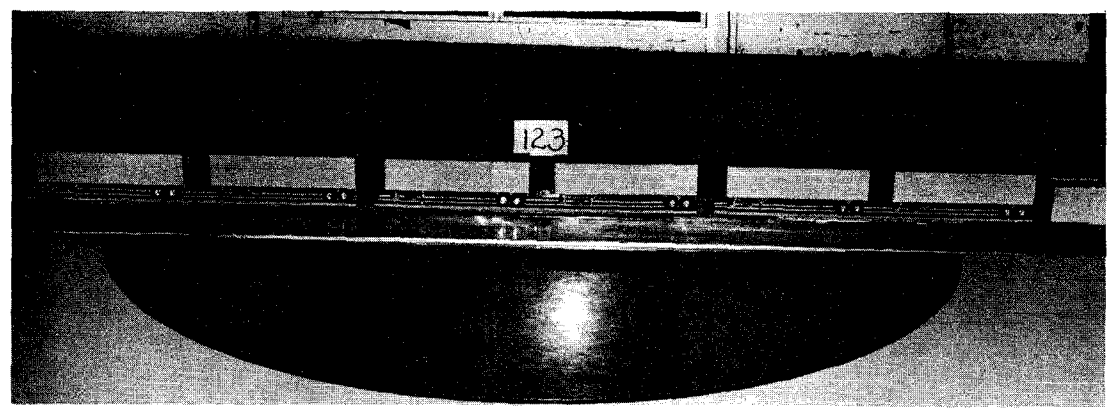

Figure 20b. Smooth sided van on TTX car in wind tunnel

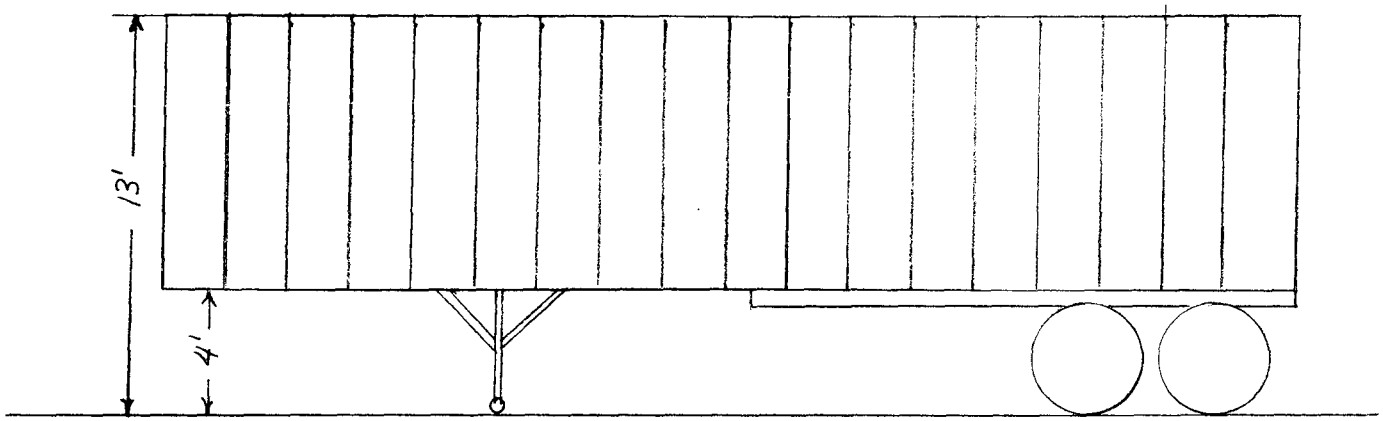

Figure 21a. Vertical post van

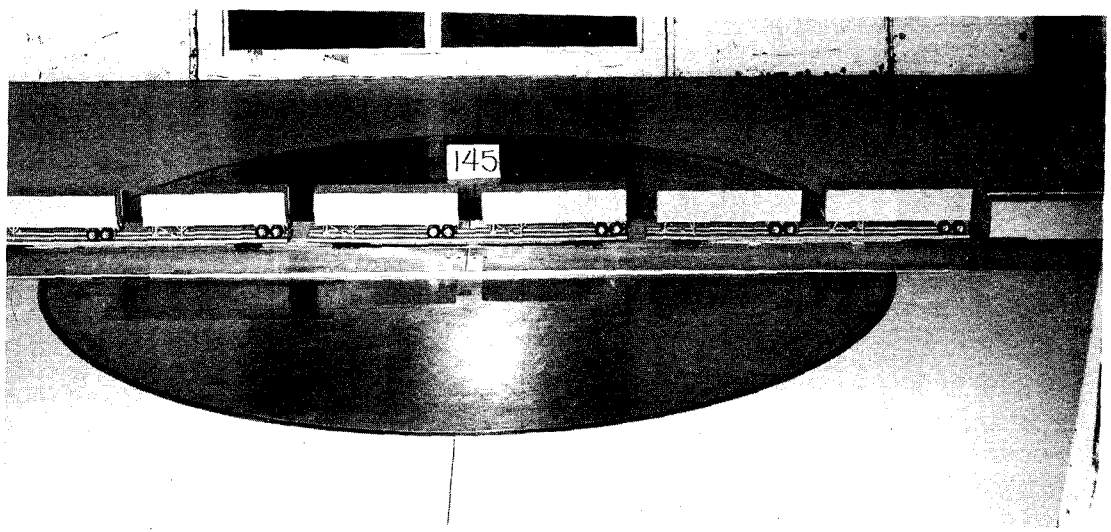

Figure 21b. Vertical post van on TTX car in wind tunnel

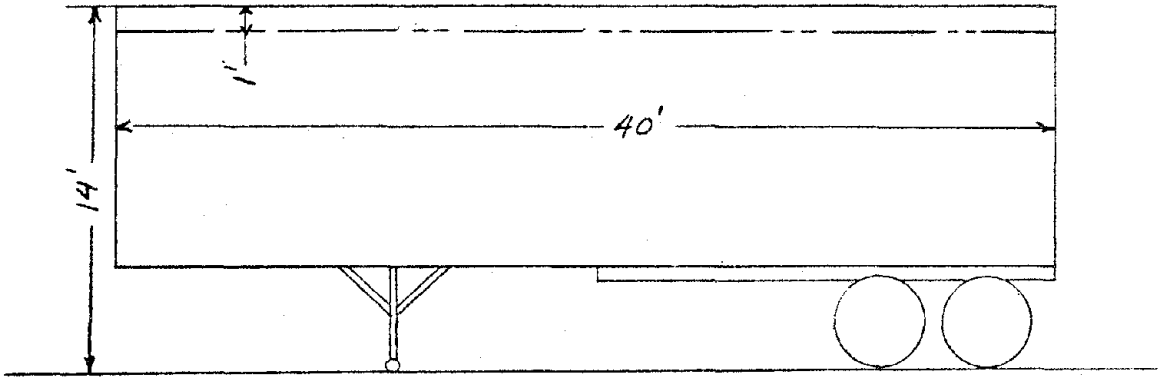

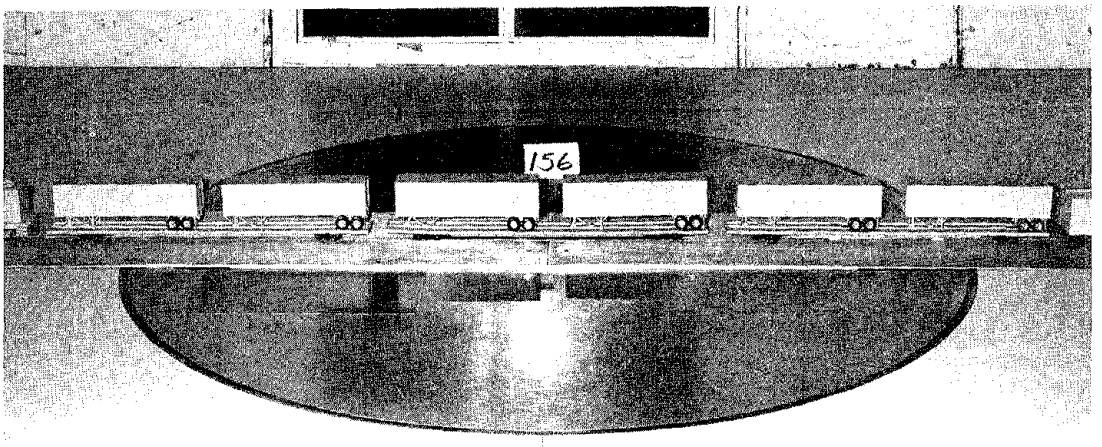

Figure 22a. Fourteen-foot-high trailer

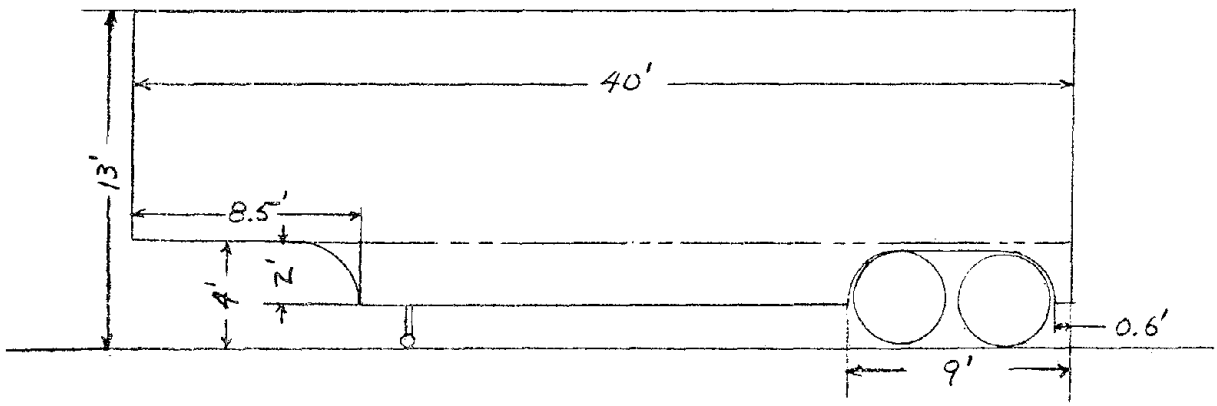

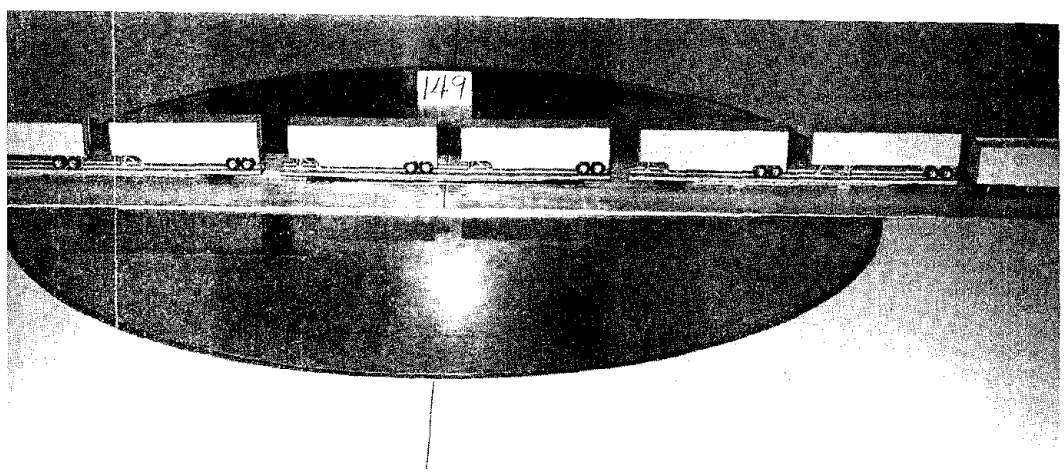

Figure 22b. Moving van

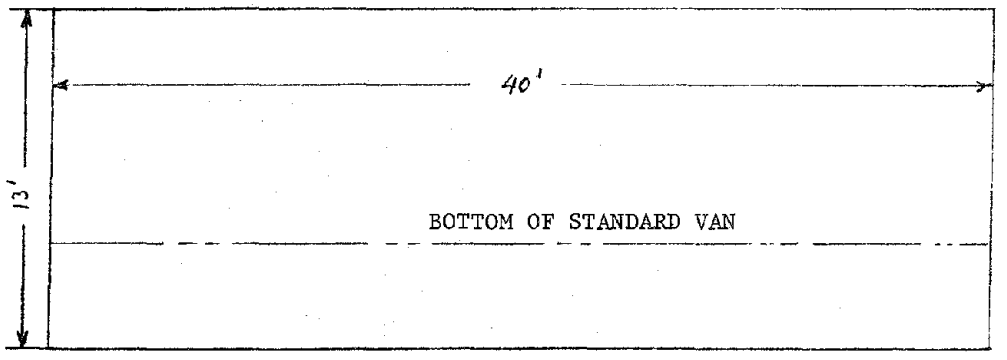

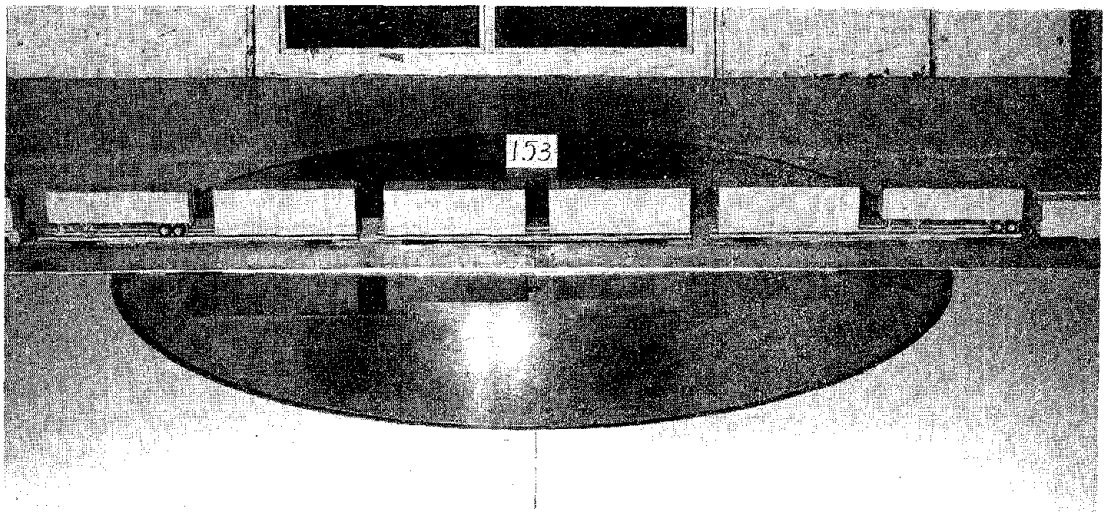

Figure 23. Trailer with full skirt fairing

TABLE 4. MATRIX OF RAILROAD CAR, TRAILER AND CONTAINER TEST CONFIGURATIONS

Railroad Cars	Trailers					Containers	
	Standard	Posts	Moving Van	Full Fairing	High	Standard	Round Corner
TTX	x	x	x	x	x	x	x
TTX close coupling	x						
TTX with bridge plates	x						
TTX faired underbody	x					x	
Trailer well car	x						
Container well car						x	x
Container well car with streamlined fairings						x	

TABLE 5. RAILROAD CAR TESTS

Tests at yaw angles between 0 and 30°. Train consists of locomotive, 3 flat cars (of which the center car is metric), and a box car.

Configuration Number	Flat Car Model	Flat Car Loading		
		1	2	3
STANDARD CONFIGURATIONS				
1	TTX	2 TS	2 TS	2 TS
2	TTX	E	2 TS	2 TS
3	TTX	2 TS	2 TS	E
4	TTX	2 TS	E	2 TS
5	TTX	E	2 TS	E
6	TTX	E	E	E
7	TTX	2 TS	1 TS F	2 TS
8	TTX	2 TS	1 TS R	2 TS
9	TTX	1 TS F	1 TS F	2 TS
10	TTX	1 TS F	1 TS R	2 TS
11	TTX	2 TS	1 TS F	1 TS R
12	TTX	2 TS	1 TS R	1 TS R
13	TTX	2 CS	2 CS	2 CS
14	TTX	E	2 CS	2 CS
15	TTX	2 CS	2 CS	E
16	TTX	2 CS	E	2 CS
17	TTX	E	2 CS	E
18	TTX	2 CS	1 CS F	2 CS
19	TTX	2 CS	1 CS R	2 CS
20	TTX	1 CS F	1 CS F	2 CS
21	TTX	1 CS F	1 CS R	2 CS
22	TTX	2 CS	1 CS F	1 CS R
23	TTX	2 CS	1 CS R	1 CS R

TABLE 5. RAILROAD CAR TESTS
(Continued)

Configuration Number	Flat Car Model	Flat Car Loading		
		1	2	3
STANDARD CONFIGURATIONS (Continued)				
24	TTX	1 TS F 1 Tr R	2 Tr	2 TS
25	TTX	1 TS F 1 Tr R	1 Tr F	2 TS
26	TTX	1 TS F 1 Tr R	1 Tr R	2 TS
27	TTX	2 TS	2 Tr	2 TS
28	TTX	E	EW	E
29	TTX close coupled 1	2 TS	2 TS	2 TS
30	TTX close coupled 2	2 TS	2 TS	2 TS
31	TTX	2 TS Rr	2 TS Rr	2 TS Rr
32	TTX	E	2 TS Rr	2 TS Rr
33	TTX	E	2 TS Rr	E
34	TTX	2 TS	2 TS Rr	E
35	TTX	2 TS	2 TS Rr	2 TS
36	TTXR	E	2 TS	2 TS
37	TTXR	2 TS	2 TS	2 TS
MODIFIED CONFIGURATIONS				
38	TWC	E	E	E
39	TWC	2 TS	E	E
40	TWC	E	2 TS	E
41	TWC	2 TS	2 TS	E

TABLE 5. RAILROAD CAR TESTS
(Continued)

Configuration Number	Flat Car Model	Flat Car Loading		
		1	2	3
MODIFIED CONFIGURATIONS (Continued)				
42	TWC	2 TS	2 TS	2 TS
43	TWC	2 TS	1 TS F	2 TS
44	TWC	2 TS	1 TS R	2 TS
45	TWC	1 TS F	1 TS R	2 TS
46	TWC	1 TS F	2 TS	2 TS
47	CWC	E	E	E
48	CWC	2 CS	E	E
49	CWC	2 CS	2 CS	E
50	CWC	2 CS	2 CS	2CS
51	CWC	2 CS	1 CS	2 CS
52	CWC	1 CS	1 CS	1 CS
53	CWC	1 CS	2 CS	1 CS
54	CWCA	E	E	E
55	CWCA	2 CS	2 CS	2 CS
56	TTXA	E	E	E
57	TTXA	2 TS	2 TS	2 TS
58	TTXA	2 CS	2 CS	2 CS
59	TTX	1 TS F 1 TM R	2 TM	1 TM F 1 TS R
60	TTX	E	2 TM	E
61	TTX	E	1 TM F	E
62	TTX	1 TS F 1 TSA R	2 TSA	1 TSA F 1 TS R
63	TTX	E	2 TSA	E
64	TTX	E	1 TWA F	E

TABLE 5. RAILROAD CAR TESTS
(Continued)

Configuration Number	Flat Car Model	Flat Car Loading		
		1	2	3
MODIFIED CONFIGURATIONS (Continued)				
65	TTX	2 TS	2 TH	2 TS
66	TTX	1 TS F 1 TH R	2 TS	1 TH F 1 TS R
67	TTX	2 CSA	2 CSA	2 CSA
68	TTX	E	2 CSA	E
69	TTX	2 CSA	1 CSA R	2 CSA
70	CWC	2 CSA	2 CSA	2 CSA
71	CWC	E	2 CSA	E
72	CWC	E	1 CSA	E

KEY:

Flat Cars

TTX	Standard without bridge plate
TTXR	Standard with bridge plate
TTXA	TTX aero fairing
TWC	Trailer well car
CWC	Container well car
CWCA	CWC with aero fairing

Coupling Distance

Normal	60"
Close Coupled 1	30"
Close Coupled 2	15"

Trailers

TS	AMT* refrigerator van
Tr	AMT* exterior post van
TM	TS modified to moving van
TSA	TS with full aero fairing
TH	TS with height increase to 14 ft.

Containers

CS	Smooth container with sharp edge
CSA	Smooth container with front edge rounded to r = .1 (width)

Location On Railroad Car

F	Front
R	Rear

Other

E	Empty
W	Wheel trucks removed
Rr	Rearward facing

*Plastic model kit manufactured by AMT, Troy, Michigan.

Model Support and Balance

The California Institute of Technology GALCIT wind tunnel has an 12 foot ground plane, a 5 foot diameter yaw table, and a six component strain gauge balance mounted in the yaw table. For this experiment the models were quite long and narrow. Because of the small cross sectional area, blockage was not a problem even when yawed and no corrections had to be made to the data for blockage. Since the models used in this experiment were longer than the yaw table, a 10 foot long auxiliary mounting plate or track was provided and bolted to the yaw table. This overhung the ground plane but turned with the yaw table and allowed the entire model system to be moved with the yaw table. The metric car could not be mounted directly through the center of the yaw table so a cutout had to be made in the track and a balance plate provided that supported the metric car and bridged the distance between the points that could be connected to the balance. This mechanism is shown in Figure 24. The metric car had to be mounted on the balance plate without touching the track. An electric conductivity system was designed to indicate if contact occurred. This was found extremely useful in monitoring the performance during the tests. The other cars were fastened down to the track at the proper spacing. The same system was used in mounting the blocks. The balance plate had to be surpressed slightly below the track so that it would not touch the other blocks since they overhung the balance plate when the gap spacing between the blocks was small. The metric block was raised somewhat above the balance plate by an appropriate shim so that it was clear of the track and this clearance was monitored during the tests by the use of the electric contact system.

Forces and moments were measured using a six component balance. Forces are expressed in a set of axes fixed with the train. Drag is the force along the train, lift is the vertical force, and side force is the horizontal force at right angles to the train. This convention is somewhat different than the one used for aircraft but is felt to be more convenient in this case. For the basic block tests all coefficients are based on the frontal area of the block. The railroad car results are all expressed as force areas so no reference area need be specified. Pictures of tufts were also taken during the tests of the blocks to provide flow visualization. Tufts were mounted on the sides, tops and ends of the blocks as well as along the track beside the blocks and in between the blocks.

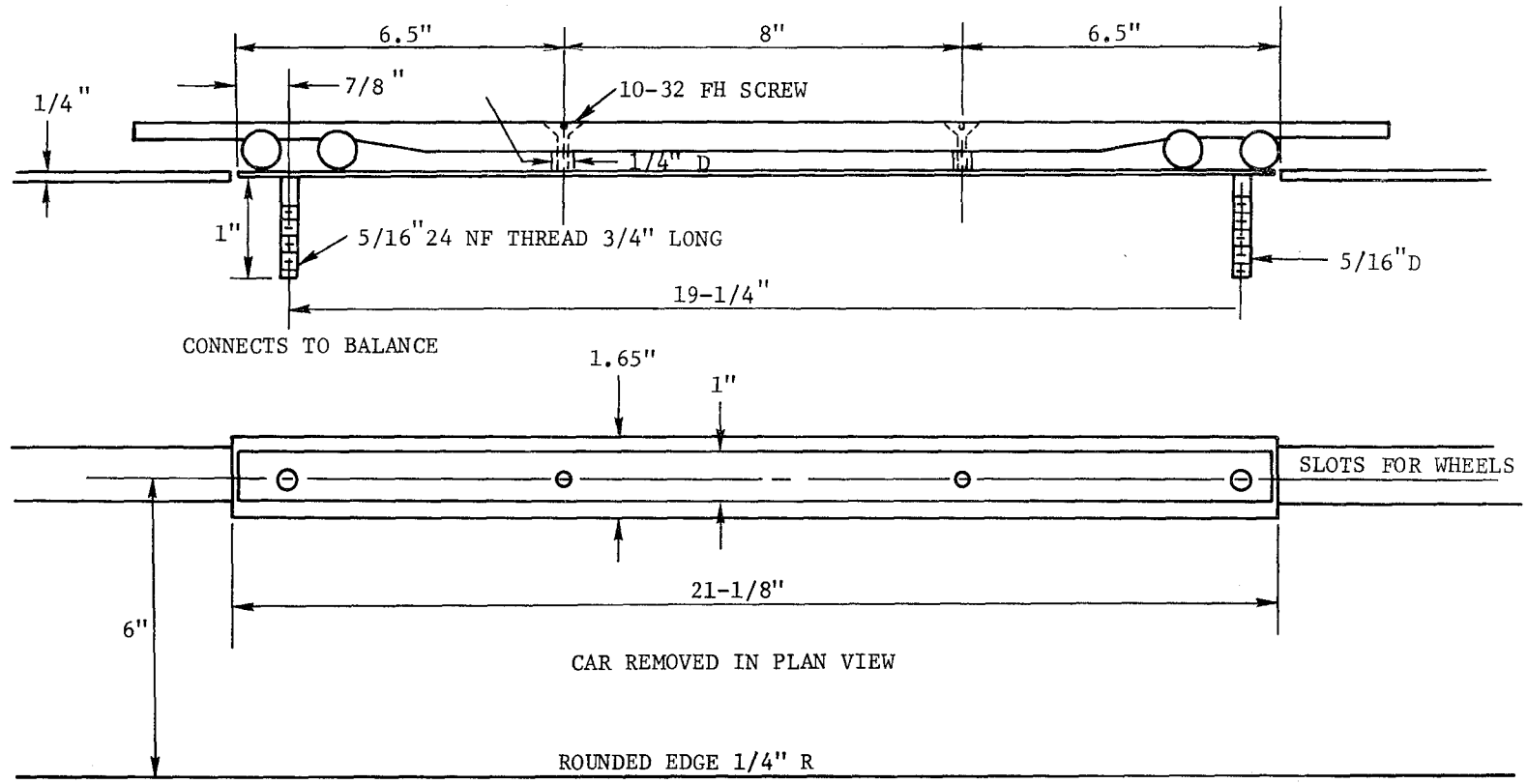

Figure 24. Balance mechanism for mounting models in wind tunnel.

6. WIND TUNNEL TEST RESULTS

6.1 BASIC BLOCK TESTS

A series of measurements were made on a set of blocks whose basic dimensions were scaled from those of containers. A line of five blocks was used and all measurements were made on the center block. The parameters that were varied were the gap spacing between blocks, corner radius, angle of yaw, and surface roughness. In addition to six component force and moment measurements on the center block, photographs were taken of the blocks with a series of tufts attached. These tests were run to obtain some basic information on the effects of gaps, corner radius, and roughness. Initial tests were made over a range of dynamic pressures. Typical results are shown in Figure 25. There appeared to be no trends with changes in dynamic pressure and Reynolds number. To understand the test configurations that are discussed in the subsequent sections, references to Tables 2 and 3 and Figure 12 may be useful.

6.1.1 Drag

Figures 26 through 29 show the drag coefficient as a function of yaw angle for different gap spacings. Figure 26 shows the conditions for blocks with sharp corners. There was very little effect as the gap spacing was increased up to a value of about 0.4. All gap spacings and corner radii are expressed as a multiple of block width. For these small gaps there was also almost no effect of angle of yaw. One must conclude that this central block in the series of five blocks was acting almost like a section of a continuous block and that there was very little flow through or effect of the gaps. At larger gaps, between 1 and 6, the drag increases with gap size and also with yaw angle. A single block was also tested. The results for this case are shown with the designation of infinite gap spacing. The drag at a gap spacing of six was rather close to that at infinity for $\phi = 30°$ but considerably less at lower angles of yaw. This is logical since the effects of the preceding blocks are reduced by increasing yaw. As the radius of the vertical and top horizontal corners on the front face was increased from zero to 0.05 and 0.1 (Figures 27 and 28), the same pattern continued. However, at a corner radius of 0.2, quite a different situation occurred (Figure 29). The effect of angle of yaw was small for all spacing except infinite. The data seems to break into three distinct bands, gaps of 0.1 and 0.4, 2 through 6, and infinity. At low angles of yaw the drag increased continuously with gap size.

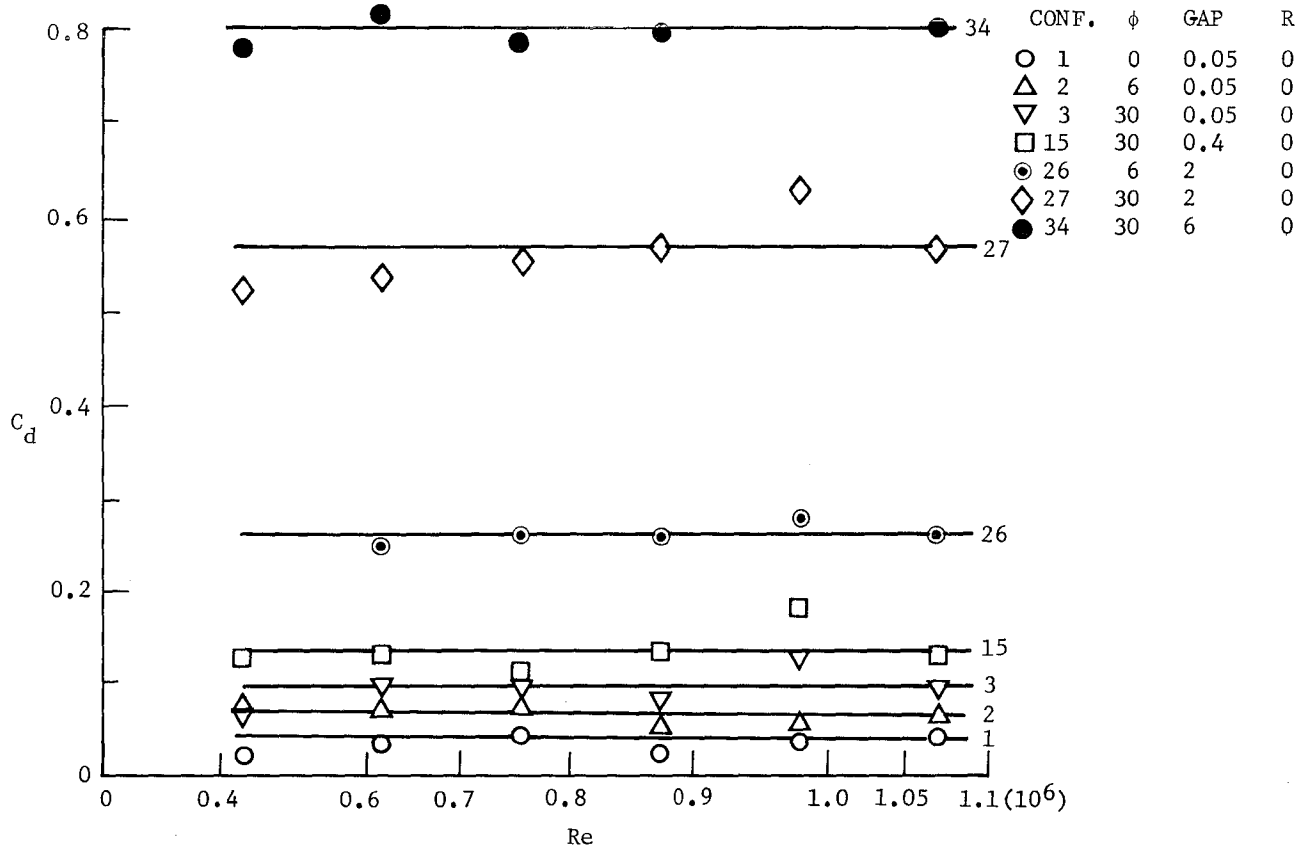

Figure 25. Drag coefficient of sharp cornered basic blocks as a function of Reynolds number for different gap spacings and yaw angles. Reynolds number based on block length.

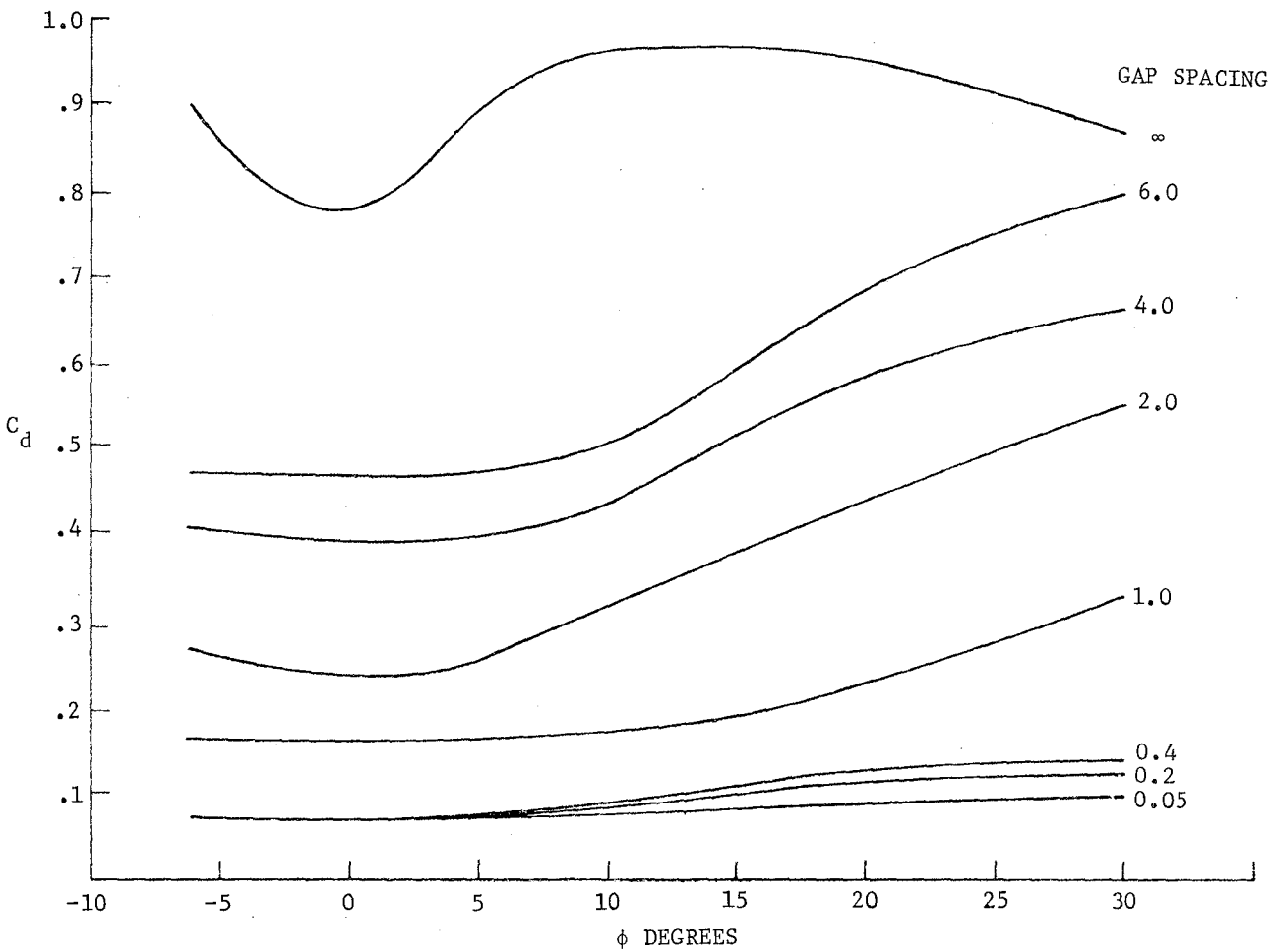

Figure 26. Drag coefficient of sharp cornered basic blocks as a function of angle of yaw for different gap spacings. Re = 10^6

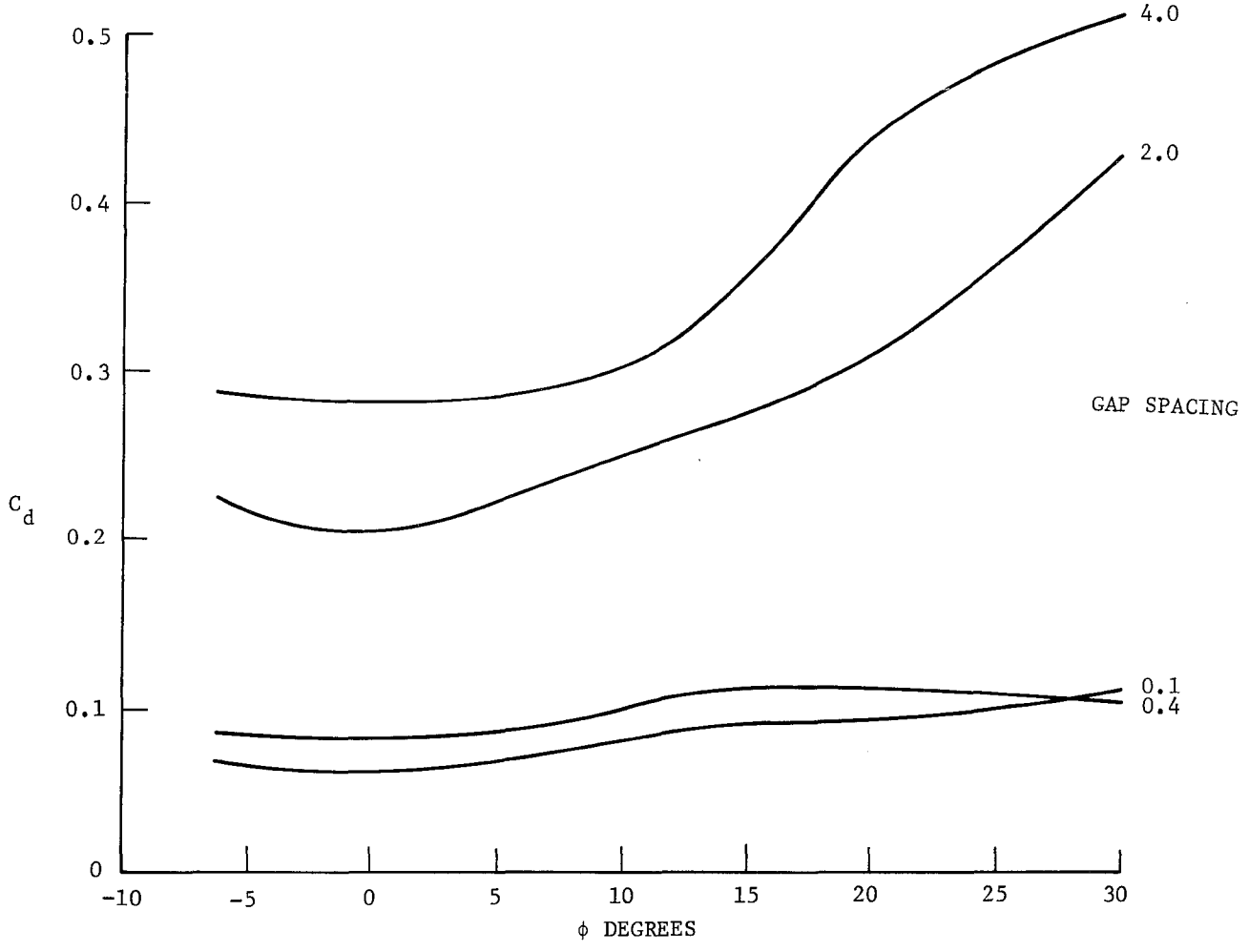

Figure 27. Drag coefficient of basic blocks with 0.05 corner radius as a function of yaw angle for different gap spacings. Re = 10^6

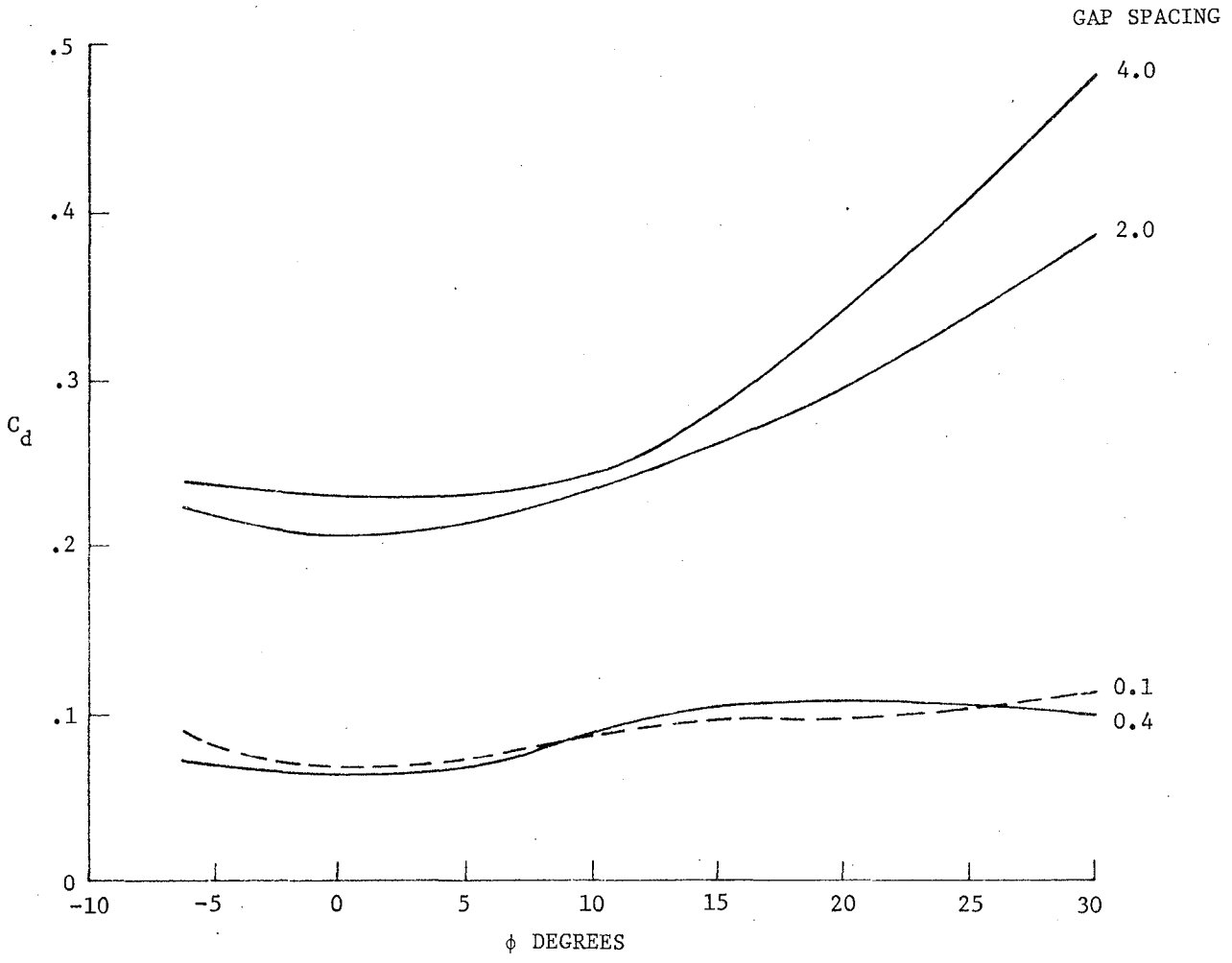

Figure 28. Drag coefficient of basic blocks with 0.1 corner radius as a function of angle of yaw for different gap spacings. Re = 10^6

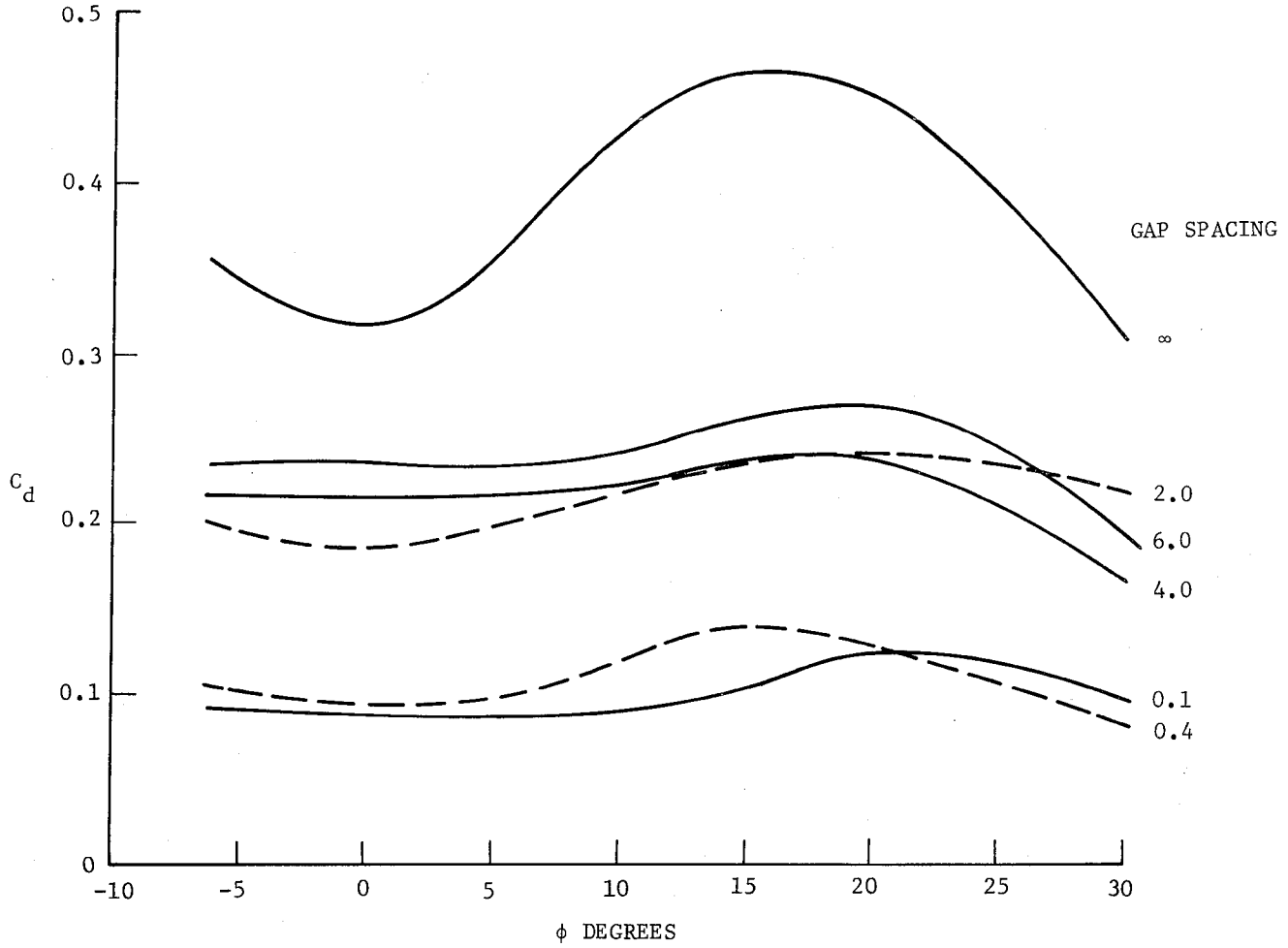

Figure 29. Drag coefficient of basic blocks with 0.2 corner radius as a function of yaw angle of different gap spacings. Re = 10^6

However, at larger yaw angles, particularly 30°, the curves crossed and there appeared to be no logical variation with gap size. It was unfortunate that the gap spacing of 1 was not tested. The steps in gap size from 0.1 to 0.4 to 2 were about a factor of 4; while from 2 to 4 and 6 were only 2 and 1.5. This was probably partly responsible for the apparent split between the two lower bands.

The effect of gap size may be better understood by reference to Figures 30 and 31. In these two figures, drag coefficient is plotted against gap size. The gap size is shown on a log scale so that equal distances represent an equal factorial change in gap size. Curves are plotted for different angles of yaw. An important change in the effect of gap size for the sharp corner blocks occurred at a gap size of about 0.5, Figure 30. The drag coefficient for a gap size of infinity to which these curves should be asymptotic is shown on the right hand side of the figure. The same plot for a corner radius of 0.2 is shown in Figure 31. The trend in the data is not nearly as clean for this corner radius. Since the effect of yaw angle is considerably reduced at this radius, the curves lie on top of each other and scatter, confusing the plot. For both radii, the drag at 30° angle of yaw is the largest at small gaps and is less than that for 5° and 12° at an infinite gap. This requires that there be some crossing of the curves.

Another way of looking at this same data is shown in Figures 32 and 33. Here the drag coefficient is plotted against the corner radius for various gap spacings. Figure 32 is for a yaw angle of 0°. The effect of corner radius on drag is similar to that shown in Reference 17 for single bodies but no direct comparison is possible. Since there were tests at only two radii in the present series at infinite spacing, the shape of this curve cannot be determined. However, at the smaller gap spacings, the shapes of the curves are determined and the infinite spacing case has been drawn to be consistent with the others. These test results show that there is a drag reduction caused by even a small radius of 0.05 which appears to be in disagreement with the results of

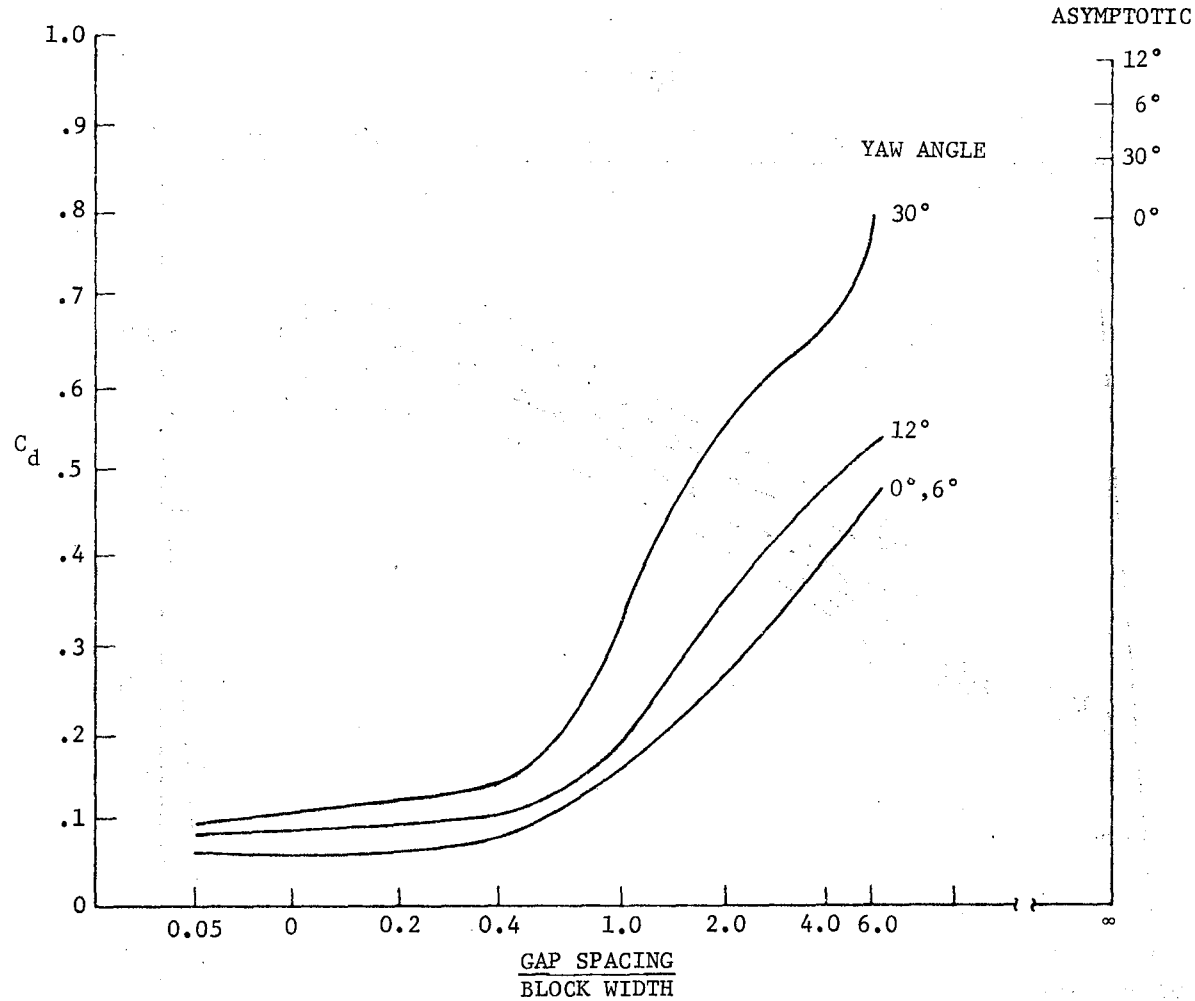

Figure 30. Drag coefficient of basic blocks with sharp corners as a function of gap spacing, for different yaw angles. Re = 10^6

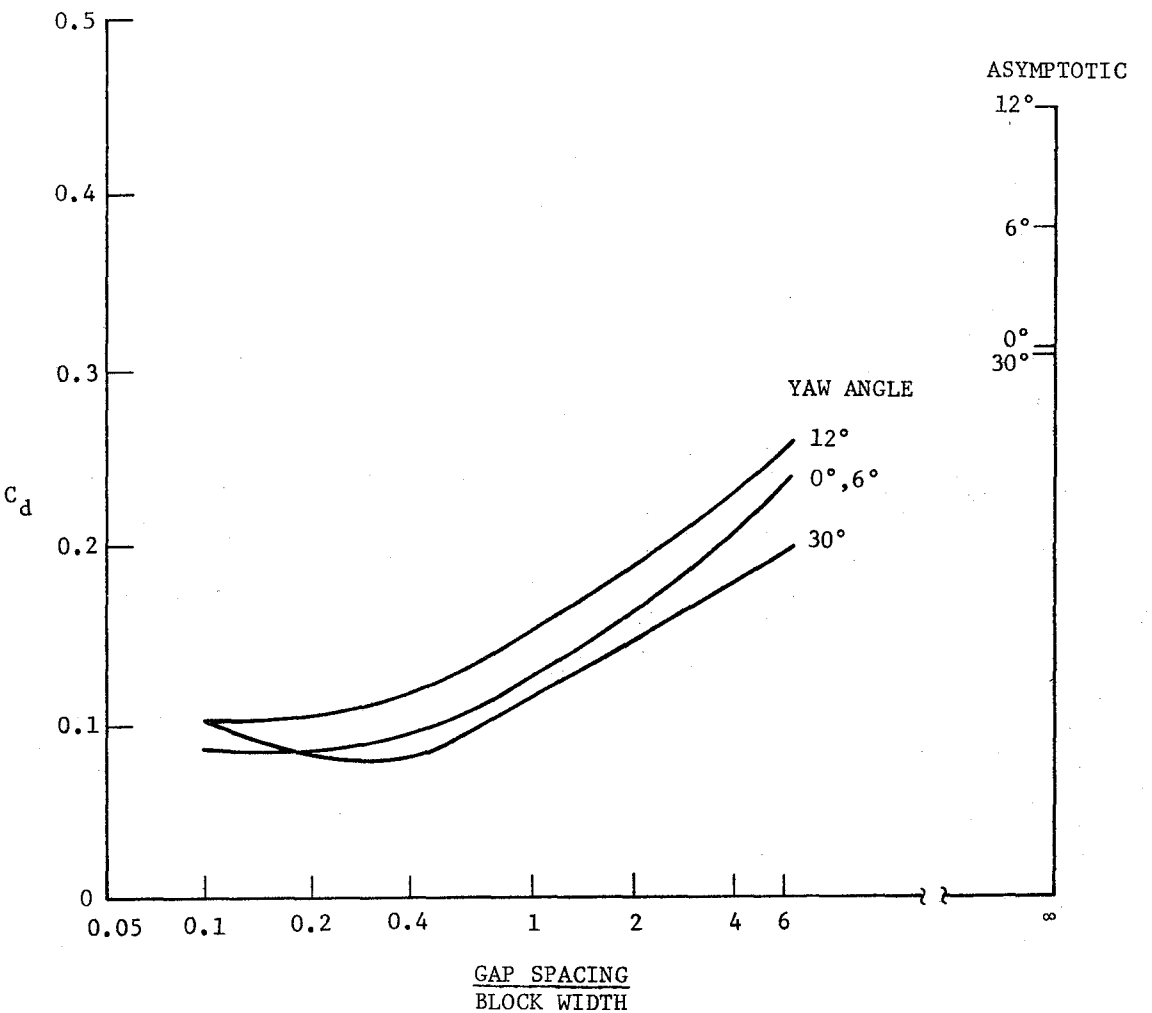

Figure 31. Drag coefficient of basic blocks with 0.2 corner radius as a function of gap spacing, for different yaw angles. Re = 10^6

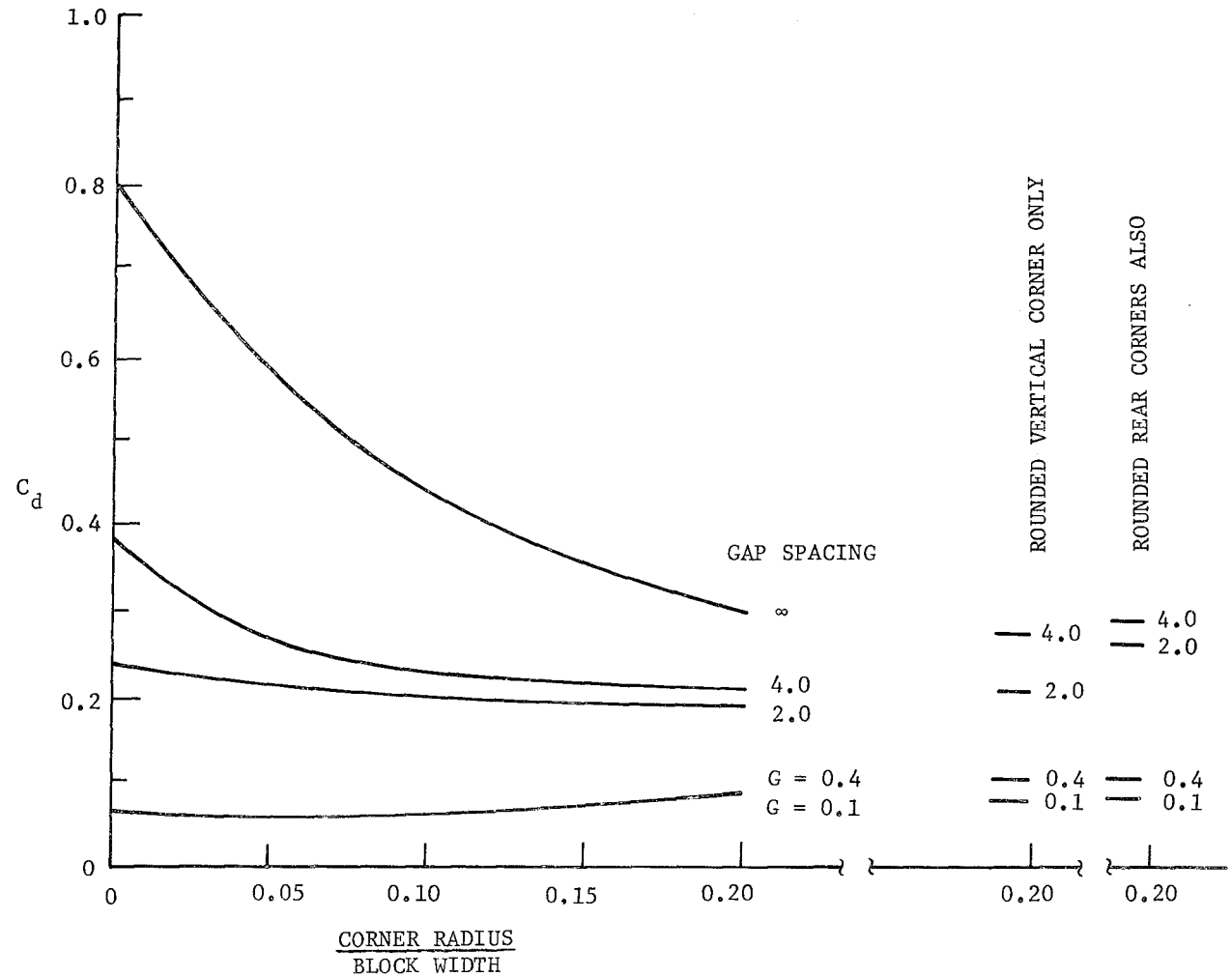

Figure 32. Drag coefficient of basic blocks as a function of corner radius for different gap spacings at 0° yaw angle. Re = 10^6 Section at right of figure shows drag coefficient for 0.2 corner radius when only vertical corners are rounded and when rear corners are also rounded.

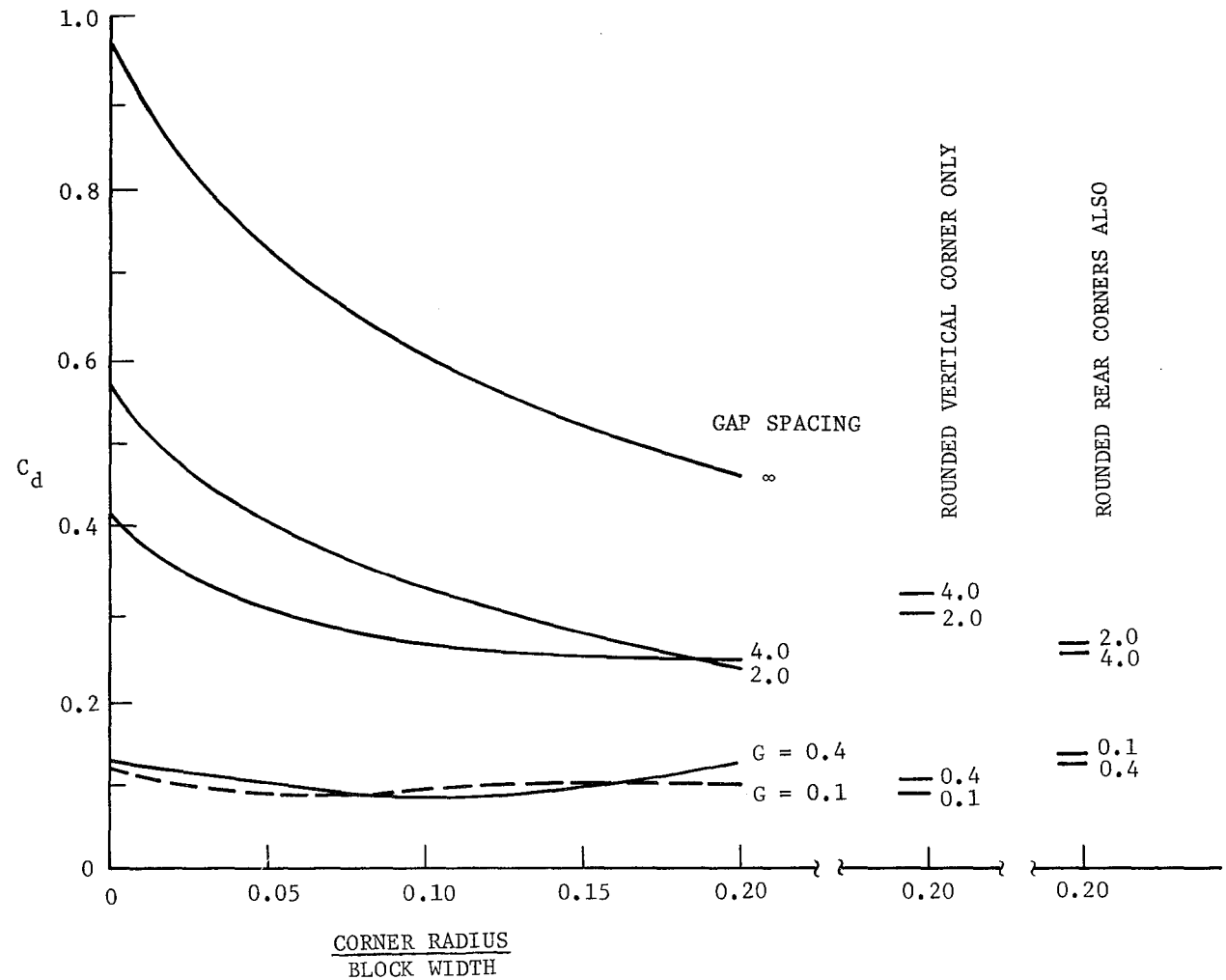

Figure 33. Drag coefficient of basic blocks as a function of corner radius for different gap spacings at 18° yaw angle. Re = 10^6 Section at right of figure shows drag coefficient for 0.2 corner radius when only vertical corners are rounded and when rear corners are also rounded.

Reference 17. However, both sets of data show that rounding the corners has an important effect in reducing the drag which reaches its asymptotic value for relatively small radii. These figures also show results when only the frontal vertical corners are rounded and when the rear corners are also rounded. The results for these different types of corner rounding will be discussed subsequently.

Photographs of tufts were also made which help in visualizing the flow pattern about these blocks. Figure 34 is a picture taken at a gap spacing of 0.1 and a yaw angle of 0°. The tufts on the first block are the only one which show much difference in pattern from those on the other blocks. On the other blocks the pattern is basically similar indicating that the flow is established around the first block. It should also be noted that the pattern does not change much along each individual block showing that there is hardly any effect of the gaps between the blocks. Figure 35 shows such a photograph taken at a gap spacing of 0.1 and a yaw angle of 30°. The flow on the lee side of the first block, which is the side towards the camera, is considerably different than on the subsequent blocks. The other blocks show a progressive change which is not appreciably influenced by the gaps between the blocks. The tufts on the tops of the blocks appear to show more of a cyclic pattern that repeats itself from one block to the next and is somewhat similar, the first block being the most different. However, this cyclic pattern does show an effect of the gaps. It is surprising how well the tufts on top of the blocks line up with the axis of the blocks and not the direction of the flow. Figure 36 shows the same blocks still at a yaw angle of 30° but now with a gap spacing of 6. The tufts on the lee side show a similar pattern on all of the blocks including the first. In this case each block is behaving much more like a single block as the drag data also shows. However, the tufts on the track in between the blocks are still generally lined up with the axis of the track and not with the undisturbed wind direction. The relations between these tufts pictures and theoretical predictions will be given when the side forces are discussed.

Two additional configurations were tested to further explore the effects of rounding the edges of the blocks. Figure 37 shows the drag measured on blocks with only the vertical edges rounded and not the horizontal top edge. At small gaps, 0.1 and 0.4, the drag is slightly reduced by the unrounded horizontal edge. This is consistent with the

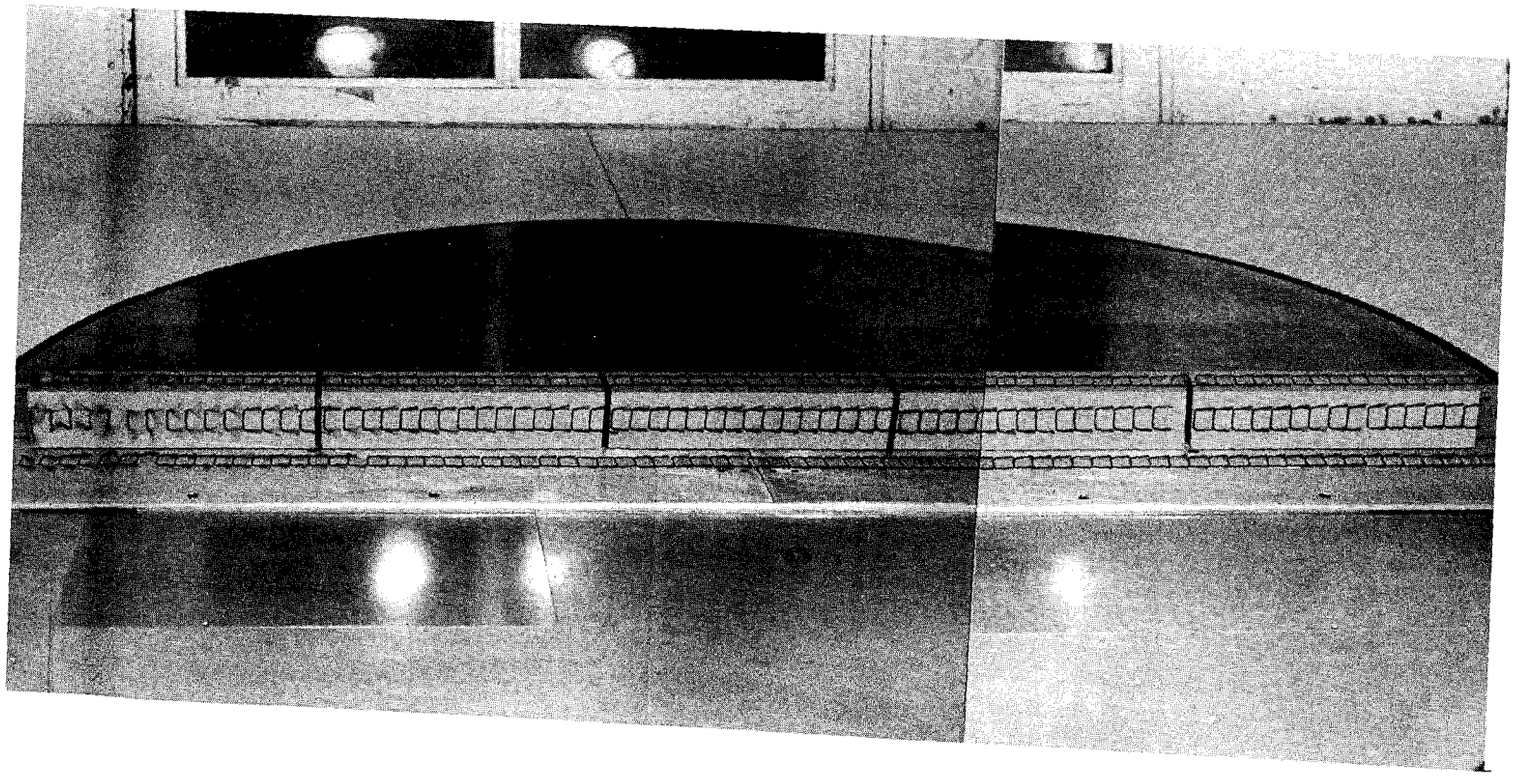

Figure 34. Basic blocks instrumented with tufts. Sharp corner, gap spacing = 0.1 block widths, 0° yaw angle, Re = 10^6

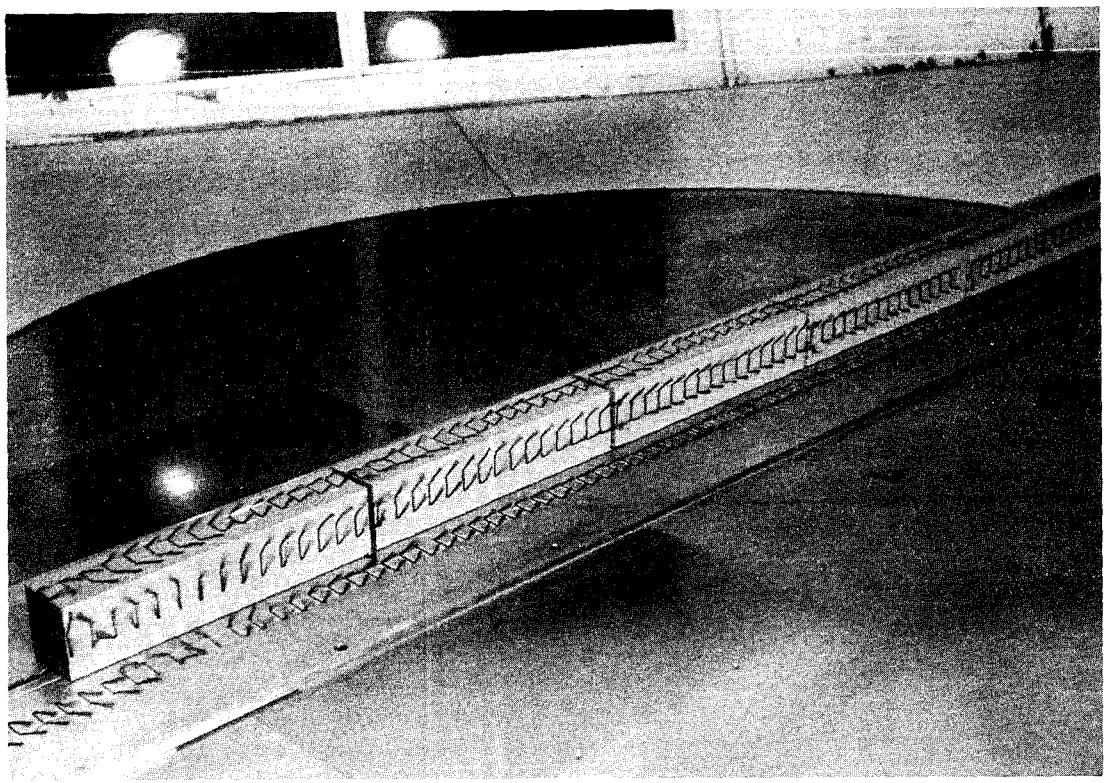

Figure 35. Basic blocks instrumented with tufts. Sharp corner, gap spacing = 0.1 block widths, 30° yaw angle. Re = 10^6

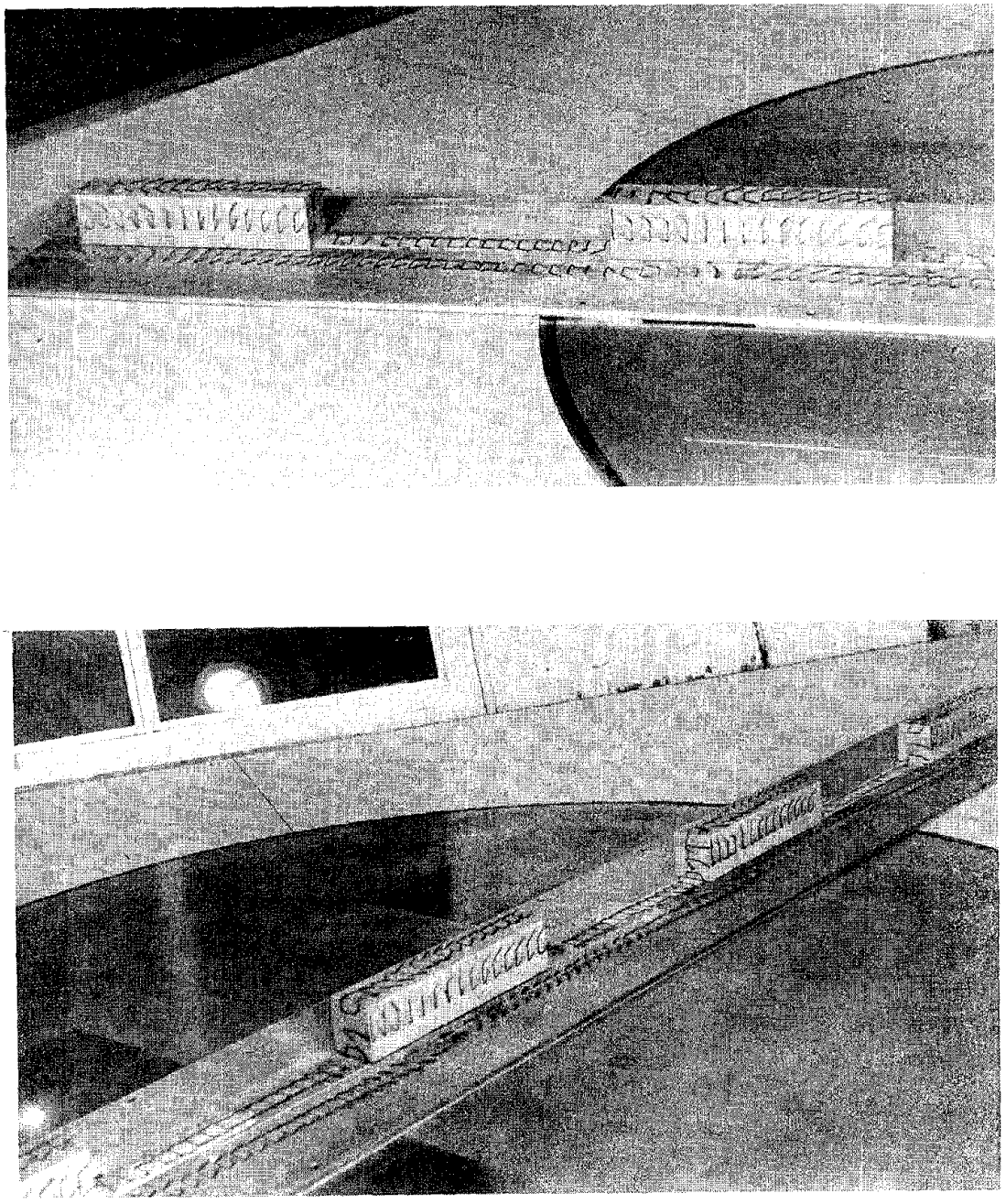

Figure 36. Basic blocks instrumented with tufts. Sharp corner, gap spacing = 6 block widths, 30° angle of yaw. Re = 10^6

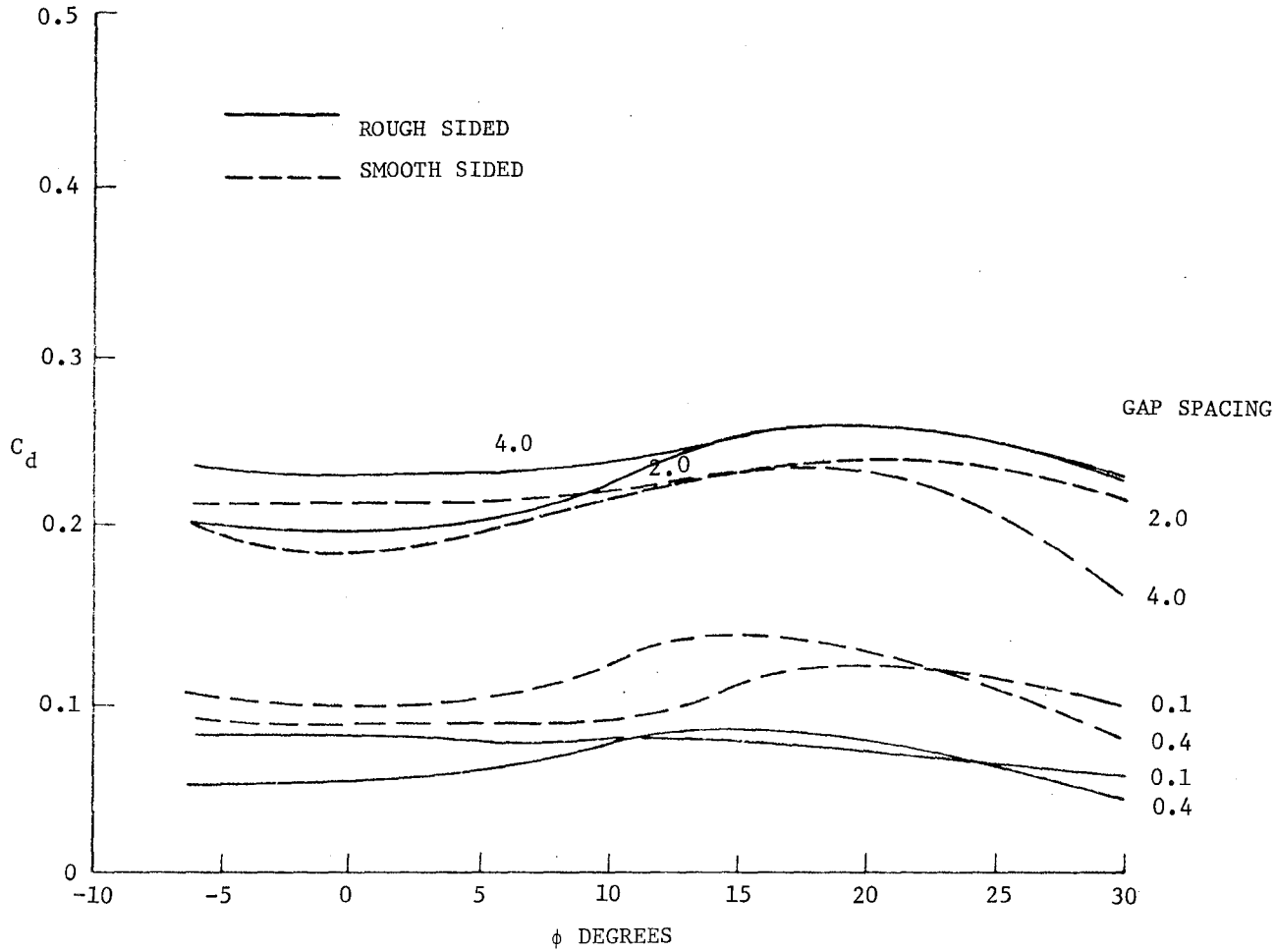

Figure 40. Drag coefficient of basic blocks with 0.2 corner radius as a function of yaw angle for different gap spacings. Comparison of smooth and rough sided blocks. Re = 10^6

increased. The results found in these tests seem to be consistent with the general result in that for the higher drag sharp-edged body, where the base drag was a smaller part of the total, the drag increased, and for the rounded nose body, where the total drag was less, the total drag decreased. However, it is not felt that these tests are adequate to determine the full nature of these effects. The principal conclusion that should be drawn is that the changes in drag caused by the changes in surface roughness are not large.

6.1.2 Side Force

The side forces on the blocks were measured and are shown in Figures 41 and 42. The general trend is an increase in side force as the gap size increases and an increased linearity with yaw angle as the gap size increases. However, at the smaller gap sizes, 0.05 to 0.4, the side force decreased with gap size. A comparison of Figures 41 and 42 shows that the effect of nose radius was rather small.

The side force is better predicted by theory than the drag force and, for this reason, it is logical to compare these results with theory. An application of slender body cross flow theory applied to ground vehicle has been carried out in Reference 24. The theory divides the effects into linear and second order terms. The linear result is simply that the side force is located at or near the nose of a long slender body and that it is given by the relation

$$C_y A = \pi \phi h^2$$

where ϕ is in radians and h is the height of the body. It also predicts a trailing vortex which causes a downwash behind the body such that the flow is turned by an amount equal to the yaw angle of the body. The second order term is more complicated and is related to the cross flow over the body. In its simplest form it says that the cross flow force is equal to the drag caused by flow across the body at the cross flow value of the dynamic pressure. In Reference 24 a more sophisticated approach is taken in which the variation of the cross flow drag coefficient with the time that the fluid has been flowing over the body is taken into account.

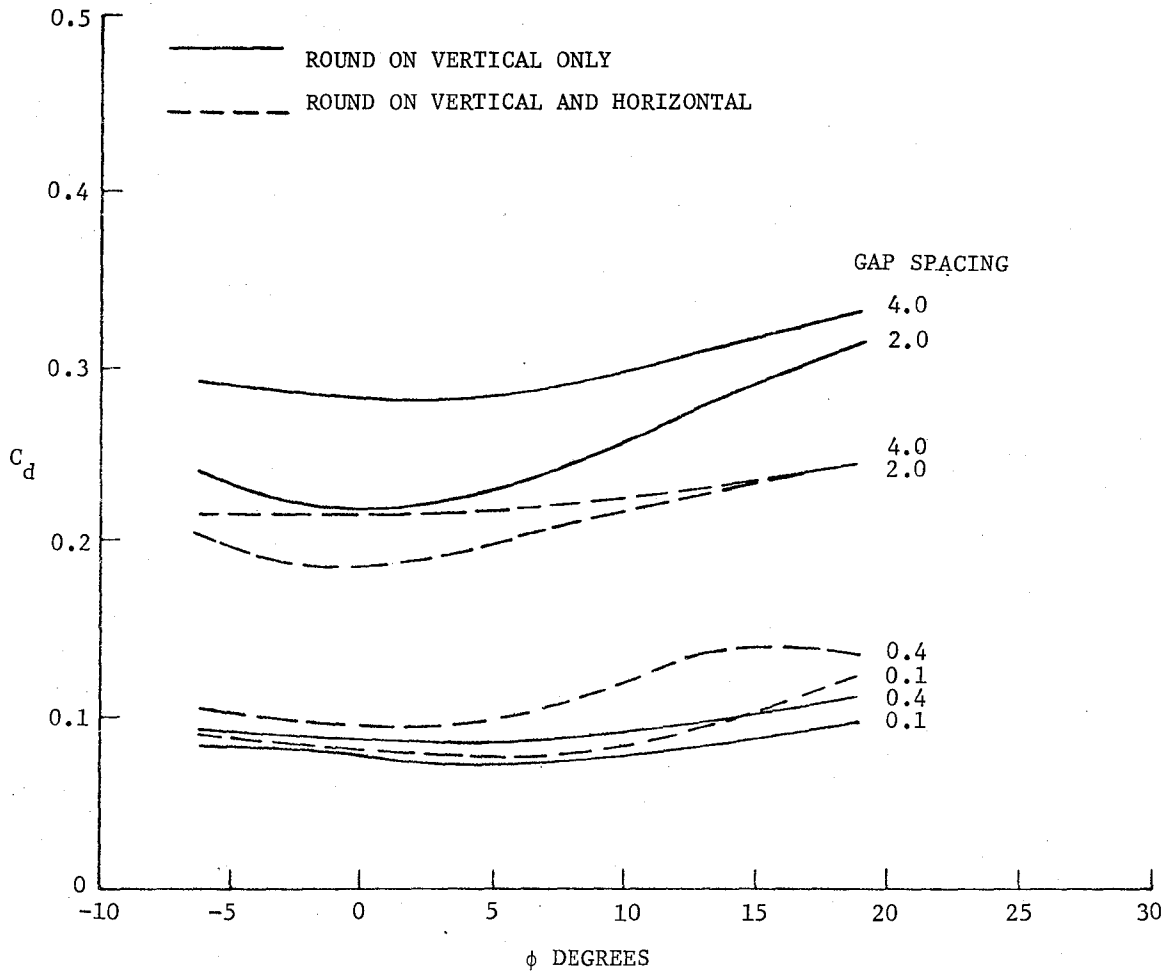

Figure 37. Drag coefficient of basic blocks with 0.2 corner radius as a function of yaw angle for different gap spacings. Comparison of blocks with rounded and sharp horizontal top corner. Re = 10^6

fact that a block with zero radius corner has a lower drag at low yaw angles than one with rounded corners as shown in Figure 32. Figure 37 shows that this effect is less pronounced at larger yaw angles but the effect of yaw angle on the flow on the horizontal edge should be less than on the vertical edges. At the larger gap spacings, 2 and 4, the unrounded edge increases the drag appreciably at all angles of yaw. However, the drag is considerably less than it would be if the vertical edges were also sharp. It might be expected that the majority of the air would flow around the side edges of the block and therefore rounding these edges would be most important since distance to the side edges is on the average less than to the horizontal edge.

The effect of rounding the rear of the block as well as the front was tested and the results are shown in Figure 38. For all but the smallest gap of 0.1, the effect of rounding the rear of the block was to increase the drag. This increase in drag was less at the higher angles of yaw, 12° and 18°, than at lower angles. It seems logical that this increase in drag was caused by the flow pattern about the preceding block and not by the flow about the rear of the metric block. The rounded rear corner encouraged the air to follow the contour and flow into the gap between the blocks. This resulted in more air impinging on the nose of the next block. Although a single block of this configuration was not tested, it would seem likely that there would be no drag increase caused by rounding the rear corners. The reduced amount of the effect of the higher yaw angles was probably caused by the decrease in the shielding at these angles.

The effect of surface roughness was tested by putting vertical posts on the side of some of the blocks. The resulting drags are shown in Figures 39 and 40. The results are mixed. For sharp edged blocks, the vertical post blocks gave a somewhat higher drag coefficient, especially at the larger gap spacings. However, for the rounded nosed blocks, the vertical posts decreased the drag at small gap spacings. It is well known that surface roughness on bodies with blunt bases can have either effect. The roughness increases the skin friction and causes a thicker boundary layer that results in a lower base drag. Either effect may dominate depending on the other parameters. For short bodies with low skin friction the decrease in base drag causes a decrease in total drag. For long bodies, the skin friction is dominant and the total drag is

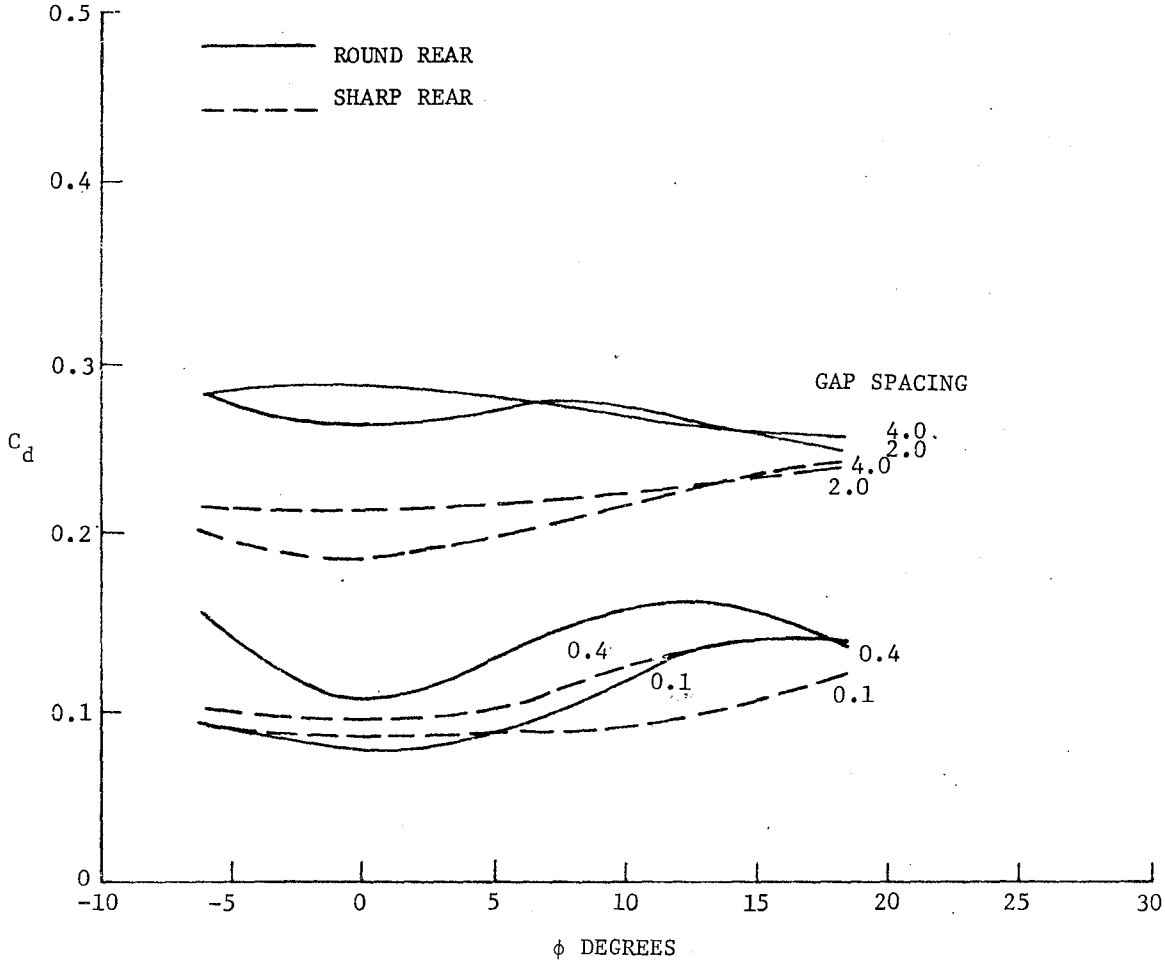

Figure 38. Drag coefficient of basic blocks with 0.2 corner radius as a function of yaw angle for different gap spacings. Comparison of blocks with rounded and sharp rear corners. Re = 10^6

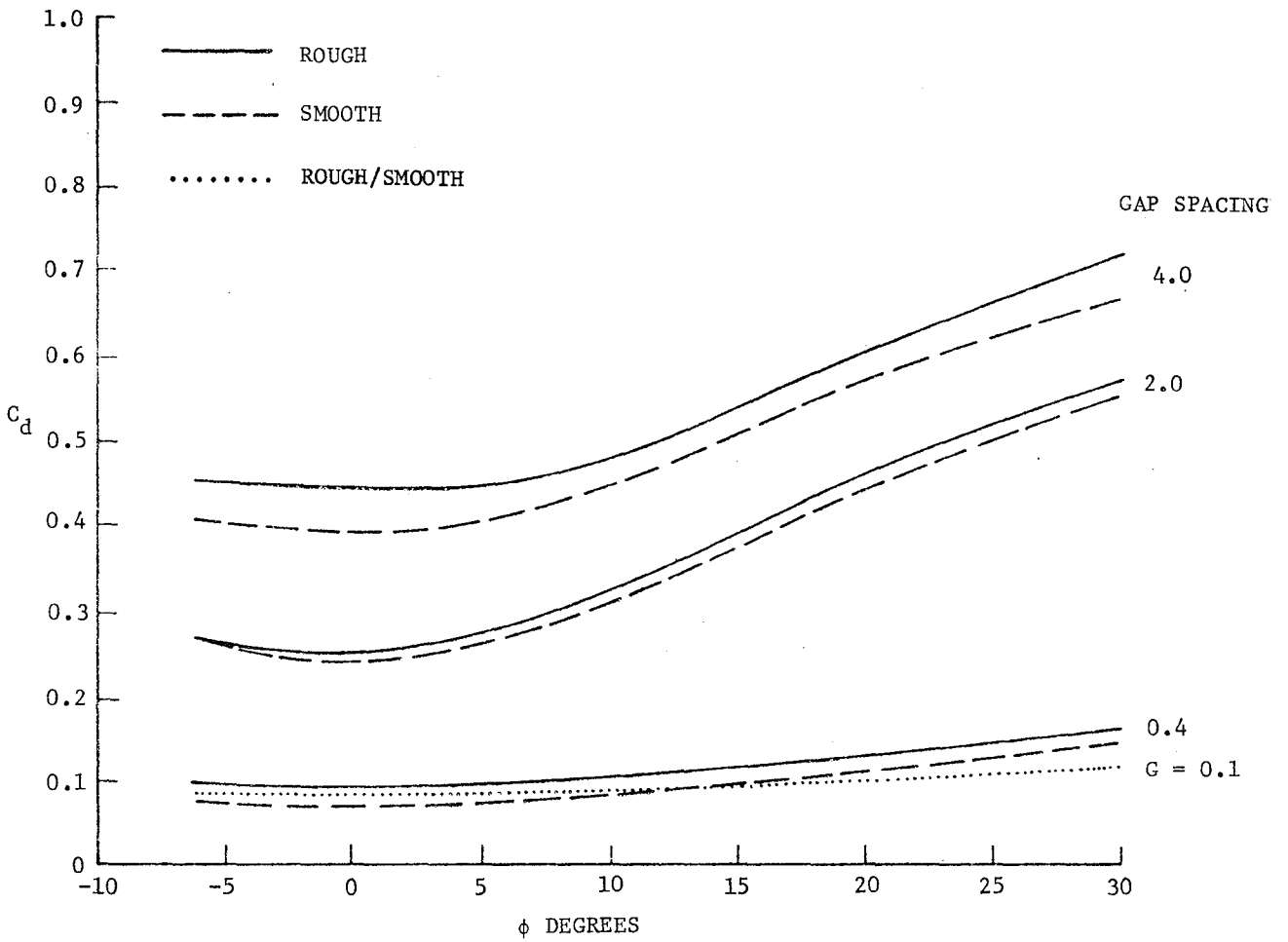

Figure 39. Drag coefficient of basic blocks with sharp corner radius as a function of yaw angle for different gap spacings. Comparison of smooth and rough sided blocks. Re = 10^6

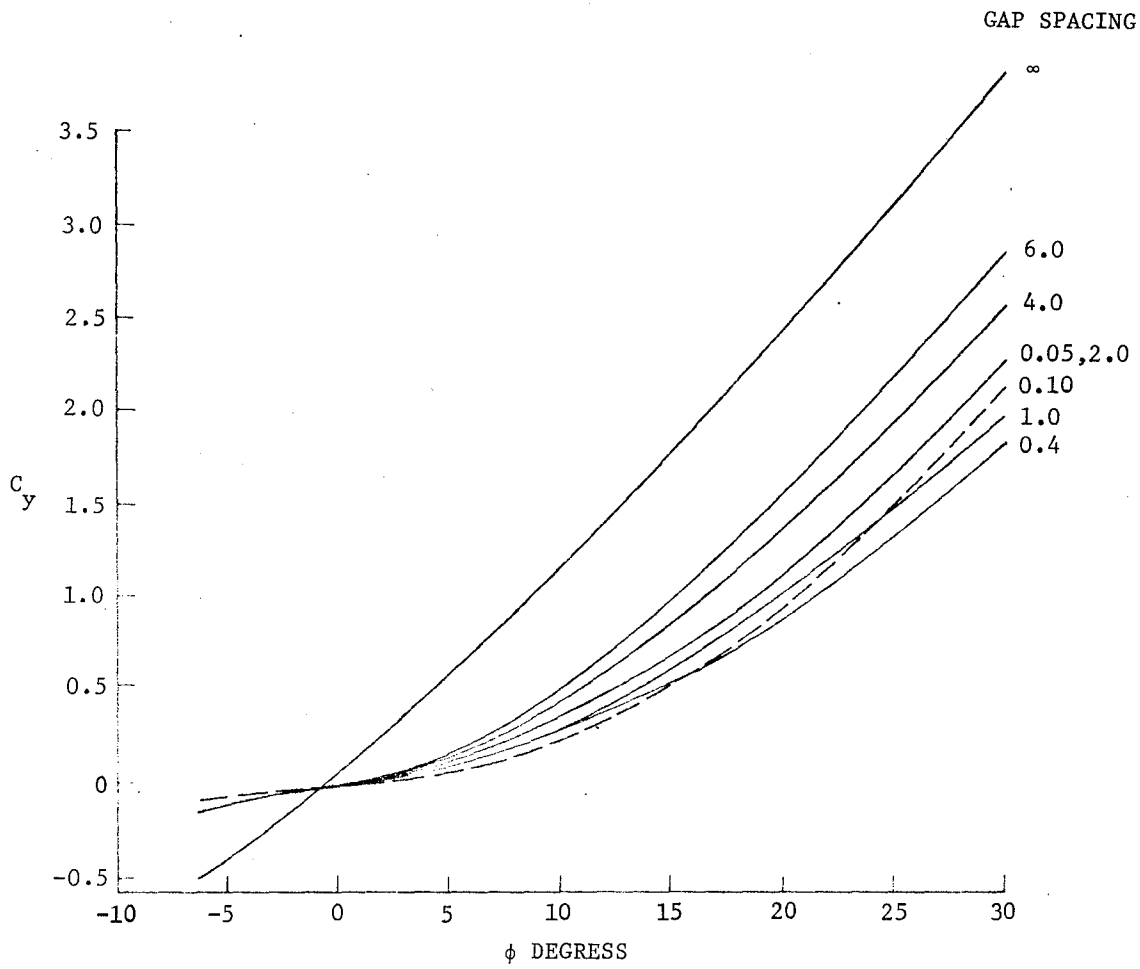

Figure 41. Side force coefficient of basic blocks with sharp corners as a function of yaw angle for different gap spacings. Re = 10^6

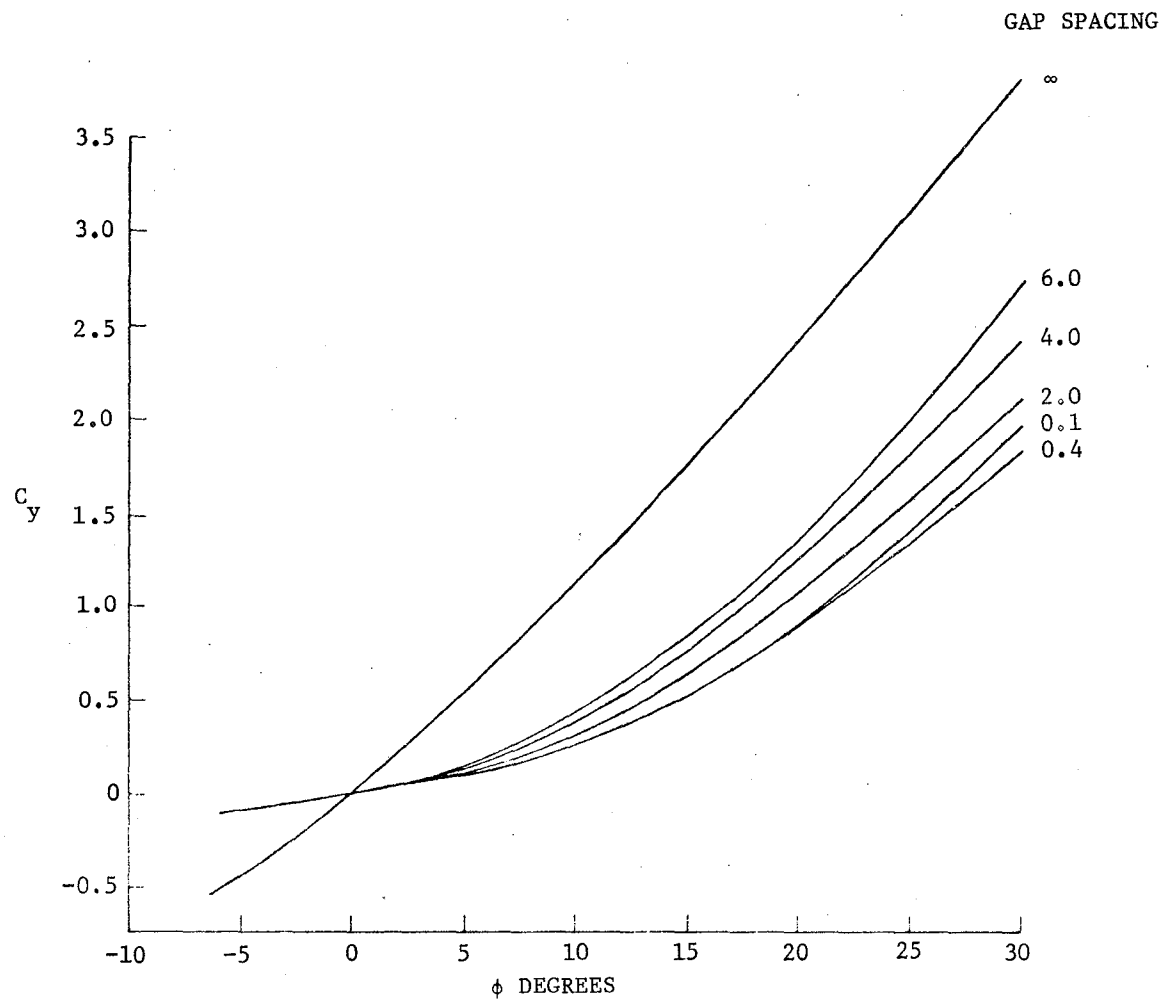

Figure 42. Side force coefficient of basic blocks with 0.2 corner radius as a function of yaw angle for different gap spacings. Re = 10^6

The time for the cross flow to establish itself over the body is related to the amount of fluid which has flowed across the body ahead of the point in question. For closely spaced blocks the force predicted by the linear term should be applied to the first block only and the forces predicted by the second order terms should be spread along the length of the train according to the local cross flow drag. If the blocks are spread far enough apart, then each block should be independent and should form a new leading edge. The forces on the central metric block should vary from the forces that would be applied to the central portion of a long block, for the closely spaced arrangement (the second order term), to the forces on a single block (the linear and second order terms), for blocks with infinite spacing. The results show that the side force on the metric block increases as the gap size increases. The shape of the curve also becomes more linear as the gap size increases. In order to obtain a more quantitative expression of this effect, the side force curves have been fitted with second order polynomials. The coefficients of the first and second order terms so obtained are shown in Figure 43. While there is considerable scatter, the coefficient of the first order linear term does increase with gaps size while the coefficient of the second order term is about constant. On the far right hand side of the figure, the theoretical value of the coefficient of the linear term at infinite gap size is shown. The coefficient of the second order term based on a drag coefficient of one is also shown. The value of the coefficient of the second order term of .00135 per degree^2 obtained from the curve fit process corresponds to a cross flow drag coefficient of 1.30. In order to better understand the theoretical predictions, Figure 44 has been prepared to show the different predictions. The second order term has been calculated using the method of Reference 24 for both the first block and for the third block in the series of closely spaced blocks. The second order term is given by the relation

$$C_{yc} A = \phi^2 h^2 \int_{\lambda_1}^{\lambda_2} g \, d\lambda$$

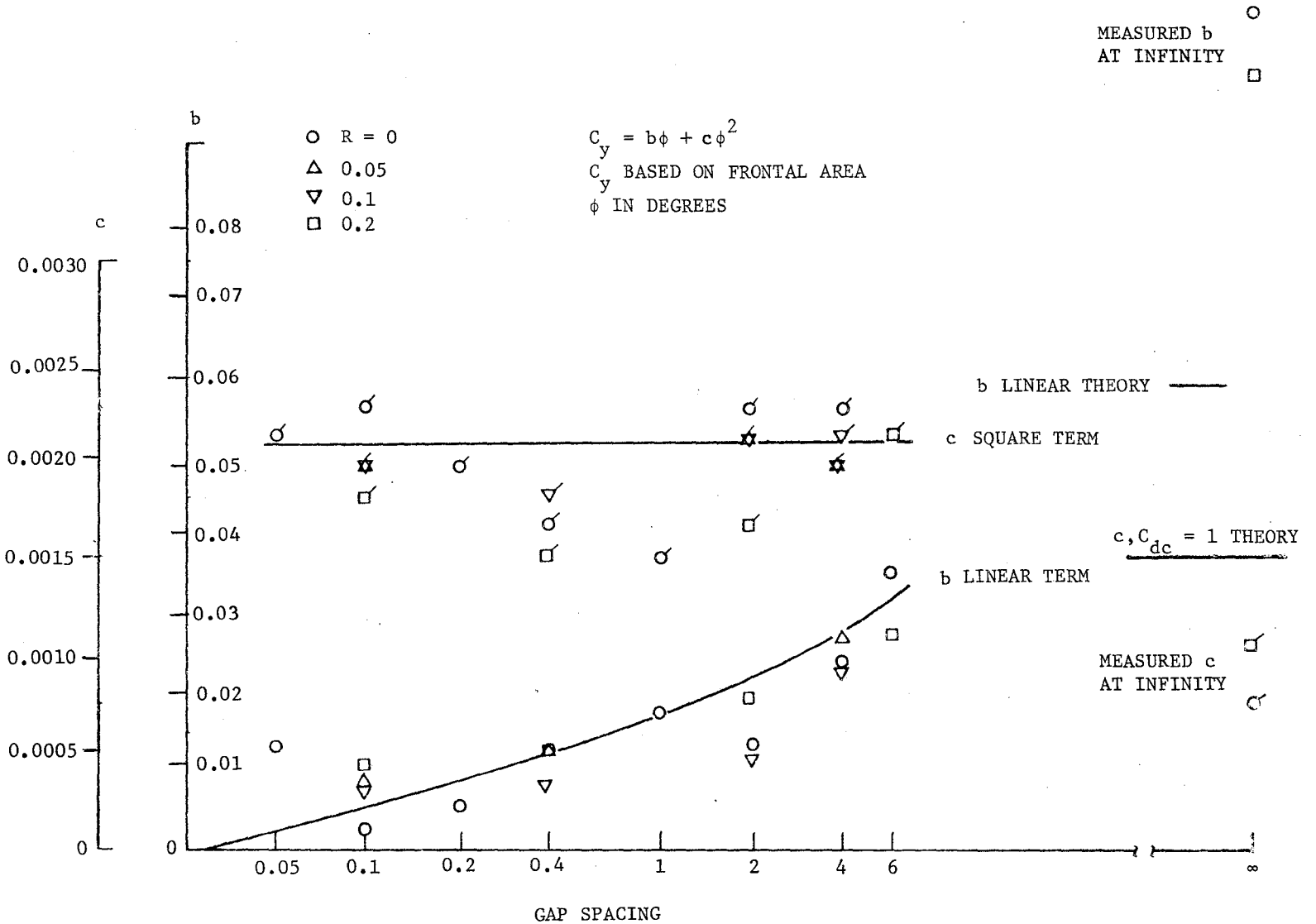

Figure 43. Coefficients determined from quadratic curve fit to side force coefficient curves as a function of gap size. Re = 10^6

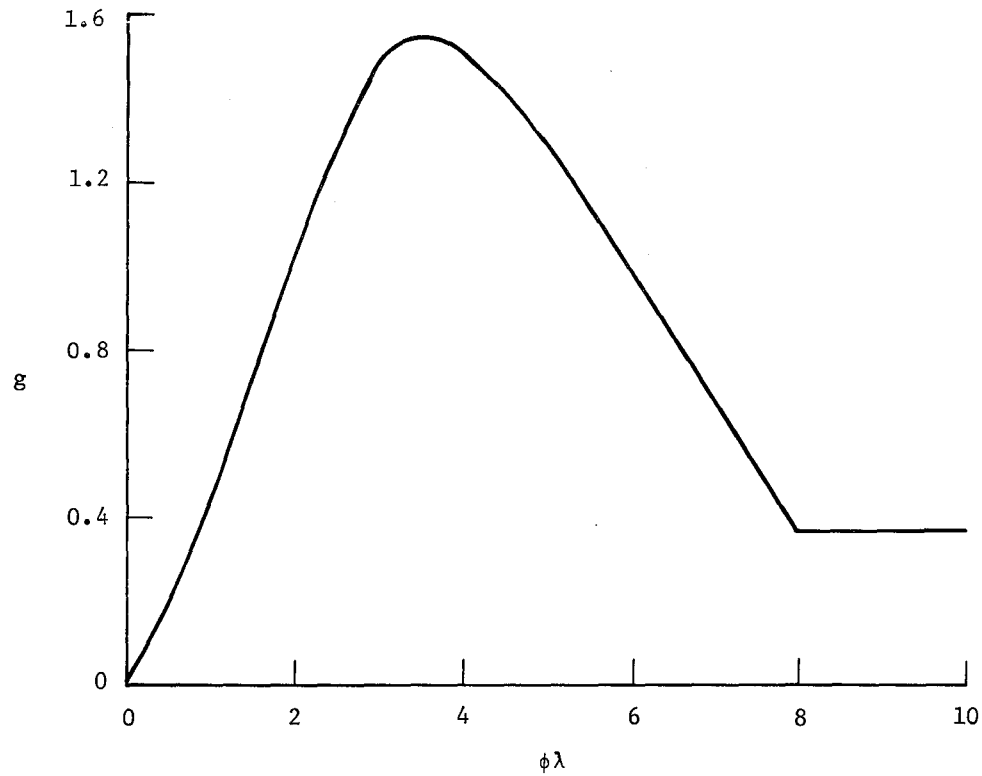

Figure 45. g function used in predicting side force coefficient as a function of yaw angle times dimensionless length (Ref. 24).

downwash in the gaps between the blocks. The theory is really for streamlined shapes that do not cause separation in their wakes. The blunt bases and noses of the blocks do cause separation which has a major effect on the flow in this region and is responsible for the position of the tufts in these regions.

A yawing and rolling moment was also experienced by the blocks when at an angle of yaw. These moments were caused chiefly by the side force but there could be some contributions from drag and lift if these forces were not applied on the centerline. These contributions should be considerably less than that of the side force since the width of the body was considerably less than its length and the magnitude of these forces was less than the side force. If it is assumed that the entire moment was due to the side force, then it is possible to determine the point of application of the side force. Specifying this point of application seems to be a good way to express this information since it correlates the data at different angles of yaw and for different configurations and expresses the results in a way which is more easily understood. The average height and standard deviation of the point of application for all yaw angles is shown in Table 6 for different gap sizes and nose radii. A comparison of these average values shows no change with gap size or nose radius. The average of these average values and their standard deviation is shown at the bottom of the table. The standard deviation of the averages is less than the standard deviation of the data obtained by averaging the data over the different yaw angles. There appears to be no significant changes with any of these parameters. The average height of this point of application of the side force is just about half the height of the block. One might expect that this point of application would be raised by the reduced velocity flow in the boundary layer along the ground plane of the wind tunnel. The location of the point of application may be somewhat different in the wind tunnel than for a vehicle moving over the ground since in this case only the cross wind velocity, which causes the yaw angle, would also be subject to the boundary layer effect. It might also be expected that the pressure difference would be somewhat reduced near the top of the block as pressure near the tip of a wing is reduced by spanwise flow. This later consideration would

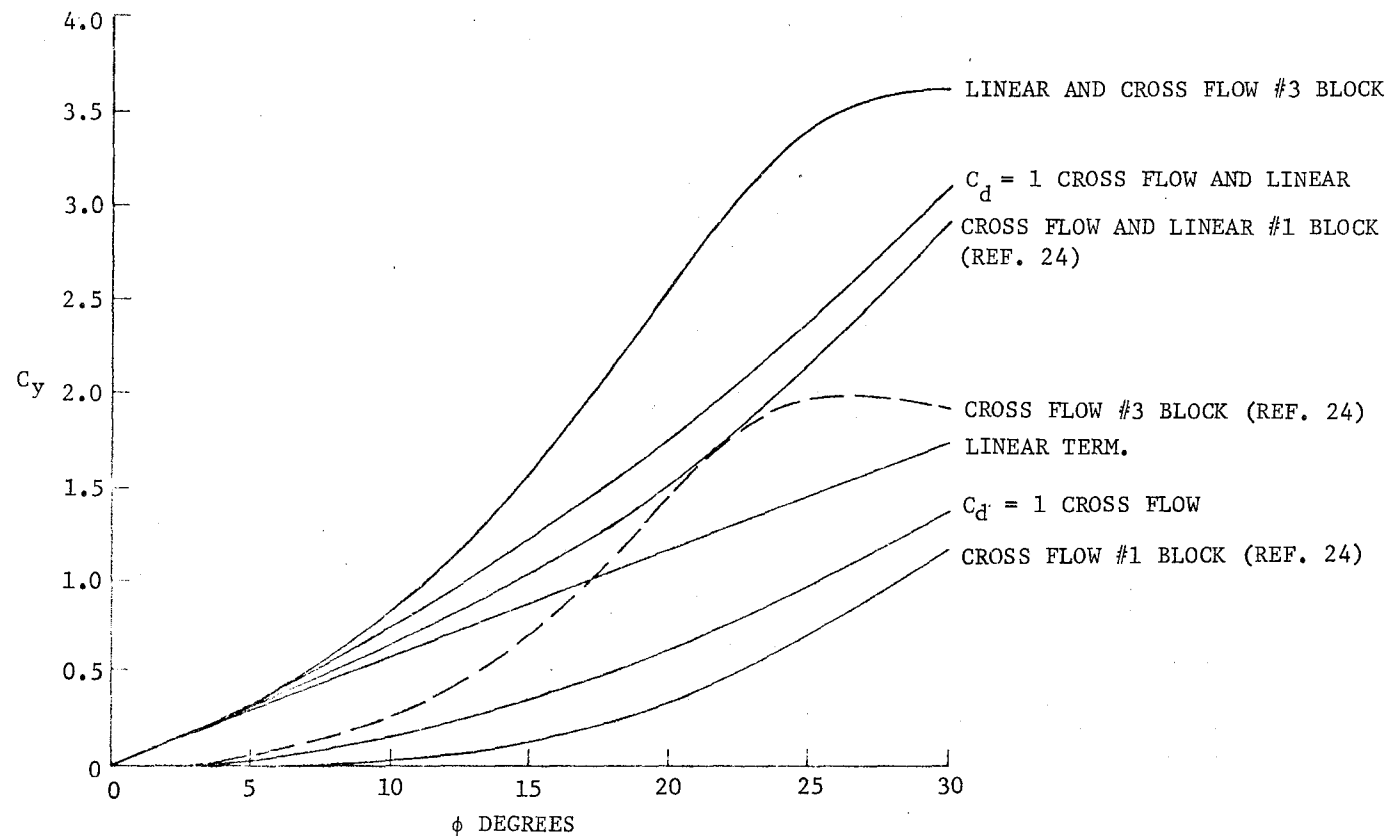

Figure 44. Theoretical predictions of side force coefficient as a function of yaw angle using different prediction methods.

where λ is the body length from the leading edge over the height. The factor g is taken from Figure 45. Since g depends on yaw angle ϕ, the value of $\int g\, d\lambda$ depends on ϕ. At a yaw angle of 30°, the maximum value of $\phi\lambda$ is 2.464 for the first block and 7.39 for the third block in the series of closely spaced blocks. Throughout the range of interest, g is not a constant. Since for the third block in the series it passes over the region in which it reaches the maximum, the relatively odd shape of the curve shown in Figure 44 results.

This comparison of theory and experiment shows that the theory predicts the correct general form of behavior. The magnitude of the side forces does increase as the gap size increases and the importance of the linear term does increase. The magnitude of the theoretical prediction of the linear term at infinite spacing is a reasonable asymptote for the coefficients of the linear term at finite spacings found by the curve fit process, but does not fit with the result for infinite spacing. The curve fitting process gives a coefficient of the second order term more or less independent of gap spacing, which corresponds to a cross flow drag coefficient of 1.30. The second order side force predicted by this term is about on the same order as that predicted by Reference 24. While the detailed shape of the curve predicted by Reference 24 is different than that given by a constant cross flow drag coefficient of 1.30, it is felt that the data is not sufficiently accurate to distinguish between these two results.

It is now interesting to return to an examination of the tuft pictures (Figures 34 through 36). Slender body theory says that the force applied near the nose of the body causes a vortex to be shed and a downwash which turns the flow in a direction parallel to the body. First order slender body theory says that this downwash will continue indefinitely and undiminished. Second order theory says that some force will have to be applied to the body to maintain the downwash as the shed vortex is swept downstream by the cross flow. The pictures show that the flow along the blocks is more or less lined up with the blocks even when their spacing is considerable. The pictures are really not adequate to show a development in the cross flow or decrease in the

TABLE 6. VERTICAL LOCATION OF SIDE FORCE ON BASIC BLOCKS

Nose Radius / Block Width	Gap Spacing / Block Width	Height / Block Height	Standard Deviation / Block Height
0	.05	.52	.067
0	.1	.57	.125
0	.2	.57	.122
0	.4	.56	.066
0	1.0	.53	.018
0	2.0	.56	.021
0	4.0	.57	.033
0	6.0	.54	.044
0	∞	.54	.034
.05	.1	.57	.146
.05	.4	.54	.032
.05	.2	.59	.054
.05	.4	.57	.018
.1	.1	.55	.063
.1	.4	.62	.172
.1	2.0	.56	.049
.1	4.0	.56	.021
.2		.55	.059
.2		.57	.055
.2	2.0	.55	.042
.2	4.0	.54	.028
.2	6.0	.57	.014
.2	∞	.52	.031
Average of all configurations		.56	.023

infer that the center of pressure would be below the middle of the block. Considering these different effects and the data itself, there seems to be no reason to conclude more than that the point of application is near the middle of the block in the vertical direction. The location of the point of application of the side force in the longitudinal direction is shown in Figure 46. There appears to be a definite relation between gap spacing and the location of the point of application. The point of application is always forward of the centerline of the block and tends to move further forward as the gap spacing is increased. The location is relatively independent of the angle of yaw. The results shown in Figure 46 are averaged over all angles of yaw. The leading edge radius also seems to have an important effect at the larger gap spacings. One might expect that the sharp leading edge would cause greater separation than the rounded leading edge. The locations of the points of application for infinite spacing and both leading edge radii are also shown. In this case the change in nose radius causes a considerable change in location.

The theory predicts that the force linearly proportional to the yaw angle should be located near the leading edge of the block and the force related to the second order of the yaw angle be located near the middle of the block. For closely spaced blocks, the force proportional to the linear term should be absent. As the blocks are spread apart, this force will increase with the result that the location of the point of application will move towards the leading edge. The behavior of the round cornered blocks seems to bear out this reasoning. The point of application of the force on the sharp cornered block moves forward as the gap width increases to about 2 to 4 and then returns towards the middle of the block as the gap space continues to increase to infinity. Theory would also predict an effect of angle of yaw on location because of the change in relative importance between the linear and second order term. This effect is not seen in the data.

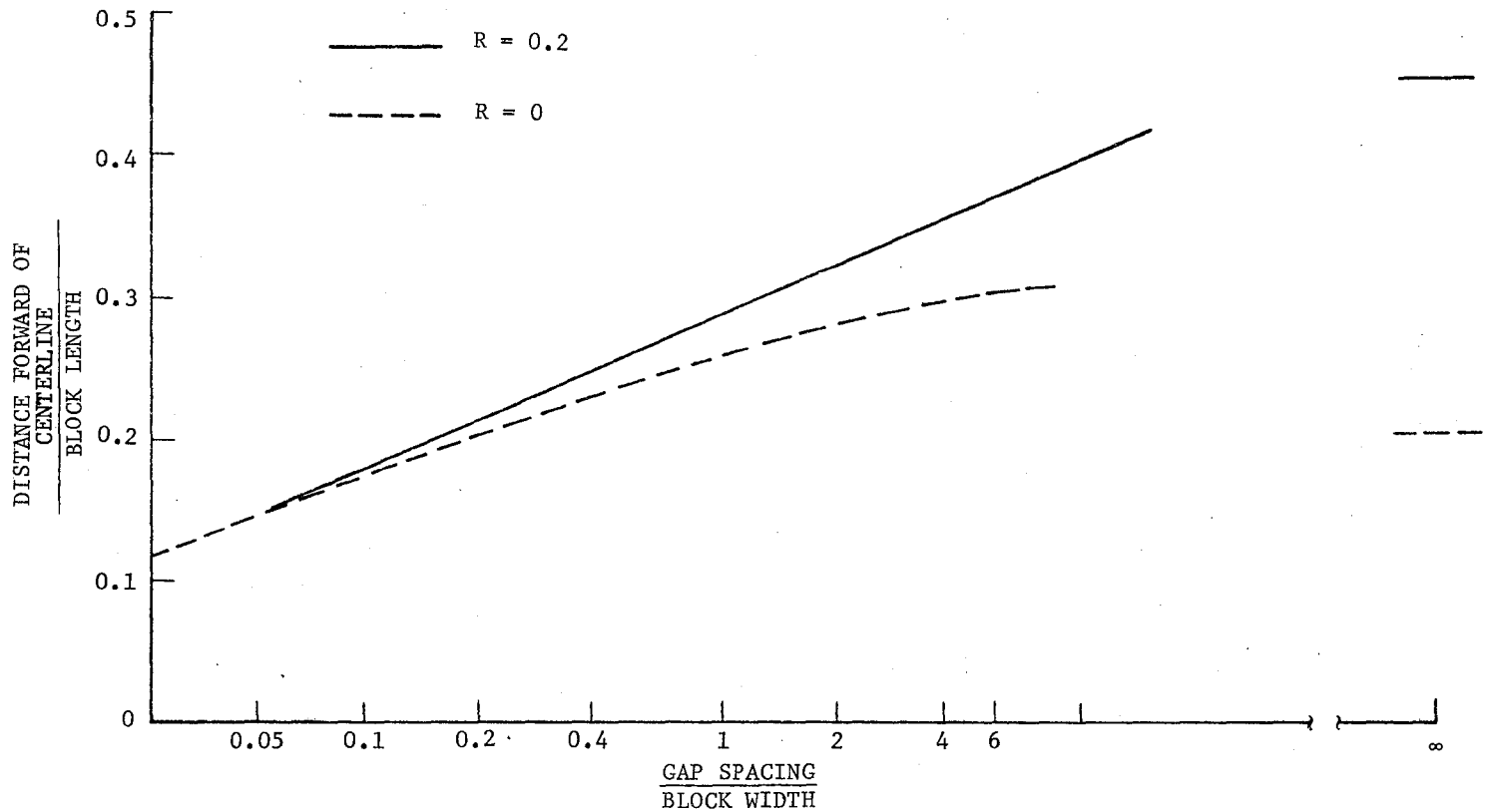

Figure 46. Location of the point of application of the side force forward of the centerline measured in block lengths as a function of yaw angle. Re = 10^6

6.1.3 Lift

The lift force as a function of both angle of yaw and gap spacing is shown in Figures 47 and 48. The lift is practically zero for zero yaw angle and close block spacing. The lift force increased with yaw angle and block gap size. Since increasing the gap size decreased the downwash effect from the preceding block, it effectively increased the yaw effect and thereby the lift. Nose radius does not appear to have an important effect on lift as can be seen by comparing Figures 47 and 48.

To determine the point of application of the lift force, the effect of drag on pitching force must be removed. If the assumption is made that the drag force is applied at the mid height of the block, then the moment caused by the drag may be removed and the point of application of the lift force determined. The effect of the drag force is particularly important at small angles of yaw where the lift force is very small. The location of the point of application of the lift force is shown in Figures 49 and 50 for two different nose radii.

At large angles of yaw, the location of the point of application was a little in front of the center of the block. As the yaw angle decreased, the curves break up into two different groups. For gap spacings of 0 to 1, the point of application continues to be near the middle of the block, but for gap spacings greater than 2, the point of application moves towards a point about half way between the front and the middle of the block.

6.2 RAILROAD CAR TESTS

6.2.1 Trailers

The aerodynamic measurements on the TOFC models were made in order to determine the magnitude of the forces and their variations with changes in the rail car and trailer design. All three forces and moments were measured. Of these forces drag is the most important and will be considered in greater detail than the other forces. The side force is of next importance along with information on the point of location of the side force in both the vertical and longitudinal direction.

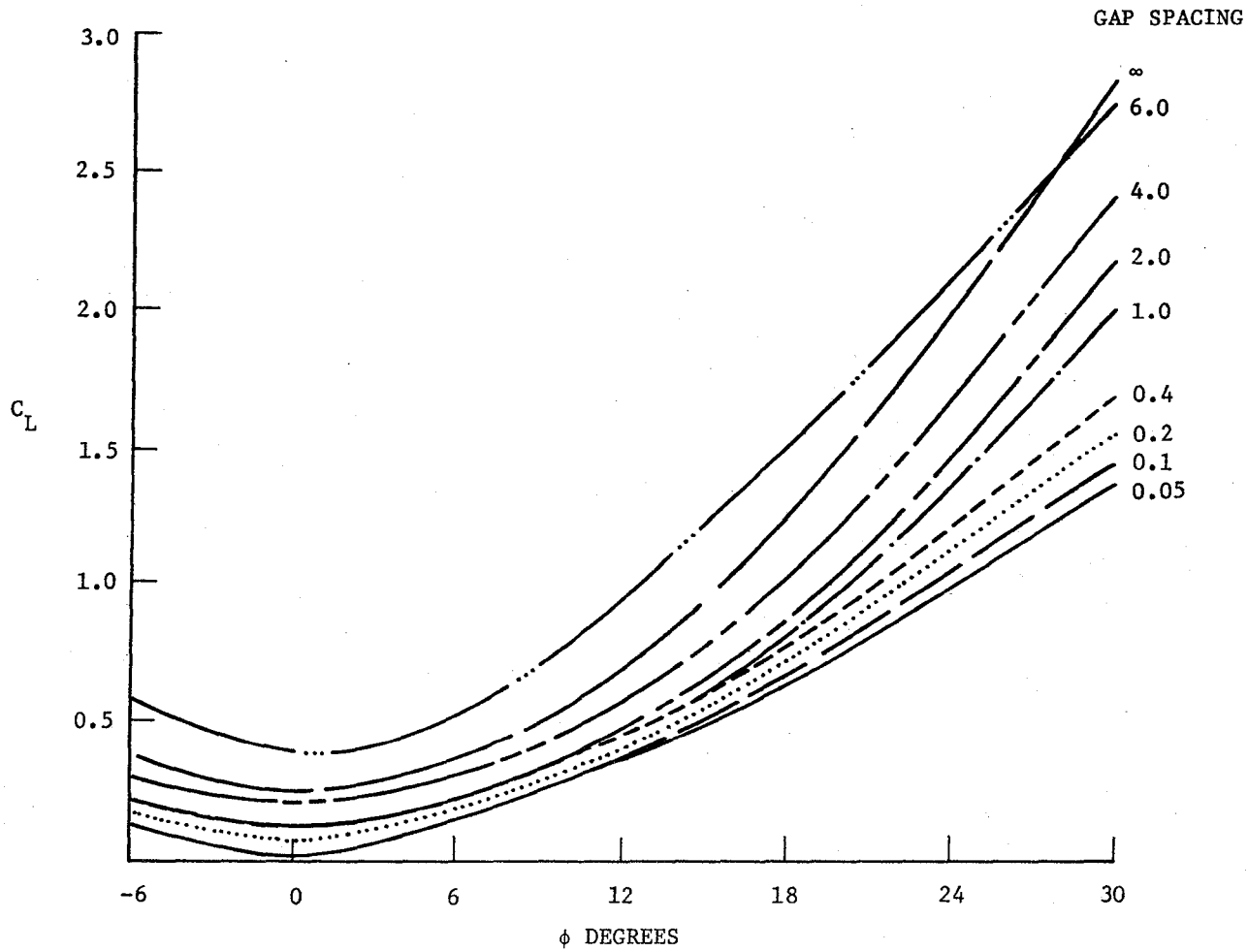

Figure 47. Lift coefficient of basic blocks with sharp corners as a function of angle of yaw for different gap spacings. Re = 10^6

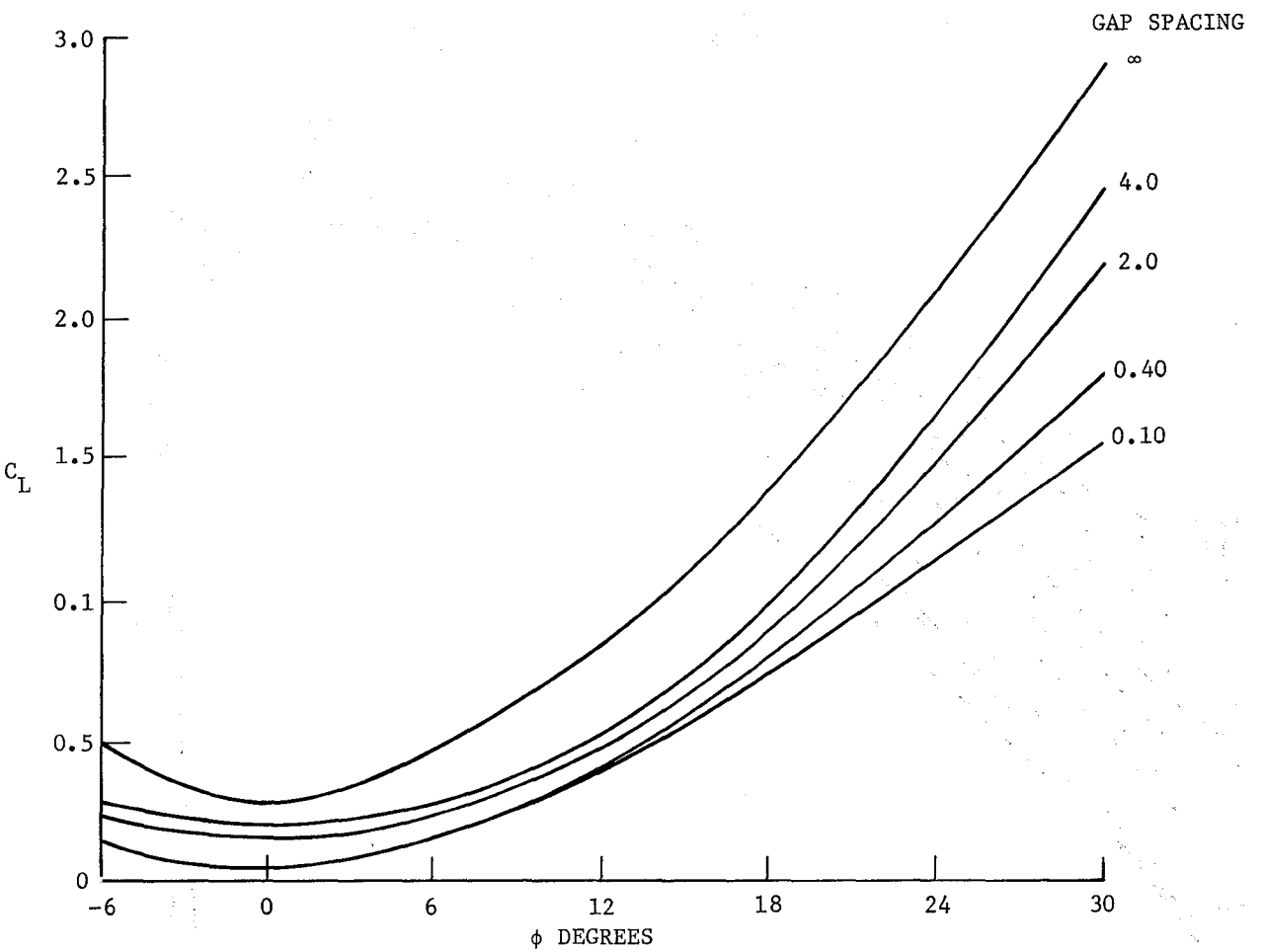

Figure 48. Lift coefficient of basic blocks with 0.2 corner radius as a function of angle of yaw. Re = 10^6

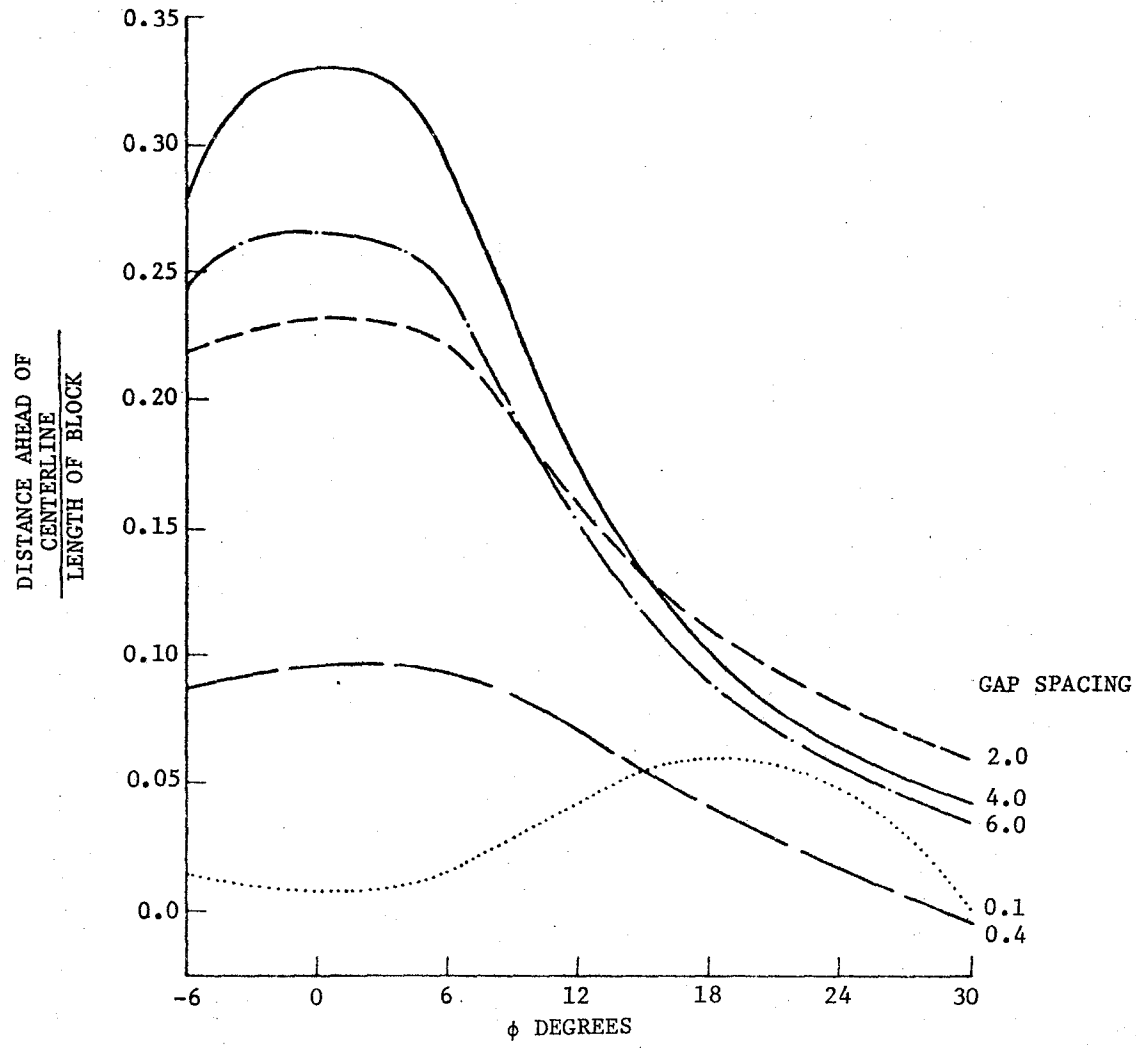

Figure 49. Location of the point of application of the lift force on basic blocks with sharp corners forward of the centerline of the block measured in block lengths. Re = 10^6

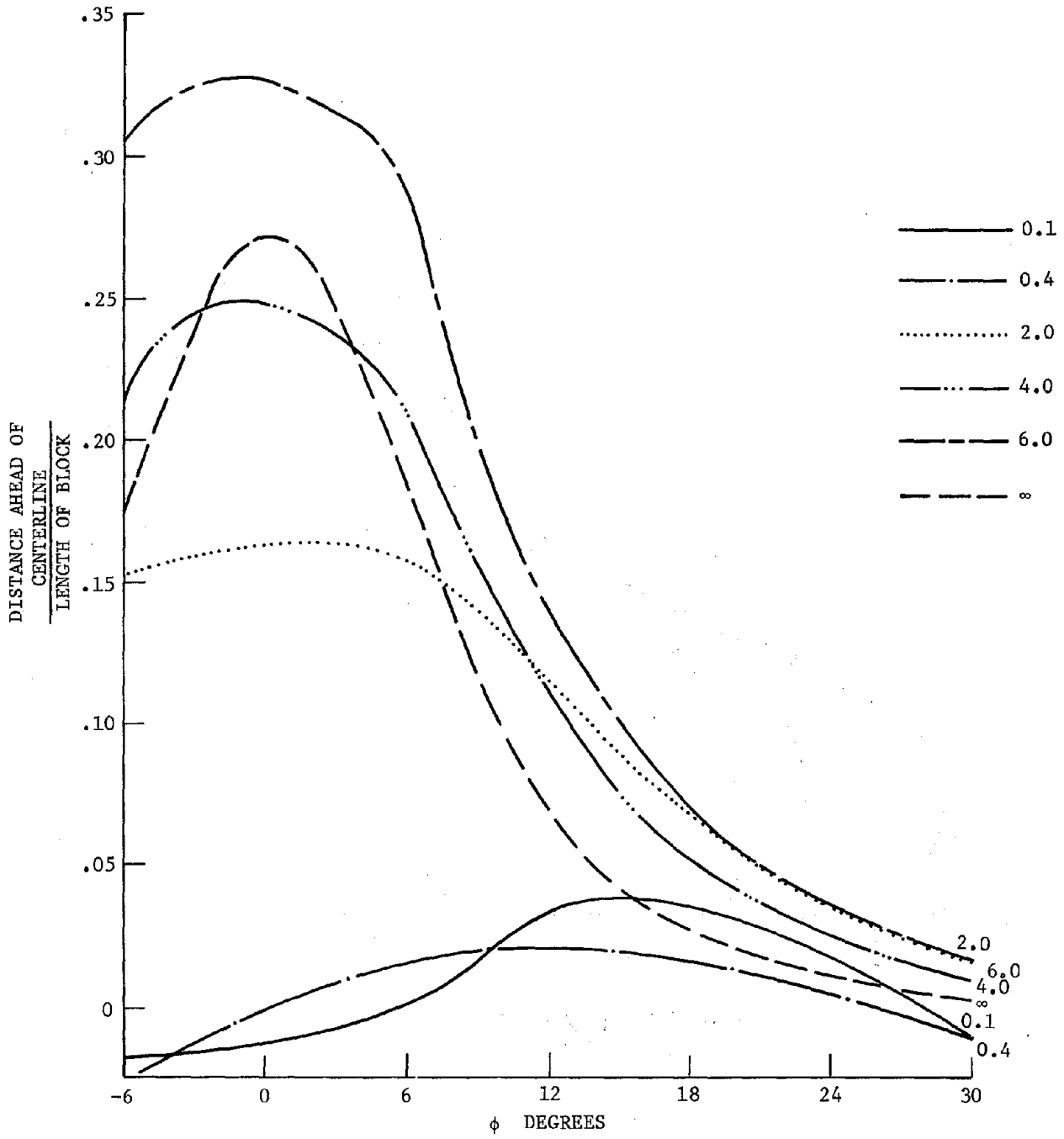

Figure 50. Location of the point of application of the lift force on basic blocks with 0.2 radius corners forward of the centerline of the block measured in block lengths. Re = 10^6

This point will be determined on the basis of the assumption that the side force is the only force contributing to the roll and yawing moments. Visualizing the point of application is more meaningful than just considering the moments. The lift effect is of least importance and only minimal attention will be given to it. In order to determine the effect of Reynolds number on the aerodynamic forces runs were made over a range of dynamic pressure, Figure 51. The aerodynamic coefficients were found to be independent of Reynolds number.

6.2.1.1 Drag

Drag on the TTX car fully loaded with two trailers and different loadings on the preceding and trailing cars is shown in Figure 52. In this figure and others showing railroad car data the configuration description used is as given in Table 5. In this figure the drag area is plotted against the angle of yaw ϕ. It is seen that the drag is minimal when ϕ is zero and increases as ϕ increases. The shape of the curve for different conditions of loading on the leading and trailing cars is basically the same. An empty car behind the metric car increases the drag of the metric car by a small amount and an empty car ahead of the metric car increases the drag by a larger amount. The drag of an empty car among other empty cars and with loaded cars on each side of it is also shown. It can be seen that a loaded car shields the next car from considerable aerodynamic load. The drag of a loaded car between two empty cars (105 ft^2) is about the same as the drag of two loaded cars (2 x 53 ft^2). The conclusion is that a train of alternately loaded and unloaded cars has a drag comparable with a fully loaded train even though it is only carrying half as many trailers.

The amount of drag caused by the wheels and trucks was assessed by removing the trucks from the metric car when the 3 TTX cars were empty. There was no measurable change in the drag.

An alternate way of presenting this same data is also shown in Figure 53. In Figure 52 the drag area has been found by dividing the force along the axis of the train by the total dynamic pressure. These same curves are also shown in Figure 53. The second set of curves in Figure 53 are obtained by dividing the force along the axis by the dynamic pressure calculated by taking only the component of the velocity

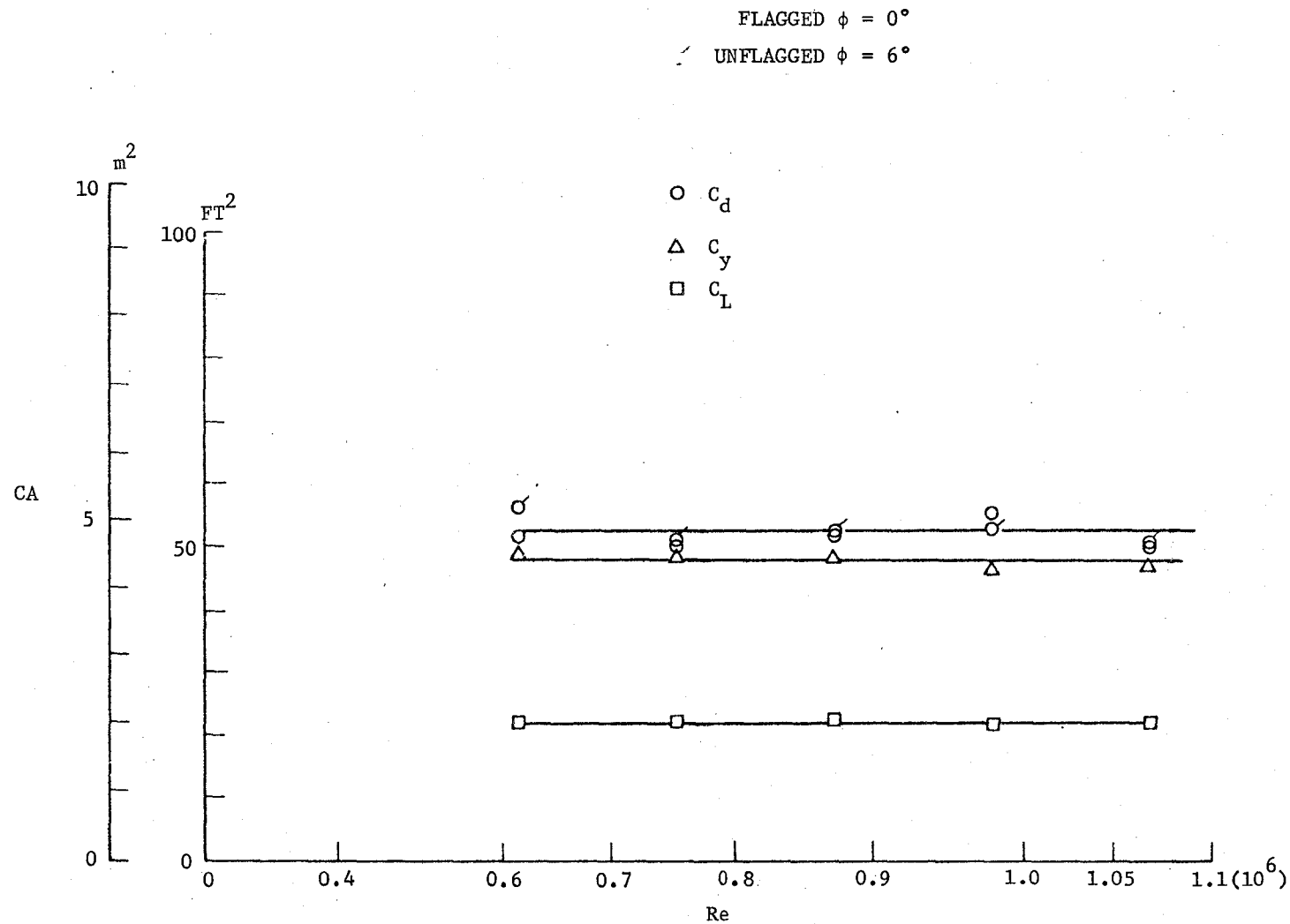

Figure 51. Drag, lift and side force area as a function of Reynolds number for Configuration 1. Reynolds number based on trailer length.

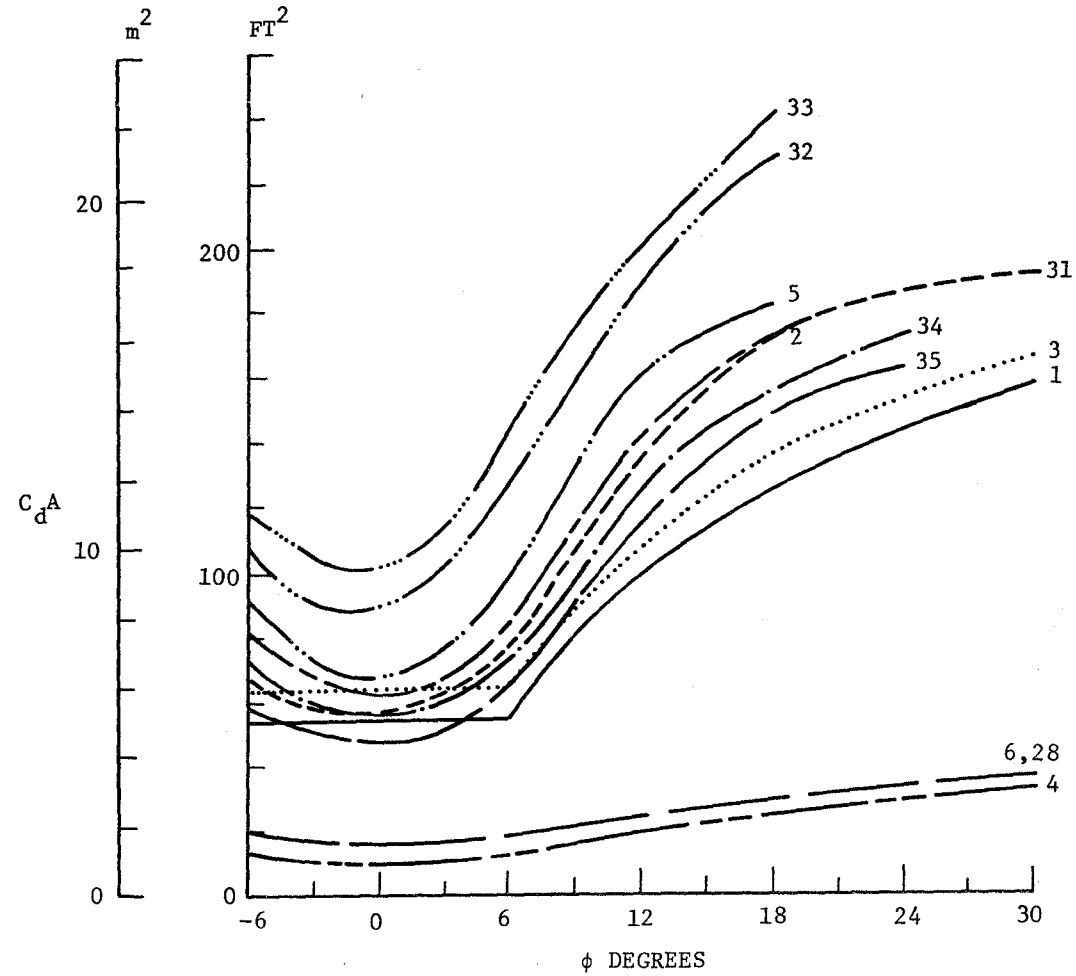

CONFIGURATION				
1	TTX	2 TS	2 TS	2 TS
2	TTX	E	2 TS	2 TS
3	TTX	2 TS	2 TS	E
4	TTX	2 TS	E	2 TS
5	TTX	E	2 TS	E
6	TTX	E	E	E
28	TTX	E	EW	E
31	TTX	2 TS Rr	2 TS Rr	2 TS Rr
32	TTX	E	2 TS Rr	2 TS Rr
33	TTX	E	2 TS Rr	E
34	TTX	2 TS	2 TS Rr	E
35	TTX	2 TS	2 TS Rr	2 TS

Figure 52. Drag area of TTX cars either fully loaded with two TS trailers or empty as a function of yaw angle. Re = 10^6

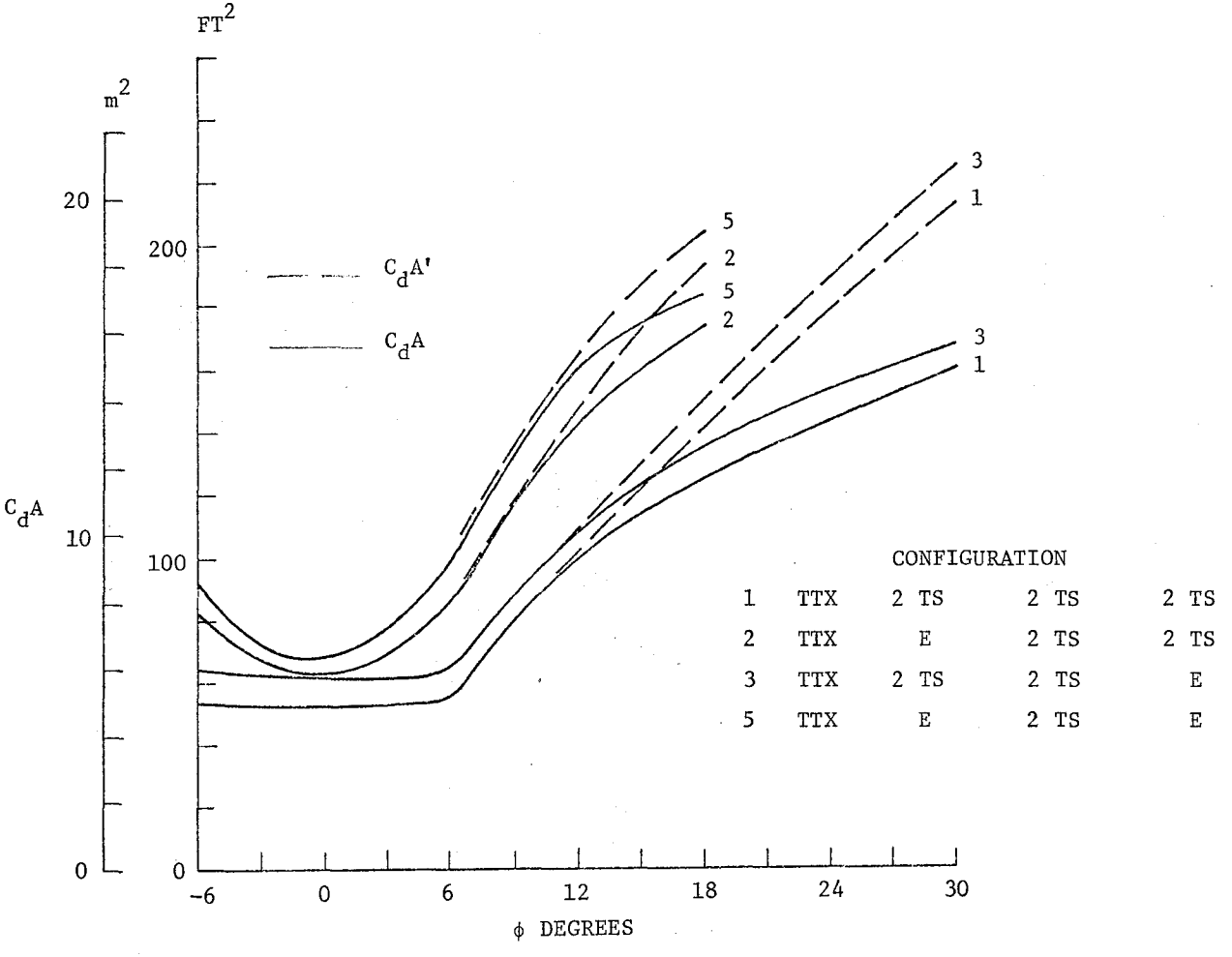

Figure 53. Drag area of TTX cars as a function of angle of yaw. Dynamic pressure based both on full velocity and velocity component along direction of track. Re = 10^6

along the axis of the train. The relation between the two drag areas is as follows

$$C_dA' = \frac{C_dA}{\cos^2 \phi}$$

C_dA' does not show the reverse curvature shown by C_dA. It is obvious that C_dA must go to zero when ϕ is about 90°; however, this is not true of C_dA'. There are reasons to argue whether C_dA or C_dA' would be a better way of presenting the data. They both appear to have advantages and disadvantages. C_dA will be used in presenting the rest of the data, but selection is rather arbitrary and it is useful to understand how a presentation using C_dA' would differ.

For the cases in which the car in front of the metric car is loaded, a pecularity exists in the neighborhood of 6° of yaw. This pecularity exists for many of the different configurations as well as that shown in Figure 52. The drag is essentially flat up to 6° yaw and then rises rapidly thereafter. When this pecularity of the drag data occurs, the yawing moment also appears to be erratic. The reason for this pecularity is not understood. It might be speculated that it is related to the flow separating at about this angle but this has not been established.

Figure 52 shows the results for the trailers facing in the rearward direction compared with forward facing trailers. For all of the different configurations in which all of the trailers are facing rearward, the drag is substantially increased for the higher crosswind angles. However, the drag has about the same value at zero degree yaw as in the forward facing case. If forward facing trailers are placed on the car ahead of the metric car, then an even lower drag is obtained at low angles of yaw. In this case the gap between the cars is formed by the square ended back of one trailer and the back of the trailer on the metric car. One might conclude that trailers with sharp square corners at both ends would be advantageous to reduce the drag at small yaw angles. However, as the angle of yaw increases, and the flow enters the region between the cars, the drag is higher for the sharp corner case.

A comparison of smooth and rough sided trailers is shown in Figure 54. The vertical post trailer has a rougher surface in the direction of flow than the standard trailer. The results of these tests are somewhat mixed. A comparison of fully loaded cars shows an increase in drag when rough sided trailers are placed on the metric car both when all smooth trailers are placed on the preceding car and when the rear trailer on the preceding car is a rough sided one. However, with only one trailer on the metric car, the rough sided trailer gives a lower drag than the smooth sided trailer. The changes are not particularly large, so the general conclusion might be that the smoothness of the trailer is not of particular importance.

Figure 55 shows the effects of only a single trailer on the metric car and some trailers missing on both the surrounding cars. One trailer on the front of the metric car with two trailers on the car in front reduces the drag over that with two trailers on the metric car. The removal of the second trailer reduces the drag more than the increase in the gap behind the existing trailer increases the drag. Increasing the gap further by removal of the trailer on the front of the following car does not seem to have any additional effect. If the single trailer is located on the rear of the TTX car with a gap in front, the drag is almost the same as when two trailers are located on the TTX car. Increasing the size of the gap in front of the trailer by removing the trailer from the rear of the TTX car preceding it gives only a small additional increase. Removing a trailer on each side of the trailer located on the metric car provides the maximum increase in drag. This was done both by removing the trailer from the front of the following car when the trailer on the metric car was in the rear and by removing the rear trailer on the preceding car when the trailer on the metric car was in front. This latter arrangement seemed to produce the larger drag, but it is not clear why this should be so.

For the metric car with one trailer directly behind the trailers on the preceding car, the force is about half that for two trailers. If there is a trailer's width gap directly ahead of one trailer on the metric car, the force is about half that for two trailers on the metric car with the preceding car unloaded.

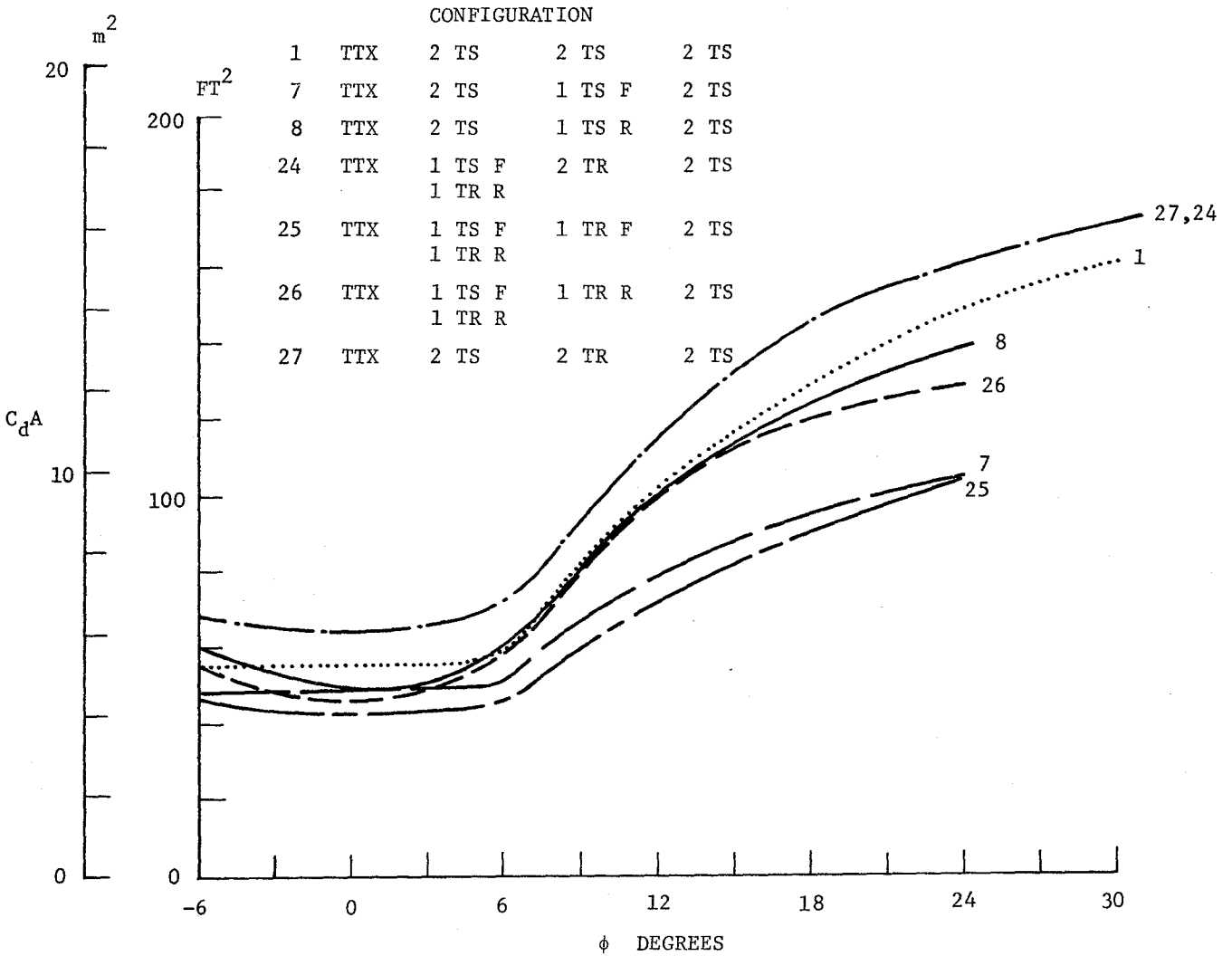

Figure 54. Drag area of TTX cars loaded with rough and smooth sided trailers as a function of angle of yaw. Re = 10^6

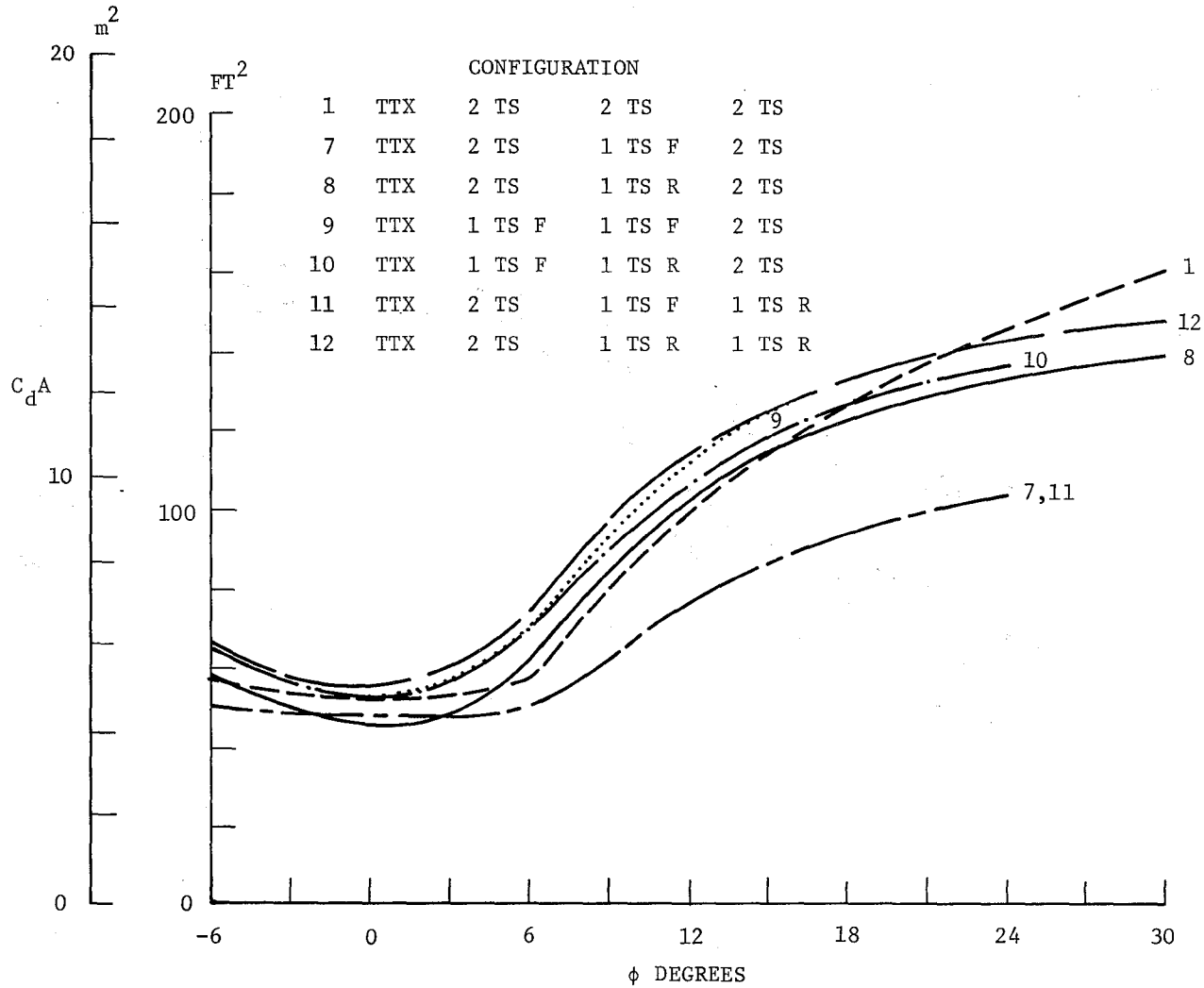

Figure 55. Drag area of TTX cars loaded with one TS trailer in different configuration as a function of angle of yaw. Re = 10^6

The effect of spacing between cars was also investigated. The coupling spacing was changed from the normal value of 60 inches to 30 and 15 inches. The results shown in Figure 56 are that there was no measureable difference between these two configurations. This result should be compared with that found for the basic block tests. To do this, the spacings between the trailers are probably the more critical distances. These distances are 94 inches, 64 inches and 49 inches, respectively. If these distances are expressed in trailer widths they are 0.625, 0.3125, and 0.1562 for the spacing between cars and 0.979, 0.666 and 0.510 for the spacing between trailers. The effect of changing gap spacings for basic blocks is shown in Figures 30 and 31 for 0 and 0.2 corner radii. The corner radius of the trailers lies between these values, at about 0.1. The curves for the drag of the blocks would have led one to expect a decrease in drag as the gap spacing was reduced. The reason this did not occur is not clear. The drag curve with gap spacing is quite flat for the block tests up to a spacing of 0.4. Table 3 shows that the next gap measured was 1 for the 0 corner radius case and 2 for the 0.2 radius case. The change in drag between a gap spacing of 0.4 and 1 shown for 0.2 corner radius is caused by the way in which the curve is faired since there was no measurement at this spacing. In summary, the block tests as presented would suggest some increase in drag at the larger gap, however, the data is not sufficiently detailed so there can be said to be a definite discrepancy.

The tests on a variety of modified car and trailer configurations are shown in Figure 57. Two trailer designs were investigated which seemed to have possibilities in reducing the drag by blocking all or part of the passage underneath the trailer. The first was the moving van with a lower floor and the second was an idealized arrangement with a skirt extending down to the deck of the TTX. The moving van provided some reduction in drag but not a very substantial amount. The trailer with the full aerodynamic skirt gave a much larger reduction in drag, especially at the larger angles of yaw.

Another configuration tested was that of the trailer well car. In this car, the wheels of the trailer were located in a well which was set down between the trucks of the rail car. The trailers were also placed in a back to back arrangement with the fronts of the trailers at the ends of the car. The drag of this car was a little higher than for the standard TTX car with the trailers with full aerodynamic fairings. This result is somewhat surprising since the total height of this car is less

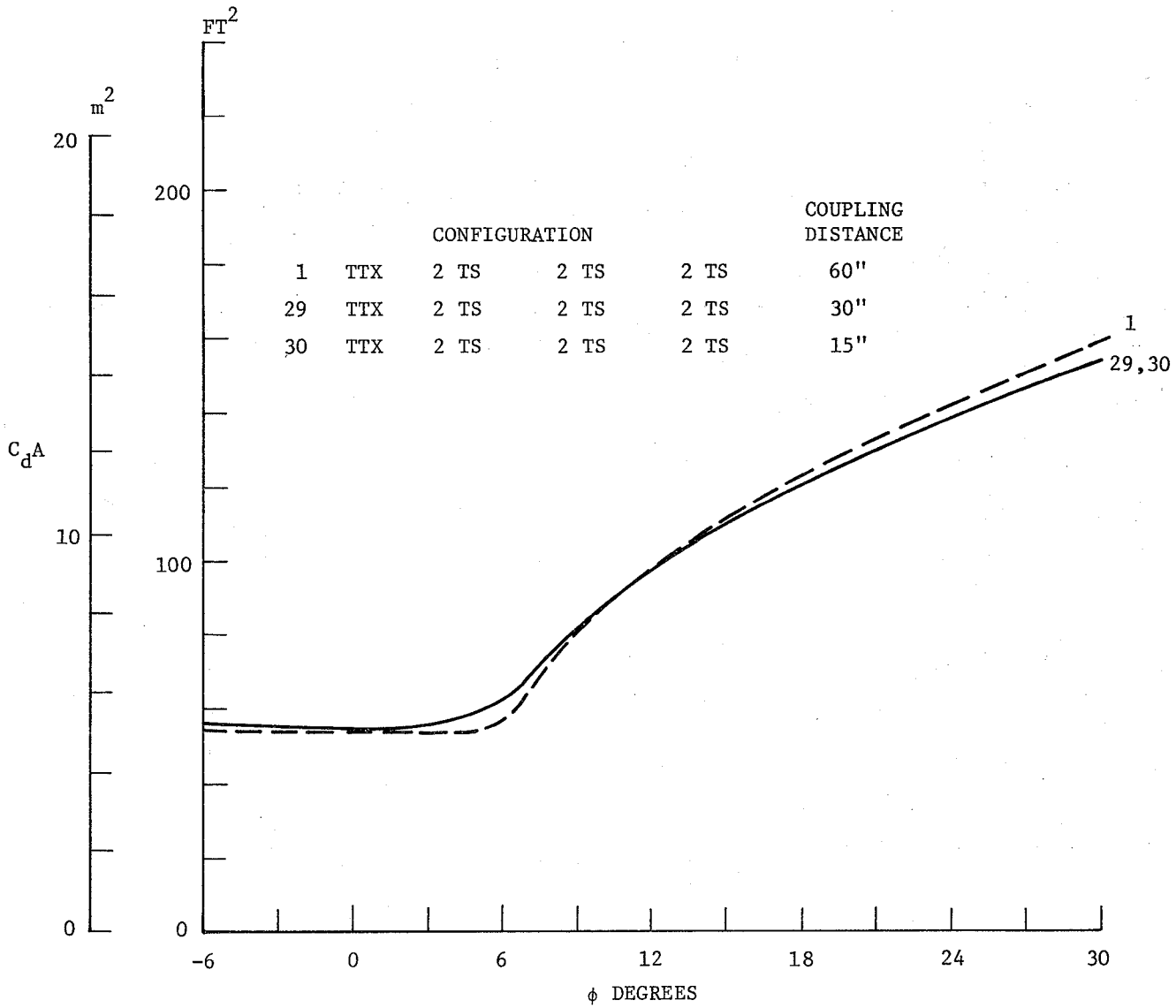

Figure 56. Drag area of TTX cars fully loaded with two TS trailers as a function of yaw angle for different spacings between the cars. Re = 10^6

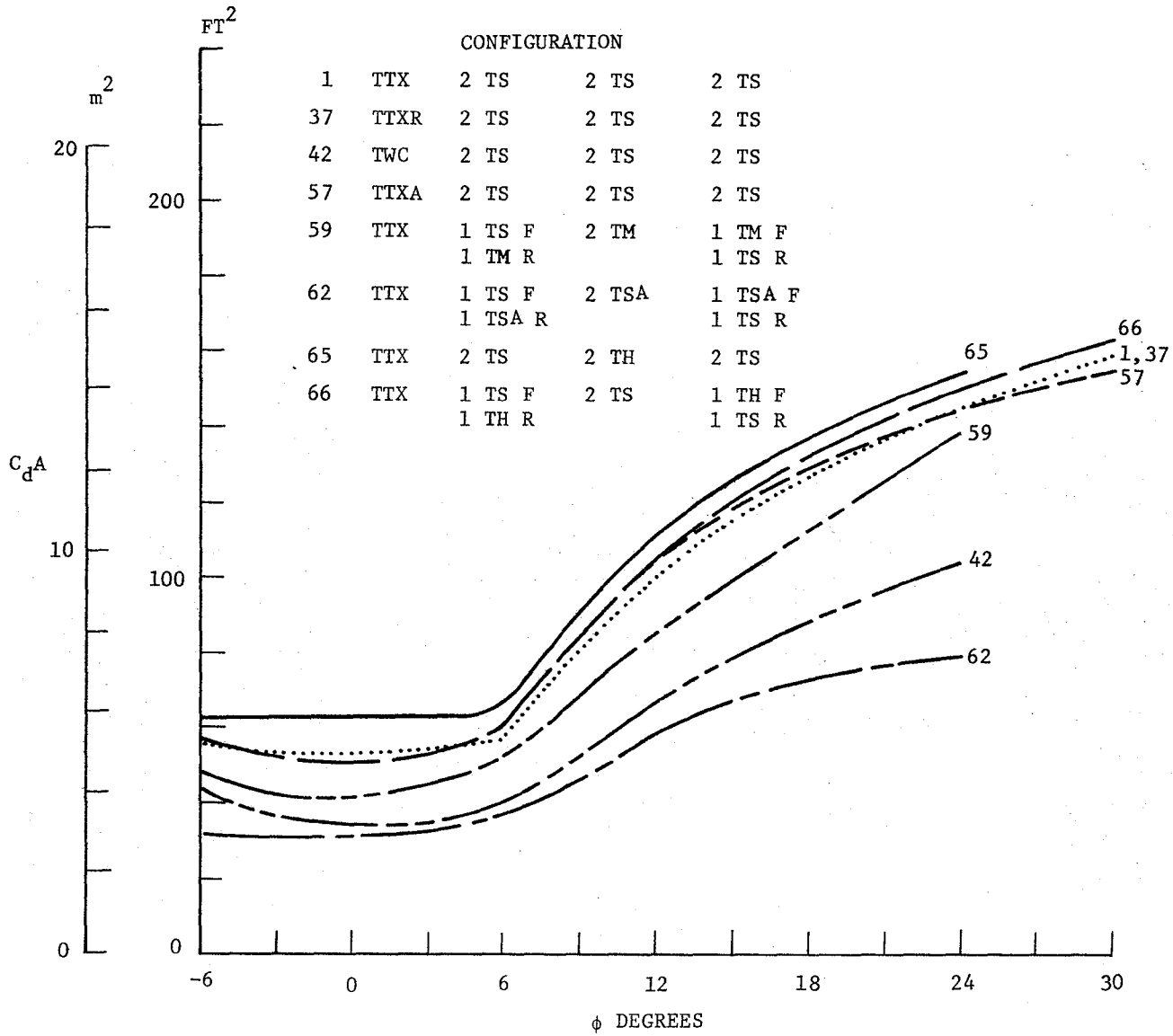

Figure 57. Drag area for a variety of different flat car and trailer combinations as a function of angle of yaw. Re = 10^6

than the loaded TTX car and the passage under the trailer is blocked. One other difference was that the trailers are facing in opposite directions but this should not account for the higher drag.

A streamlined version of the TTX was also tested. The underbody of this car was faired to remove the protuberances which existed in the normal car. However, the test showed no improvement over the standard TTX car design. Apparently there is not much to be gained by changes of this type. However, it should be remembered that the wind tunnel tests may well be less sensitive to such changes than in the actual case because of the inexact simulation of the ground plane.

Tests were also made with trailers which were 1 foot higher on the metric car. This caused only a small increase in drag over the standard trailer. The effect of locating the higher trailers on the ends of the TTX cars ahead of and behind the metric car and locating lower standard trailers on the metric car was also tested. This might be expected to shield the metric car and reduce its drag. However, this did not appear to be the case and the drag was about the same as it was with standard trailers on the cars on each side of the metric car.

Another effect that was considered was that of the bridge plates on the drag. These are plates which are used to provide a bridge between the cars when loading and are normally carried in a vertical position when the train is underway. All of the tests were carried out with these bridge plates removed except for a few tests designed to show the effects of the bridge plates. Figure 57 shows that the effects are quite small. Evidently the flow between the cars was sufficiently retarded so that the presence of the vertical bridge plates did not have an appreciable effect on the trailer drag.

6.2.1.2 Side Forces, Rolling and Yawing Moments

The drag is the aerodynamic force of greatest importance. Of next greatest importance are the side force and rolling moment. The side forces for the standard TTX cars with different arrangements of trailers are shown in Figure 58. The side force is less sensitive to the changes in configuration than the drag force. Figure 58 shows that there is no noticeable change in side force from the standard configuration of fully loaded cars facing forward caused by reversing the cars, unloading the following car, or decreasing the spacing between cars. An increase was

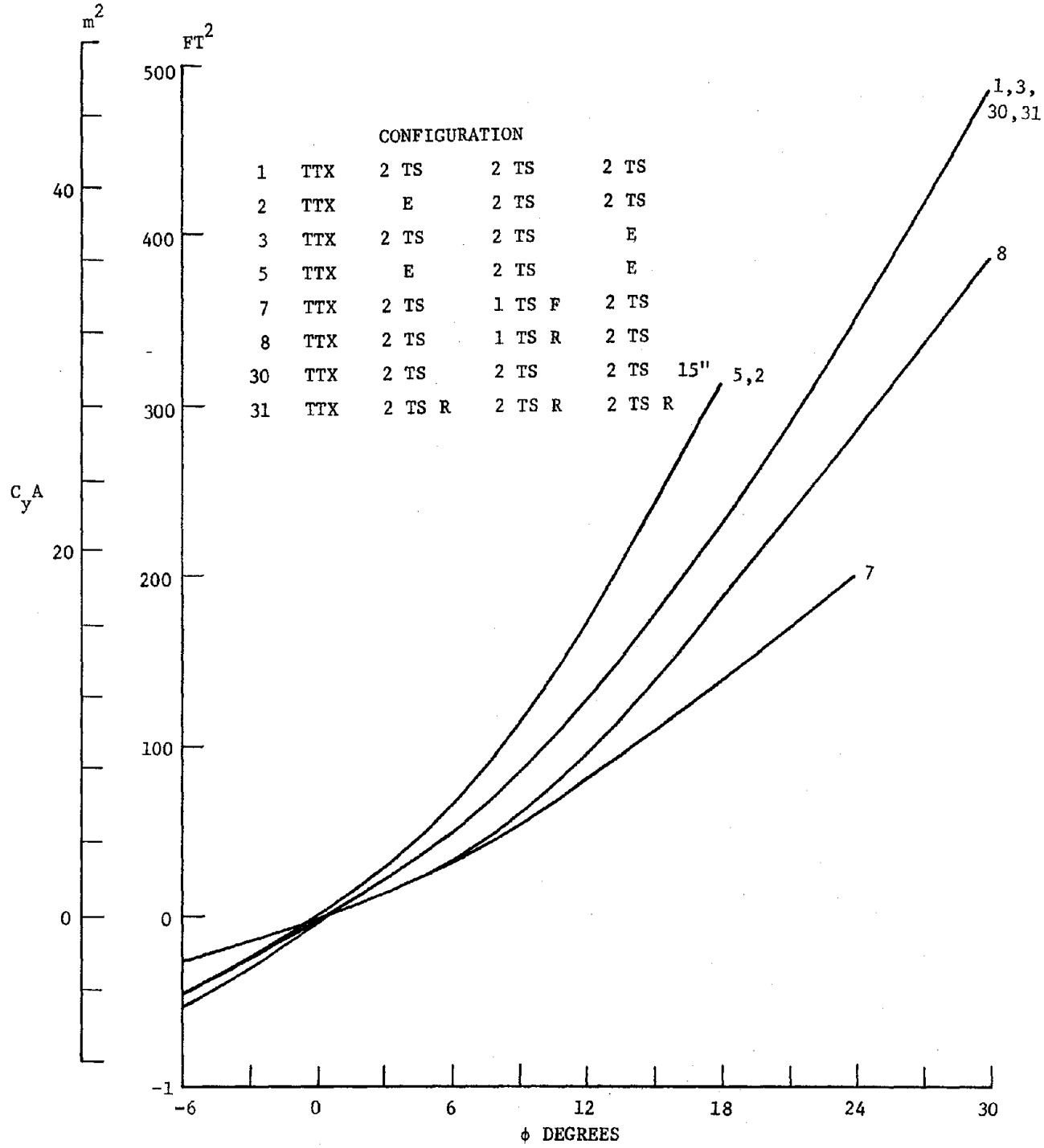

Figure 58. Side force area of a TTX car with different trailer loadings as a function of yaw angle. Re = 10^6

caused by unloading the preceding car. For this case also, the side force was independent of the condition of loading on the following car. The side force on the metric car was decreased by removing one of the trailers. The force was greater when the remaining trailer was located on the rear of the car than on the front of the car.

The side forces for different trailers and rail cars are shown in Figure 59. Replacing the TTX car with the aerodynamically streamlined TTX car had no noticeable effect. However, the trailer well car gives a reduced side load. This should be expected since it has less side area. Different trailers were also tested on the standard TTX car. The moving van and the trailer with a full aerodynamic skirt both showed an increase in side force. The trailer with the full aerodynamic skirt gave the larger side force consistent with the fact that it had the larger side area. The higher trailer also gave some increase in side force over the standard trailer and about equal to that of the moving van.

Rather than presenting the rolling and yawing moments, it seems more meaningful to provide this information by specifying the location of the point of application of the side force as was done for the basic block tests. The vertical location of the point of application of the side force, determined in this way, appears to show no systematic variation with yaw angle. The height depends chiefly on the height of the load being tested; the point of application is quite close to the mean height. Table 7 shows the height at which the side force is applied for the different configurations. The results shown are an average for the configuration at all different angles of yaw. The standard deviation is also shown to indicate the range of the data used in arriving at these average results.

The distance of the point of application of the side force in the longitudinal direction from the centerline of the car is also shown in Table 7. The general result is that for fully loaded cars, the point of application is forward of the centerline by about 5 to 6 feet. If the car preceding the metric car is empty, the point of application is somewhat further forward. If the metric car is not fully loaded, only one trailer at one end, then the point of application of the side force moves towards the loaded end of the car so that it is then near the center of the trailer. The longitudinal location is not as well defined as the vertical location of the point of application of the side force. There appears to be more random variation in the measurement of the yawing moment.

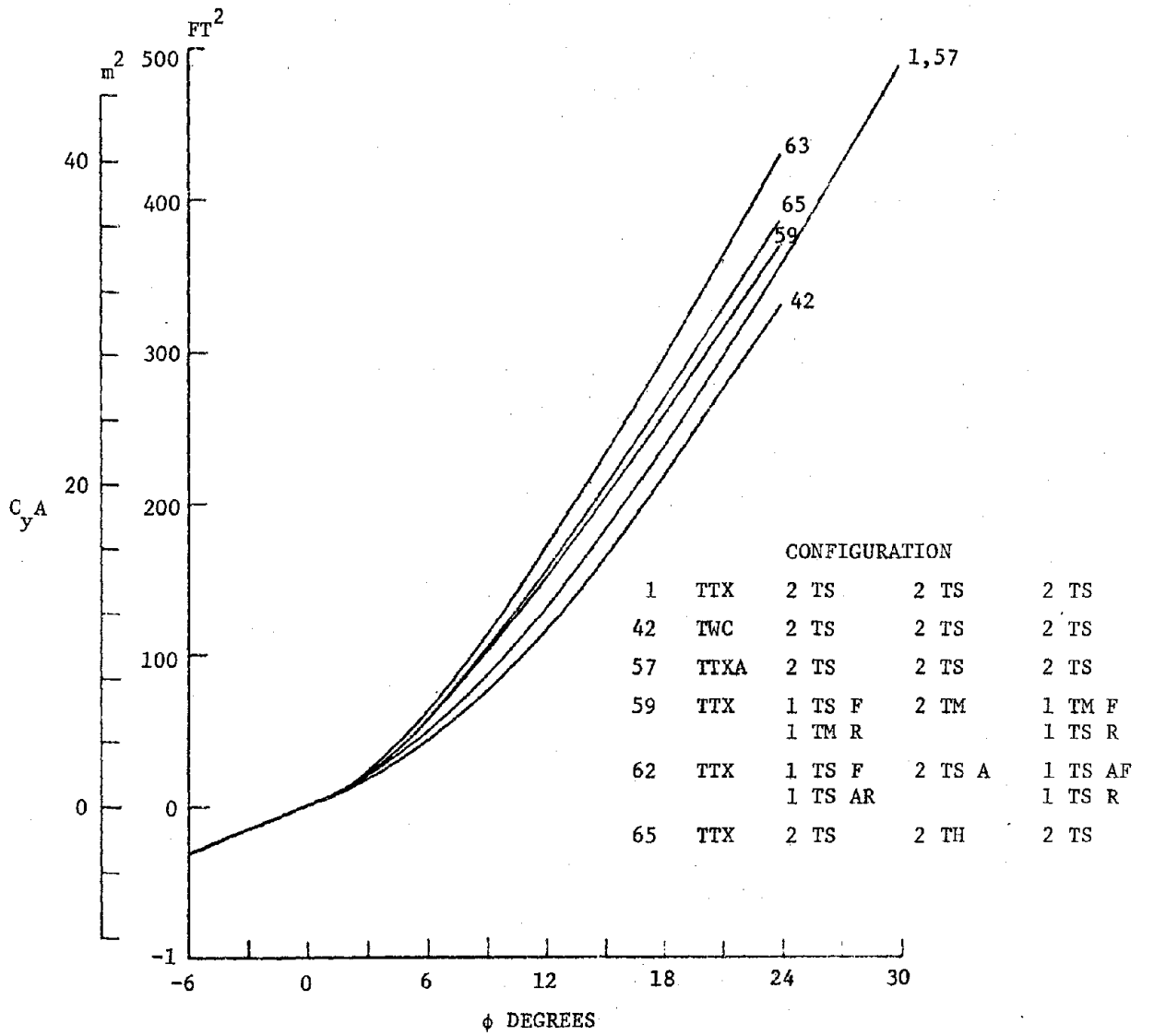

Figure 59. Side force area of a variety of different flat car and trailer combinations as a function of yaw angle. Re = 10^6

TABLE 7. LOCATION OF SIDE FORCE ON RAILROAD CARS

Configuration					Vertical Location of Point of Application				Longitudinal Location of Point of Application			
					Height		Standard Deviation		Distance Forward of Centerline		Standard Deviation	
					ft	m	ft	m	ft	m	ft	m
1	TTX	2 TS,	2 TS,	2 TS	8.2	2.5	.34	.10	not determined*			
2	TTX	E,	2 TS,	2 TS	8.5	2.6	.37	.11	5.9	1.8	1.2	.36
3	TTX	2 TS,	2 TS,	E	8.2	2.5	0.42	.13	not determined*			
5	TTX	E,	2 TS,	E	8.4	2.6	0.51	.16	4.5	1.4	2.7	.82
7	TTX	2 TS,	1 TS F,	2 TS	7.8	2.4	0.31	.09	18.1	5.5	1.0	.30
8	TTX	2 TS,	1 TS R,	2 TS	8.5	2.6	0.33	.10	-17.8	-5.4	2.3	.70
9	TTX	1 TS F,	1 TS F,	2 TS	8.4	2.6	0.62	.19	20.2	6.2	1.6	.49
10	TTX	1 TS F,	1 TS R,	2 TS	8.8	2.7	0.50	.15	-20.2	-6.2	3.6	1.1
13	TTX	2 CS,	2 CS,	2 CS	6.1	1.9	0.17	.05	6.3	1.9	0.8	.24
14	TTX	E,	2 CS,	2 CS	6.1	1.9	0.14	.04	11.6	3.5	1.4	.43
15	TTX	2 CS,	2 CS,	E	6.3	1.9	0.31	.09	6.3	1.9	0.8	.24
31	TTX	2 TS Rr,	2 TS Rr,	2 TS Rr	8.2	2.5	0.51	.16	8.1	2.5	2.0	.61
33	TTX	E,	2 TS Rr,	E	8.4	2.6	0.18	.05	6.4	1.9	2.7	.82
35	TTX	2 TS,	2 TS Rr,	2 TS	8.2	2.5	0.28	.08	5.1	1.6	1.0	.30
43	TWC	2 TS,	2 TS,	2 TS	6.8	2.1	0.18	.05	7.8	2.4	2.4	.73
51	CWC	2 CS,	2 CS,	2 CS	8.5	2.6	0.56	.17	5.6	1.7	0.3	.09
56	CWCA	2 CS,	2 CS,	2 CS	8.9	2.7	1.1	.33	5.1	1.6	0.2	.06
58	TTXA	2 TS,	2 TS,	2 TS	8.2	2.5	.20	.06	-1.4	-.43	2.2	.67

TABLE 7. LOCATION OF SIDE FORCE ON RAILROAD CARS (CONTINUED)

Configuration					Vertical Location of Point of Application				Longitudinal Location of Point of Application			
					Height		Standard Deviation		Distance Forward of Centerline		Standard Deviation	
					ft	m	ft	m	ft	m	ft	m
60	TTX	1 TS F, 1 TM R,	2 TM,	1 TM F 1 TS R	7.9	2.4	.39	.12	3.4	1.0	0.8	.24
63	TTX	1 TS F, 1 TSA R,	2 TSA,	1 TSA F 1 TS R	8.3	2.5	.60	.18	5.9	1.8	0.8	.24
68	TTX	2 CSA,	2 CSA,	2 CSA	6.1	1.9	.23	.07	6.2	1.9	0.9	.27

*Location varies erratically with yaw angle. Data appear unreliable.

Height of standard trailer loaded on TTX car is 16.5 feet (5.03 m).

Height of standard container loaded on TTX car is 12 feet (3.66 m).

Length of TTX car is 90 feet (27.43 m).

6.2.1.3 Lift

The lift area for trailers loaded on TTX cars is shown in Figure 60. It can be seen that the lift force is practically zero at zero yaw angle but increases with yaw angle in a way similar to the side force. The lift is less dependent on changes in loading and configuration than the drag. Removal of the trailers from the preceding and following cars had only a minor effect on lift. Loading the trailers in the rearward direction or use of the high trailers seemed to reduce the lift at 30° yaw angle. Since both of these points depended upon one measurement only, the possibility of error exists. The use of the trailers with the aerodynamic skirts gave a small increase in the lift. The removal of one of the trailers from the metric car considerably reduced the lift. It made little difference whether the forward or rearward trailer was removed. Removal of both trailers reduced the lift even further. While the lift force must be caused by pressures on the horizontal surfaces, the change in pressure clearly depends upon the vertical cross sectional area of the load. The other changes in load configurations, in addition to those shown, were little different than the most closely related cases shown.

The location of the point of application of the lift force is shown in Table 8. These locations have been calculated from the pitching moment by subtracting out the part of the pitching moment caused by the drag and then dividing by the lift force similarly to the method used for the block configurations. For these calculations, it was assumed that the drag force was applied at the mean height of the car plus trailer. The location of the lift force depended critically on the location of the trailer. The location of the lift force is at the trailer or, if two trailers, then somewhat forward of the mean. The values determined are most accurate for the higher angles of yaw. At small yaw angles, especially zero yaw, the calculated locations have considerable scatter. Because the drag force is considerably larger than the lift force at small yaw angles, the position of the point of application of the lift force is not considered reliable and has been left out in preparing Table 8. The location for small yaw angles is of little practical interest since the lift force is so small.

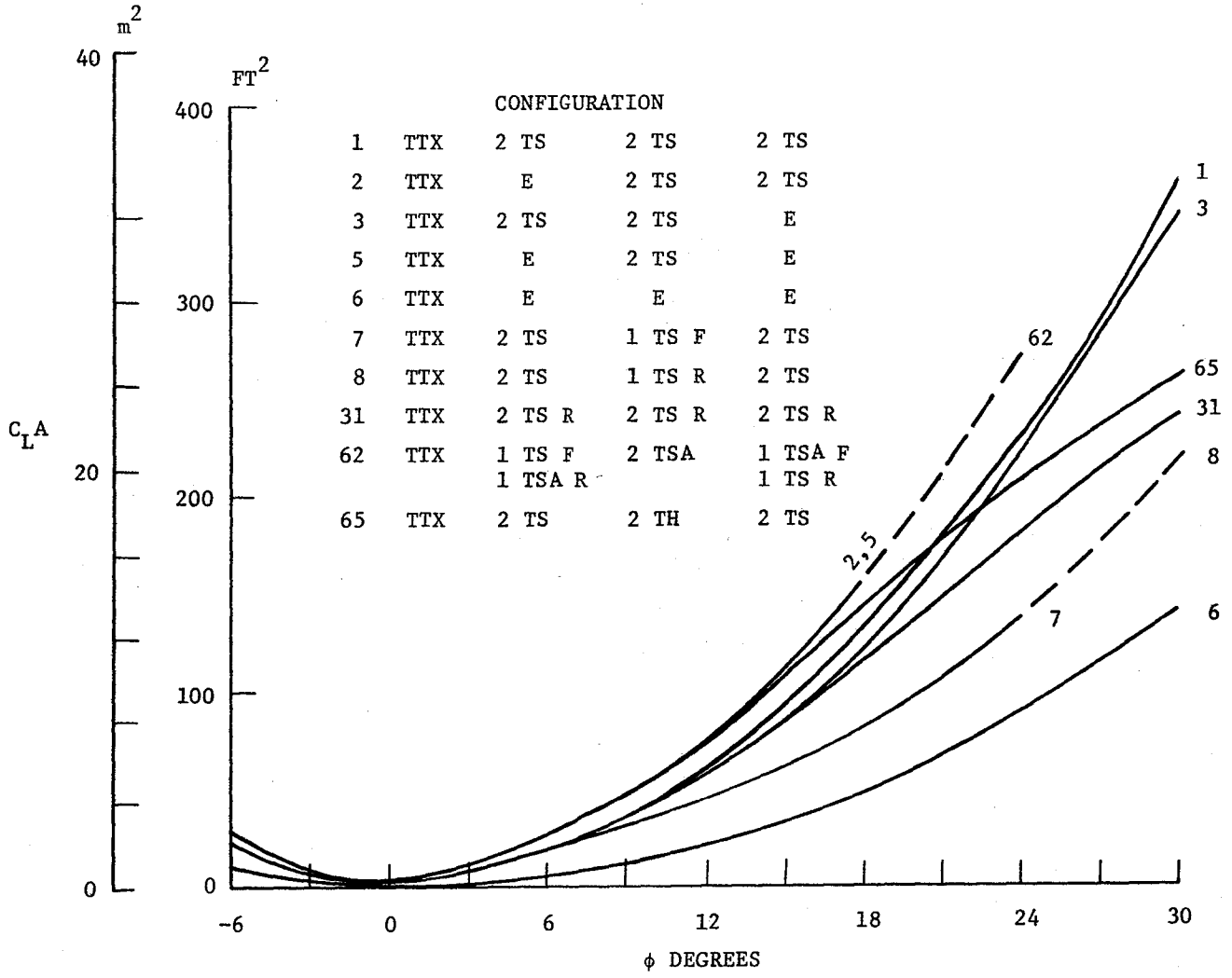

Figure 60. Lift area of a TTX car with different trailer loadings as a function of yaw angle. Re = 10^6

TABLE 8. LOCATION OF LIFT FORCE

Configuration					Longitudinal Location of Point of Application			
					Distance Forward of Centerline		Standard Deviation	
					ft	m	ft	m
TRAILER CARS								
1	TTX	2 TS,	2 TS,	2 TS	4.7	1.4	2.2	.67
5	TTX	E,	2 TS,	E	4.8	1.5	1.2	.36
7	TTX	2 TS,	1 TS F,	2 TS	12.4	3.8	8.5	2.6
8	TTX	2 TS,	1 TS R,	2 TS	-10.3	3.2	3.4	1.0
CONTAINER CARS								
13	TTX	2 CS,	2 CS,	2 CS	0.1	.030	1.5	.46
17	TTX	E,	2 CS,	E	2.7	.82	3.4	1.04
18	TTX	2 CS,	1 CS F,	2 CS	15.5	4.7	4.7	1.43
19	TTX	2 CS,	1 CS R,	2 CS	-19.5	-5.9	2.7	.82
51	CWC	2 CS,	2 CS,	2 CS	-9.8	-3.0	3.9	1.19
56	CWCA	2 CS,	2 CS,	2 CS	.9	0.27	1.6	.49

Length of TTX car is 90 feet (27.43 m).

6.2.2 Containers

6.2.2.1 Drag

A similar set of tests has been run using containers. Tests were run using the TTX car and a container well car. Figure 61 shows test results for fully loaded TTX cars with different mixes of full and empty cars. The most important result is that the drag forces on containers are considerably less than on trailers. The vertical scale used in this figure is twice as large as that used in Figures 51 through 57 for trailers. The reduced drag of containers has been well known and had previously been measured by full scale tests on railroads. The effect of using the component of the wind velocity in the direction of motion of the trailer to calculate the dynamic pressure is also shown on this figure as was done in Figure 53. The flattening of the curves at the higher yaw angle is removed by this way of plotting. The results for containers are similar to those found for trailers in that the removal of containers from the car following the metric car does not cause as large an increase in drag as the removal of the containers from the preceding car. The curve for the fully loaded train has the same flattened shape at low angles of yaw.

Figure 62 shows results for only one container on the metric car and different loadings on the other cars. The results are generally similar to those found for trailers. An open space in front of the container on the metric car gave a larger drag increase than an open space behind. A single container in the forward position behind a fully loaded car had a lower drag than a fully loaded car showing that the reduction in drag caused by the removal of the rear container was larger than the additional drag caused by the open space behind the container. However, the removal of the container would cause additional drag on the following car so that there is really no advantage in removing the container from the rear position as opposed to the forward position.

The container well car which has been suggested by the Southern Pacific was also tested. This is a shorter car with two containers stacked vertically in the well between the two wheel trucks. The drag of

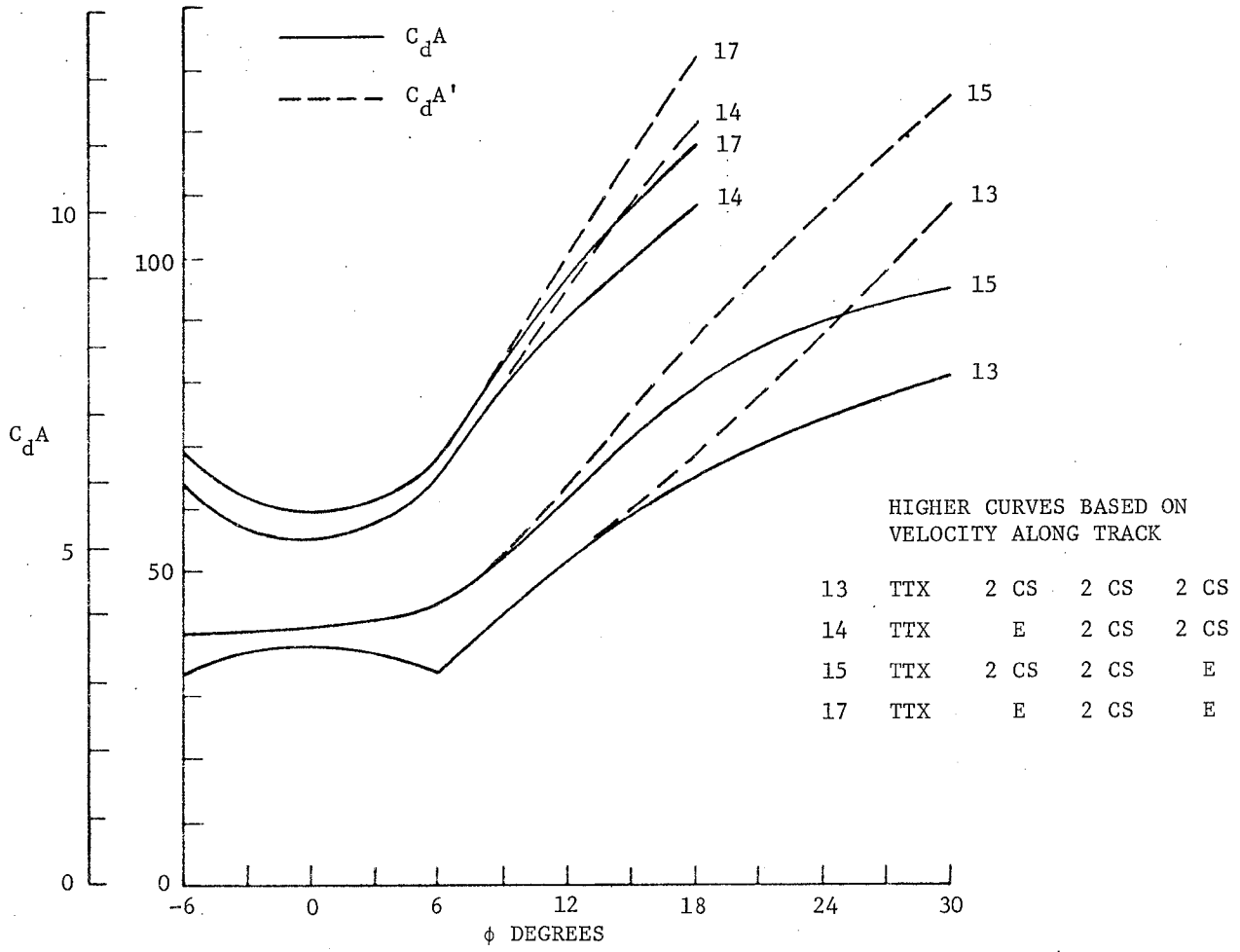

Figure 61. Drag area of TTX cars loaded with containers as a function of yaw angle. Dynamic pressure based on both full velocity and velocity component along track. Re = 10^6

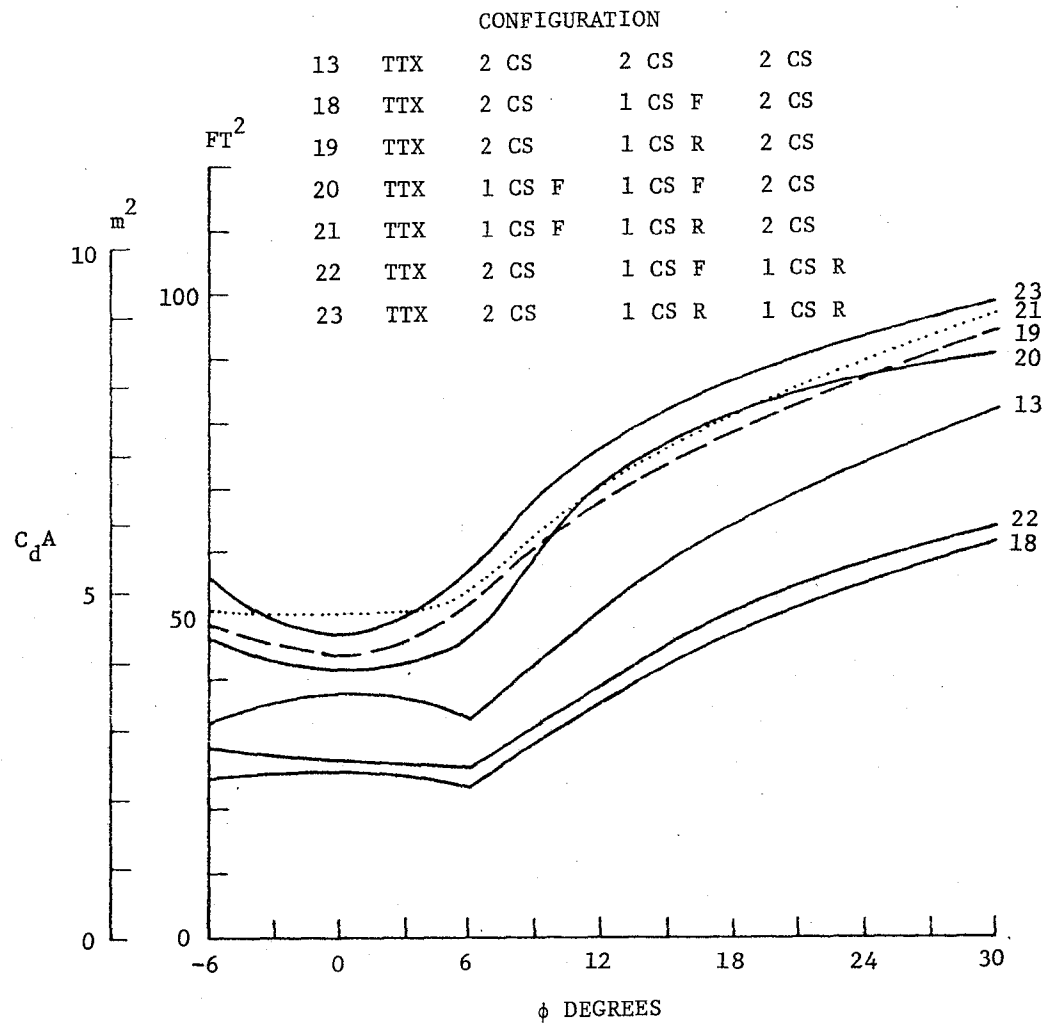

Figure 62. Drag area of TTX car loaded with one CS container in different configurations as a function of yaw angle. Re = 10^6

the fully loaded car, Figure 63, was considerably higher than the fully loaded TTX car shown in Figure 61; however, the drag of the empty car was less than the empty TTX car, Figure 52. Both of these results could have been anticipated because of the greater height of the loaded car and the reduced length which is important in reducing the drag of the empty car. The increase in drag caused by partial loadings was less with this car than the TTX car. If a partially loaded train can consist of one container per car, the drag will be considerably reduced. It might be anticipated that the high drag of this car is caused both by the height and the large open spaces between the containers on successive cars. Two methods of reducing this drag were considered. First a set of containers with rounded leading edges was used. This caused a small reduction in the drag, Figure 64. The second method tested was to provide blocks on each end of the car to fill part of the space between the cars and to provide a rounded leading edge. This change cut the drag dramatically, almost down to the empty car drag of the container well car. These fairings seem to provide a very aerodynamically efficient train in the loaded condition. However, if the car with the aerodynamic fairing in place was operated unloaded, the aerodynamic drag was very high, higher than any other container configuration tested. From an aerodynamic drag point of view the container well car offers very interesting possibilities. If the aerodynamic fairings can be used and either empty operation avoided or the fairing removed during empty operation, a very low drag system would be obtained.

Figure 65 also shows comparisons with the other models that were used to test the effect of streamlining containers and the associated cars. The use of a rounded front edge on the containers on a TTX car caused an effective drag reduction but not as large as on the container well car. The streamline TTX car in which the protrusions on the underbody were removed caused no noticeable drag reduction. This is consistent with the effects found when this car was used with trailers.

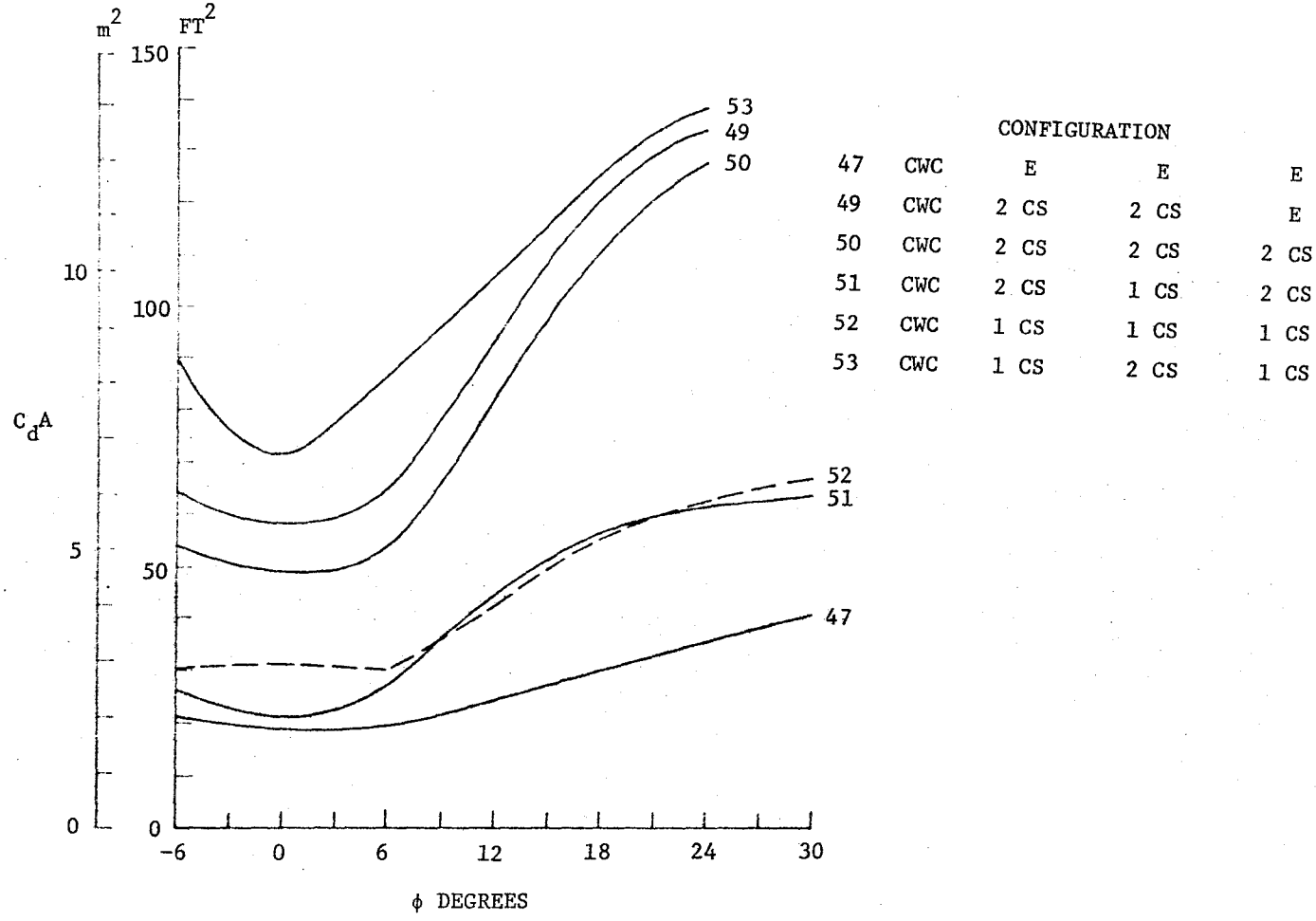

Figure 63. Drag area of container well car with different loadings of containers as a function of angle of yaw. Re = 10^6

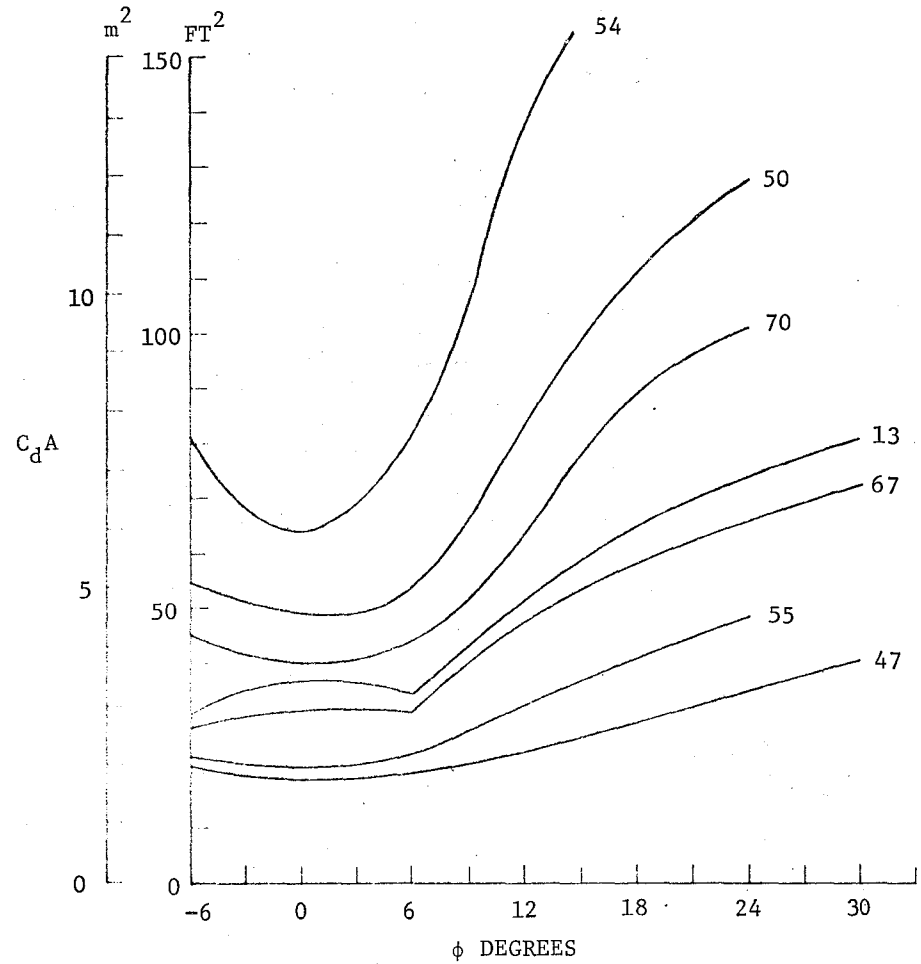

		CONFIGURATION		
13	TTX	2 CS	2 CS	2 CS
47	CWC	E	E	E
50	CWC	2 CS	2 CS	2 CS
54	CWCA	E	E	E
55	CWCA	2 CS	2 CS	2 CS
67	TTX	2 CSA	2 CSA	2 CSA
70	CWC	2 CSA	2 CSA	2 CSA

Figure 64. Drag area of TTX and container well car with various containers and loadings. Re = 10^6

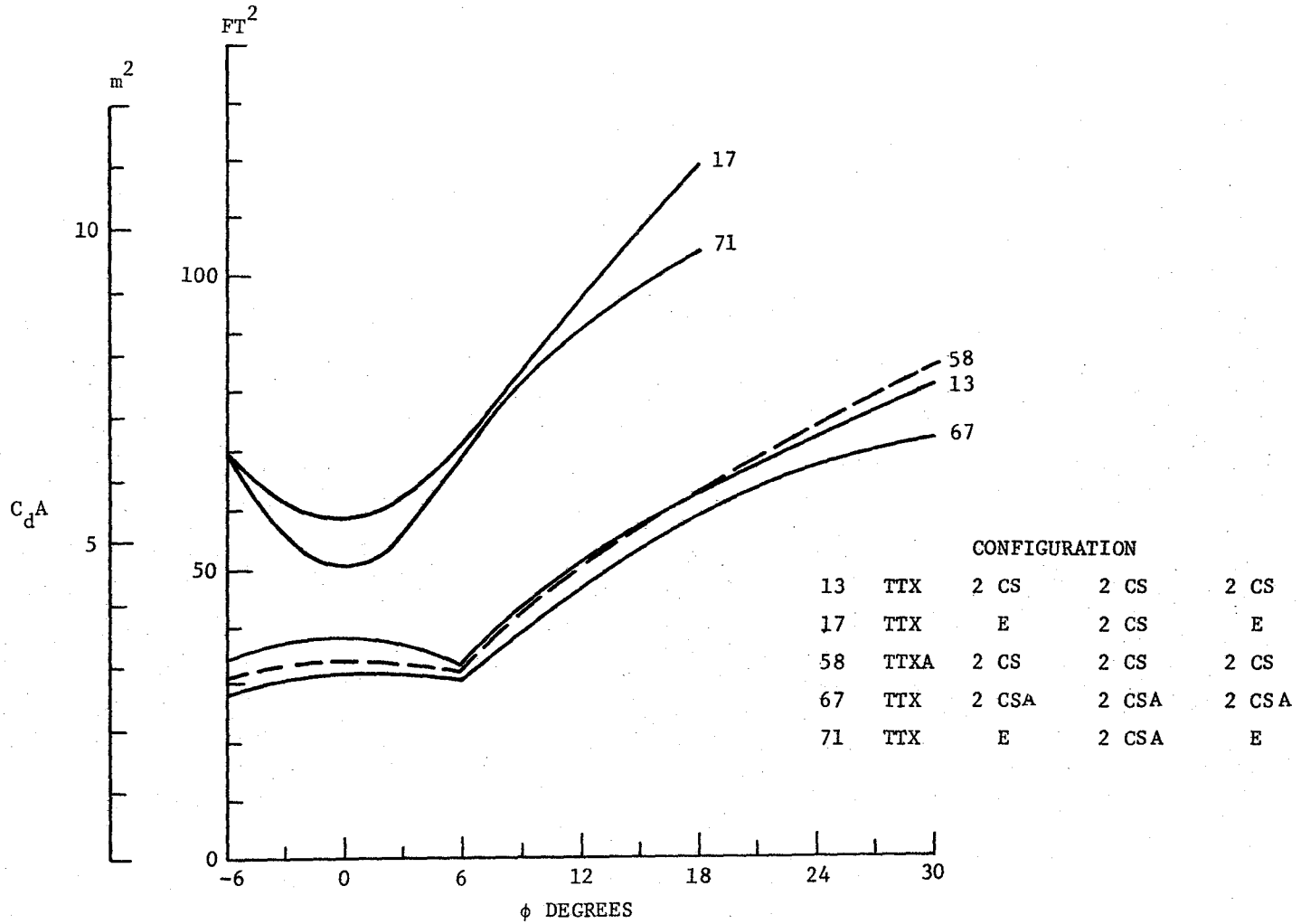

Figure 65. Drag area of TTX type flat cars with different containers loadings as a function of yaw angle. Re = 10^6

6.2.2.2 Side Force

The side force on the different container configurations is shown in Figure 66. Configurations with the same lateral area gave about the same side force. The side force was considerably lower than that on the trailers as might be expected with the lower loads. The TTX car with either the regular or rounded nosed containers gave the lowest side force. The stack car with or without the aerodynamic fairings gave a somewhat higher side force. While the lateral area of this configuration was less than the loaded TTX car, the increased gaps between the cars caused an increase in side force as was shown by the basic block tests. The addition of the aerodynamic fairings caused a considerable increase in lateral area but only a small increase in side force because the gaps between the cars were reduced.

The rolling and yawing moments data has been expressed as the location of the point of application of the side force. These results are contained in Table 7 and are very similar to those found for the trailers.

6.2.2.3 Lift

The lift forces on the cars loaded with containers are shown in Figure 67. The results for the TTX car loaded with different container configurations were similar to what would be expected from the results with trailers. The lift forces appeared to be slightly less than those measured on the trailers but the difference was hardly significant. Similarly to the trailers, the removal of one container reduced the lift considerably and it did not matter whether the forward of rearward container was removed. The results found for the container well car with two containers stacked on top of each other were interesting. This car had a smaller planform area but the load was higher than for the standard TTX car. For the container well car without fairings, the lift was almost equal to the values measured with only one container on the TTX cars. However, when the aerodynamic fairings were added to the car, the lift was increased to about the same values found for two containers on the TTX cars. The reduction in planform area seemed to be compensated by the increase in lateral area.

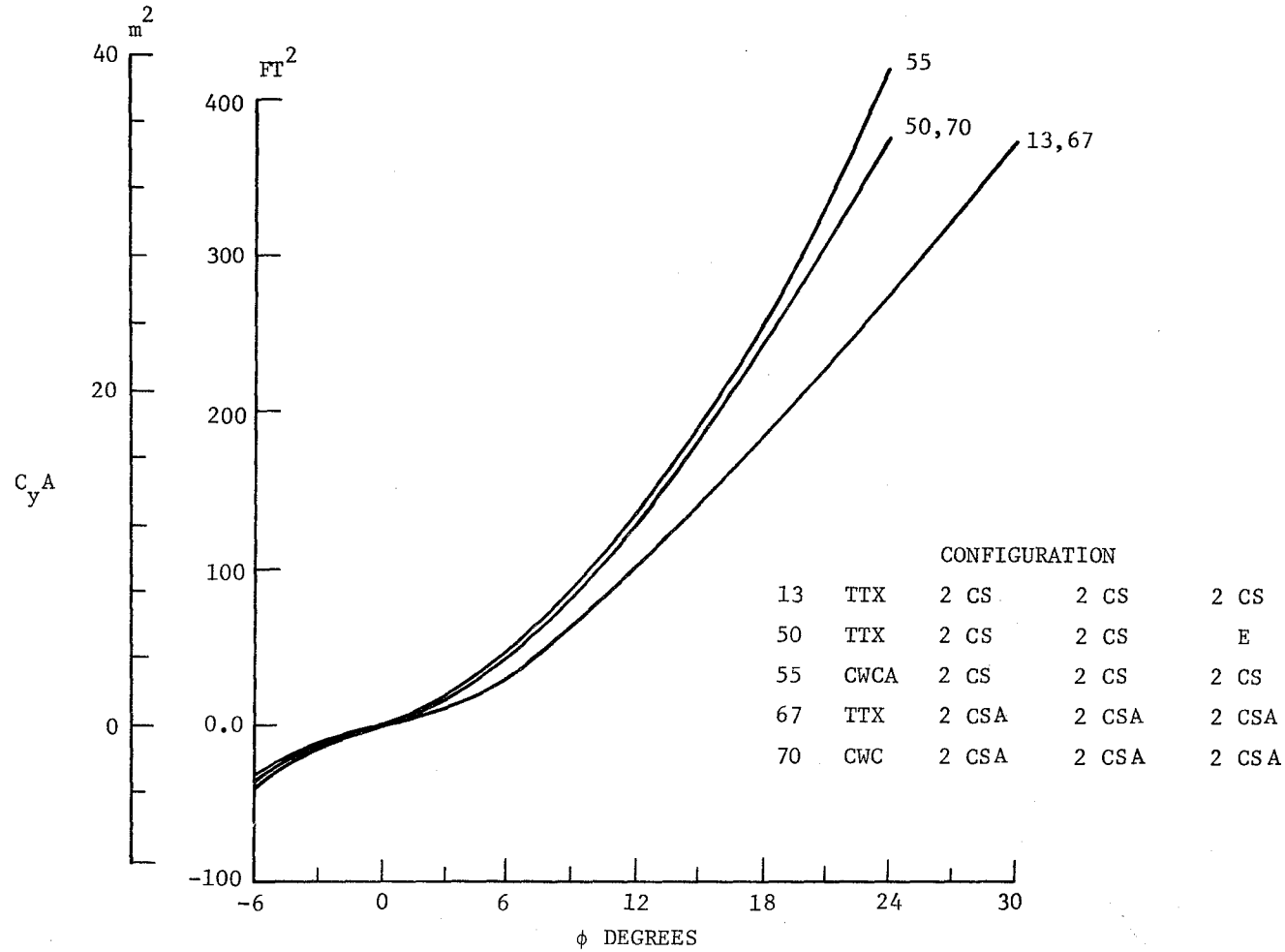

Figure 66. Side force area of various container car and container configurations as a function of yaw angle. Re = 10^6

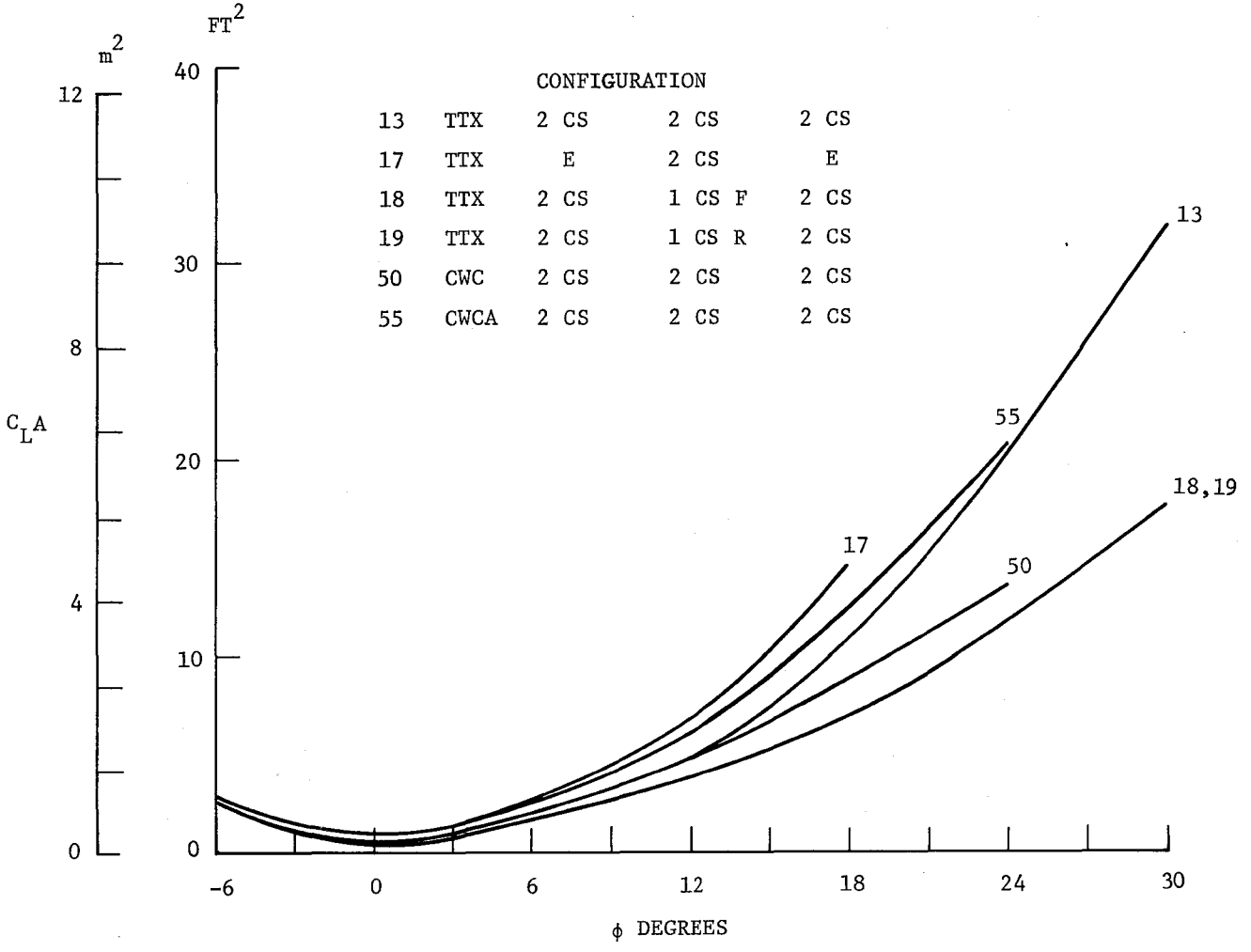

Figure 67. Lift area for various container car and container configurations as a function of yaw angle. Re = 10^6

For containers, the center of pressure for two containers on a TTX car seemed to be very near the center of the car (Table 8). There was also no effect from changing the loads on the surrounding cars. The removal of one of the containers moved the point of application of pressure towards the remaining container. The point of application for the container well car depended upon whether the aerodynamic fairings were used. When the fairings were used, the point of application was almost in the center of the car. When the fairings were removed, the point of application moves rearward almost 10 feet.

7. RESULTS AND FULL SCALE COMPARISONS

The purpose of the basic block tests was to provide information on the forces on a block located in a series of other blocks as a function of angle of yaw, block spacing, and nose radius. The primary result was that the gap widths up to about half the block width had small effect on the forces, but as the spacing was increased further the forces changed and eventually approached that of an individual block for large enough gap sizes. There was very little effect of angle of yaw on drag until the gap spacing was greater than half the width and there was little change in side force and drag from that with the minimum gap until the gap exceeded half the width. Rounding the nose of the block tended to increase the drag slightly for the gap sizes less than the half block width and decreased the drag for greater gap sizes. It would appear that the flow was not appreciably entering the gaps at small gap size and the corner radius just increased the effective roughness of the gap. At larger gap sizes the flow entered and the larger nose radius became beneficial.

The tuft pictures show that the flow along the blocks at angle of yaw was deflected from the freestream direction to lie almost along the direction of the blocks. The metric block was not only shielded by the viscous wake from the preceding blocks but the downwash effect generated by the side forces on these blocks reduced the effective angle of yaw on the metric block as well as deflecting the viscous wake so that it was not swept off directly in the downstream direction.

The effect of surface roughness was not very large and seemed to vary between the different configurations. The data showed a decrease in drag with increased roughness at small gaps and large nose radius and an increase under other conditions. It is felt that this is a sufficiently involved question that more tests are needed to fully understand the mechanisms involved. The present tests are only adequate to show the magnitude of the effects.

The effect of rounding on the side corners and of rounding the rear corners was also considered. The results showed that most of the effects obtained by rounding the corners were associated with the vertical and not the horizontal corner and this was particularly true at angles of yaw. Rounding of the rear corners appeared to increase the drag particularly at the larger gap sizes. Apparently any effect which the rounding had on encouraging the flow to fill in behind the block and thereby reduce the base drag was more than overcome by increased nose drag on the following block.

The tests on the standard TOFC and COFC car configurations showed reasonable agreement with values in the literature that was discussed in Section 2. The following table shows the comparison.

	C_dA	
	Ft^2	m^2
TOFC (C and O tests)	63	5.85
TOFC (EL tests)	78	7.25
TOFC (wind tunnel test 0° yaw)	53	4.92
COFC (NYC tests)	37	3.44
COFC (wind tunnel test 0° yaw)	35	3.25

The wind tunnel tests showed a major increase in drag caused by angle of yaw. It is hard to know what the yaw angle was for the railroad tests. It seems reasonable that they contain some effect of yaw angle and, therefore, might be expected to show higher drag than the wind tunnel 0° yaw

angle results. Considering the uncertainties, the comparison is surprisingly good.

For a train, a yaw angle can only be created by a crosswind. Figure 68 has been drawn to show the effect of a wind blowing at different angles with respect to the track based on the wind tunnel tests for Configuration 1. It may seem surprising that a crosswind causes a larger increase in drag than a headwind of the same velocity. A wind at 65° from the direction of the track of about 1/4 the velocity of the train more than doubles the drag while a headwind of the same velocity only increased the drag by about 50 percent. Since the wind has such an important effect, it is impossible to make accurate predictions of the resistance of a train without accurate predictions of the wind.

The tests showed that empty spaces along the train and the direction in which the trailers were facing had important influences on the aerodynamic drag. Having all of the trailers facing in the rearward direction increased the drag of the train by about 10 to 15 percent over most of the range of yaw angles (Figure 52). Only at 0° yaw angle was there little effect. Empty spaces in the loading increased the drag on the surrounding cars. An unloaded following car had only a small effect but an unloaded preceding car had a much larger effect (Figure 52). However, the drag on the unloaded cars was considerably reduced. At a yaw angle of 6°, a train of alternately loaded and unloaded cars has about the same drag as a completely loaded train, but the same cars arranged so that the loaded and empty cars were grouped together would have about 30 percent less drag than the fully loaded trains. Additional information on the effect of empty spaces in the train is given in Figure 55 for which loadings of only one trailer on the metric car were used. Configurations 7 and 11 are for one and two trailers missing behind the trailer on the metric car. The difference between 1 or 2 spaces had no measurable effect and these configurations gave the lowest drag of any one trailer on the metric car configurations tested. Configuration 8 is for one trailer on the metric car with one empty space ahead, and Configuration 10 has two empty spaces ahead. Empty spaces ahead gave a higher drag than empty spaces behind, and one empty space was almost the

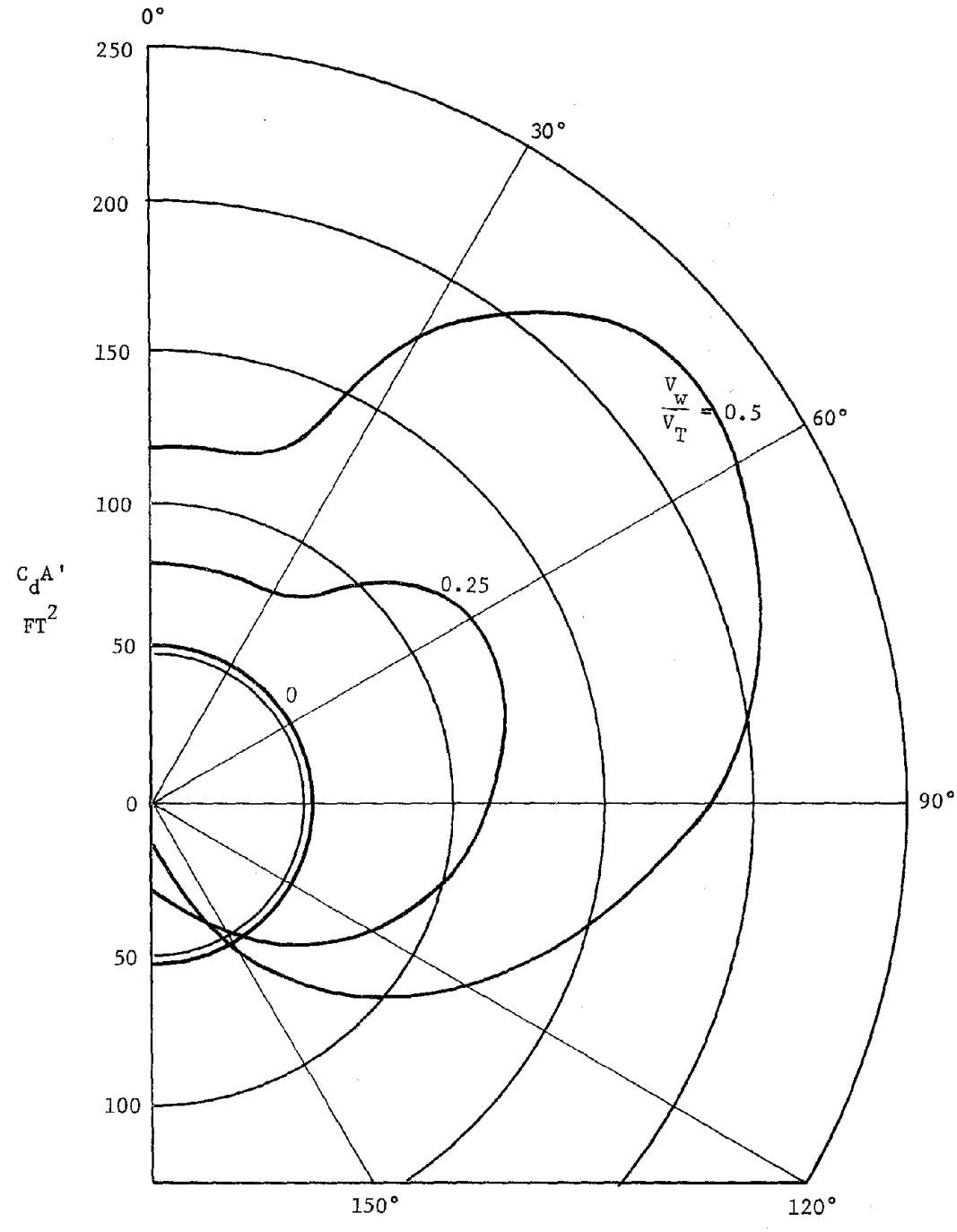

Figure 68. Polar diagram of drag area using dynamic pressure based on train velocity as a function of wind direction strengths. Re = 10^6

same as two. One empty space ahead of a trailer gave a car with only one trailer about the same drag as a car with two trailers. A train loaded with only one car per trailer with all of the trailers on the front or back of the cars is the highest drag arrangement for transporting that number of trailers. Any arrangement that groups the trailers closer together is an improvement.

A rough surface on the trailers does increase the drag (Figure 54). Decreasing the coupling distance from the nominal value of 60 inches between car faces seemed to have little effect on the drag (Figure 56). This seemed to be somewhat of a contradiction to the basic block tests. When the cars were 60 inches apart the trailers were almost 8 feet apart, or about one trailer width. Figure 30 shows a definite increase in drag when sharp cornered blocks were one width apart. With the corner radius of 0.2 (Figure 31), no tests were run at one width apart so one must judge using results of 0.4 and 2 only. Certainly the 60 inch spacing must be near the maximum for not causing a drag increase.

Several modifications of trailers and cars were tested (Figure 57). The trailer well car (Figure 18 and Configuration 42), showed a considerable decrease in drag over the standard TTX car. However, the streamlined TTX car, Figure 17 and Configuration 57, showed no effective improvement. Two modifications of trailers were tested which were felt might improve the aerodynamics. One trailer patterned after a moving van, Figure 22 and Configuration 60, showed a definite but not very substantial improvement. Another more radical modification, Figure 22 and Configuration 63, which had a fairing going completely to the deck of the car gave a substantial reduction in drag. The conclusion is that some means of covering over the openings at the sides of the trailers reduces the drag by an amount that can be substantial.

Two other modifications were tried and are shown on this figure. One which increased the height of the trailer from 13 to 14 feet, resulted in an increase in drag roughly proportional to the increase in height. Another modification was to mount the bridge plates on the TTX car in the vertical position, Configuration 37. Somewhat surprisingly this resulted in no measurable change.

The results for containers were very similar to those found for trailers. The use of containers gave a substantial reduction in drag to about 2/3 that for trailers and the zero yaw drags seemed to be in reasonable agreement with results obtained by rail tests as has already been discussed. The effect of yaw was substantial and similar to that for trailers.

From an aerodynamic point of view, the vertically stacked container well car, Figure 19 and Configuration 50, had interesting properties. Cars of this type loaded with two containers had more drag than the standard TTX car, but the removal of one container did reduce the drag substantially (Figure 63). Figure 64 shows various combinations using this well car both with containers with rounded forward corners and with a fairing placed on the ends of the well car. The effect of the fairing was quite dramatic. It produced a very low drag loaded car and a very high drag empty car.

Side forces and lift forces were quite similar between the containers and the trailers. They both depended substantially on crosswind or yaw angle. Side forces on trailers are shown in Figures 58 and 59. The magnitude of the force depended upon the side area and whether there was a trailer in the position ahead. The results for containers (Figure 66) were similar. A rolling moment was developed for both configurations which was equivalent to the side force being applied at the mid height of the car plus load. The longitudinal location of the side force was about in the longitudinal center of the car plus load. For a completely loaded car it was about in the middle and for a car with a load on only one end it was shifted towards the loaded end. The lift forces followed the same pattern as the side forces. It is the wind blowing across the train that causes the lift and not the wind along the train. The higher the load the larger the lift force. The location of the lift force was similar to the side force. It was about in the center of the car for a symmetric load and moved towards the loaded end with an unsymmetric load.

REFERENCES

1. Schmidt, Edward C., University of Illinois Bulletin #43, 1910.

2. Davis, W. J. Jr., "The Tractive Resistance of Electric Locomotives and Cars," General Electric Review, October 1926, pp. 685-707.

3. Report of the Electric Railway Test Commission, New York, N. Y. to the President of the St. Louis Louisiana Purchase Exposition, McGraw Hill Publishing Company, New York, 1906, Library of Congress TF 857 S14, pp. 488-574.

4. Tietjens, O.G. and Ripley, K. C., "Air Resistance of Trains and Interurban Cars," Trans ASME, Vol. 54, 1932.

5. Klemin, Alexander, "Aerodynamics of Railway Trains," Railway Mechanical Engineer, Part II, September 1934, Part III, October 1934.

6. Johansen, F. J., "Air Resistance of Passenger Trains," The Institute of Mechanical Engineers Proceedings, Vol. 134, 1936, pp. 91-208.

7. Gross, W. F. M., "Atmospheric Resistance to the Motion of Railway Trains," The Engineer, Vol. 86, August 12, 1898, pp. 164-180.

8. Lesher, E. J., "Wind Tunnel Study of Streamlined Passenger Trains," Tech Report M883, University of Michigan, Ann Arbor, Mich., February 1951.

9. Burlage, Harry Jr., "The Drag of Railway Cars of New Design," Case Institute of Technology, 13 December 1954.

10. Hara, T., Kawaguti, M., Fukushi, G., and Yamomota, A., "Aerodynamics of High Speed Trains," High Speeds Symposium, Vienna International Railway Congress Association Bulletin vol. 45, No. 11, 1969.

11. Bernard, M., "A New Means of Studying Railway Aerodynamics Problems. The Long Wind Tunnel at the Saint-Cyr L'Ecole," Revue Generale des Chemins de Fer, December 1973.

12. Matthews, J. T. and Barnett, W. F., "Wind Tunnel Tests of a Scale Model Railroad Automobile Pack Car," NTIS PB 180 198, June 1968.

13. Luebke, R. W., "Evaluation of TOFC Aerodynamic Resistance," Research Services Report, Planning Department, The C&O-B&O Railroad Company, August 11, 1966.

REFERENCES (Continued)

14. "E - L Test Piggyback, Rack Car Resistance," Railway Locomotives and Cars, October 1966, pp. 23-54.

15. Kaelin, C. R., The Atcheson Topeka and Santa Fe Railway Company, Private communication, October 1974.

16. "Economics of Plant Equipment and Operation," Manual for Railway Engineering, American Railway Engineering Association, Chicago, Illinois, Chapter 16.

17. Hoerner, S. F., Fluid-Dynamic Drag, Hoerner Fluid Dynamics, Box 342, Brick Town, N. J., 1958.

18. Hammitt, A. G., The Aerodynamics of High Speed Ground Transporation, Western Periodicals Co., 13000 Raymer St., North Hollywood, CA 91605 1973.

19. Tuthill, J. K., "High Speed Freight Train Resistance: Its Relation to Average Car Weight," University of Illinois Engineering Bulletin, 376, 1948.

20. Luebke, R. W., "Economics of Railroad Automobile Rack Car Aerodynamic Drag," NTIS PB 183-845, March 1969.

21. O'Leary, R.J., Southern Pacific Transportation Company, Private communication, May 1975.

22. Grunwald, K. J., "Aerodynamic Characteristics of Vehicle Bodies at Crosswind Conditions in Ground Proximity," NASA TN D-5935, August 1970.

23. Turner, T. R., "Wind-Tunnel Investigation of a 3/8 Scale Automobile Model Over a Moving Belt Ground Plane," NASA, TN D-4229 Nov. 1967.

24. Ruetenik, J. R., Zartarian, G., "Development of Methods for Predicting Airloads on TACV Configurations Due to Strong Crosswind Gusts." DOT-TSC-171-1, 27 March 1972.

APPENDIX

REPORT OF INVENTIONS

After diligent review of the work performed under this contract (DOT-TSC-1002), no innovation, discovery, improvement, or invention of a patentable nature was made. Several unconventional train configurations were tested, but all of these were either obvious from an aerodynamic standpoint or had been suggested from sources independent of the work of the contract. The main contribution of this effort was to quantify the change in drag caused by these various configurational changes.

390copies